University of Messina

Department of Engineering

PhD Course in Engineering and Chemistry
of Materials and Constructions

XXXIII cycle

Lightweight structures for marine applications:

From testing to design

Giulia Palomba

Tutor: Prof. Vincenzo Crupi

SSD: ING/IND-02 - Costruzioni e impianti navali e marini

2020

Abstract

The main objective of the thesis was to promote a broader integration of lightweight sandwich structures in the marine industry. Amongst all possible material combinations, all-aluminium sandwich structures were selected as the focus of the study.
Weight reduction and materials sustainability are becoming of primary importance for marine structures, but the simultaneous application of both of these approaches is seldom considered. The literature review regarding the use of sandwich structures for marine applications, highlighted the predominance of the composite category, whose disposal and recycling are both difficult and expensive. Therefore, a solution to both lightweight requirements and environmental issues could lie in the application of all-metal sandwich structures, and in particular of aluminium sandwich structures, which combine low-density and excellent mechanical properties with good recyclability and sustainability. In view of these considerations, a deeper knowledge on aluminium sandwich structures, based on experimental and analytical analysis, is required to support a safe and reliable design and encourage their application.
For this purpose, aluminium sandwich structures (AHS) with honeycomb core were chosen to perform an extensive experimental investigation. Particular attention was paid to two of the most critical loading condition, which may result from common in-service events: impact and fatigue loading.

Low-velocity impact tests were performed on six different AHS configurations, both single and double-layer. The latter were introduce in order to improve the crashworthiness of sandwich structures. Double-layer panels displayed a progressive collapse sequence, depending on the core arrangement and on the cell size. Such observations suggested the possibility to obtain energy absorbing structures with a controlled deformation.
A theoretical evaluation was applied to investigate the mono-layer impact response and preliminary considerations on the existence of a size effect were drawn.

The fatigue analysis, which was seldom considered in previous literature on AHS, was performed applying three-point bending loading conditions. A preliminary static analysis was performed both under three and four point

bending conditions. The static tests allowed the identification of the static bending strength and the identification of cell walls buckling buckling as the main phenomena involved in AHS bending response. The influence of boundary conditions on fatigue life and on collapse modes were investigated by considering different supports spans. For one condition the S-N curve was obtained and its equation was compared to literature results. Two different collapse mechanisms were observed depending on the supports span: for larger supports span a fracture of the tensioned skin was observed, whereas lower supports span produced core shear. In both cases, failure occurred suddenly and this should be taken into consideration in real applications. An analytical model was applied to predict fatigue collapse modes and limit loads. A fatigue failure map describing the relationship between supports span, collapse modes and fatigue limit loads was obtained, in order to provide a quantitative tool for aluminium honeycomb sandwich structures design.

Other innovative and efficient solution to the requirements of lightness and good mechanical performance for marine structures - with particular attention to crashworthiness - could be provided by the application of biomimetic principles. The idea of taking inspiration from natural strategies and structures to cope with engineering problems, was introduced and developed in collaboration with Trinity College of Dublin.

Bamboo was selected as the natural structure to analyse and mimic, especially for what concerns impact behaviour. Bamboo samples were subjected to impact both on the outside and on the inside surface. It was found that the impact strength is correlated to the thickness and to the impact side. Impact tests were also performed on specimens whose outside surface had been abraded and on whole cylindrical sections. The role of graded and hierarchical structure in impact response, suggested some guidelines for bio-inspired structures design. Four bamboo-inspired structures were designed, based on the idea of combining corrugated panels with different geometrical characteristics to resemble bamboo graded and hierarchical structure. The design choices took into considerations also the feasibility limitations for large components, which is often the case for marine structures. Some samples of the bio-inspired solutions were made using 3D printing and tested in compression. The best performance was obtained by the structure which more closely replicates bamboo's hierarchy. In addition, buckling theory was

applied to predict bio-inspired structures performance and good agreement between experimental and analytical results was observed.

Finally, a comparison of the performances of aluminium honeycomb sandwich structures and glass-fibre reinforced plastics (GFRP) sandwich panels for marine applications was provided, in order to assess the feasibility and the benefits of AHS application. The comparison was first based on the identification of the bending stiffness as a mechanical parameter equivalence, to guide the replacement of existing GFRP sandwich panels with AHS. Material charts reporting bending stiffness against other design parameters showed the significant improvements in terms of weight and volume reduction achievable with aluminium sandwich structures. Starting from bending stiffness equivalence, further suggestions for the design of AHS were introduced: a graphical approach based on plots of stiffness requirements, weight reduction goal and failure modes was applied for the identification of the main design variables. In conclusion, a case study regarding the possible substitution of a GFRP-based ship balcony overhang with an equivalent aluminium honeycomb sandwich structure was outlined. A preliminary numerical investigation to support the design of full-scale tests was developed. The results showed the possibility to simultaneously significantly reduce the weight, leave the geometry almost unchanged, and improve the mechanical response.

Keywords: *Marine structures*; *Blue economy*; *Lightweight structures*; *Sandwich structures*; *Honeycomb structures*; *Mechanical behaviour*; *Fatigue*; *Impact*; *Energy absorption*; *Crashworthiness*; *Prediction models*; *Collapse modes*; *Failure map*; *Biomimetics*; *Bioinspired design*; *Green design*; *Material charts.*

Contents

1 Introduction

1.1 Background

Structures design has changed over the past decades as a consequence of advances in manufacturing technologies, materials science, technical software availability, laws requirement, economical and environmental constraints.
Some of the main demands for mechanical design concern structures lightness and materials sustainability.
Lightweight concept has acquired considerable importance in numerous fields for several reasons. The transportation industry has a particular interest in adopting lightweight solutions, in order to reduce energy consumption and, as a consequence, CO_2 emissions.
According to the 2020 report about clean energy progress tracking of the International Energy Agency (IEA) [1], transports are responsible for 24%

of direct CO_2 emissions. Among all the transportation means, shipping and aviation are in a critical situation, being the only sectors were emissions are increasing. A decisive effort in such fields is therefore required to achieve emissions reduction demanded by international organizations and agreements.

Updating structural design philosophy in the transportation industries by taking into account weight reduction and materials environmental impact, could be beneficial not only for vehicles' fuel consumption, but also for the energy expense involved in upstream processes, which include fuels extraction and processing or energy distribution and conversion [2]. Lightweight design is not only advantageous for energy-related purposes but it is able to provide other positive outcomes, depending on the field of application and on the objectives of the design. Giving a closer look to marine industry, lightweight concept can be successfully exploited for several purposes, among which is worth mentioning easiness of building process, available volume increase and displacement decrease with consequent payload increment, stability and manoeuvrability improvement, volume and mass of building materials reduction with consequent costs and time savings for shipping, speed increase for a selected power. Hence, it is clear that a clever application of lightweight principles would be beneficial at different levels, from production, to use and even probably reuse and disposal.

Weight decrease can be achieved via two combined actions: a proper material selection and the adoption of innovative lightweight solutions. Sandwich structures are an ideal alternative for structural lightening [3]: they provide excellent mechanical properties at low densities and they allow the design of their mechanical properties through an adequate selection of face-sheet and core materials and configurations. Considering such interesting advantages, sandwich structures have gained a significant importance in the transportation industry, mainly in marine and aeronautical applications [4], [5]. The benefits of sandwich structures could be further increased by introducing new

technologies and processes, such as additive manufacturing (AM) techniques, which have opened novel paths to structure optimisation and materials innovation, owing to the possibility of producing components with complicated and customised geometries in a relatively short time [6].

1.2 Marine industry: toward a green route

According to the European Union (EU) definition [7], the expression "Blue Economy" indicates all activities that are marine-based or marine-related. The former are all those "activities undertaken in the ocean, sea and coastal areas", whereas the latter include "the activities which use products and/ or produce products and services from the ocean or marine based activities like [...] shipbuilding and repair, port activities, technology and equipment, digital services, etc".

The EU Blue Economy Report 2020 [8] points out that the EU shipbuilding industry is an innovative and competitive sector, which in the last decade specialised, with its 300 shipyards, in products with high level of technology and added value, such as cruise ships, mega-yachts, research vessels, offshore support vessels, etc. In addition, the EU plays a leadership role for high-tech and advanced maritime equipment and systems, as a results of the investments in research and innovation promoted by the major actors of the sector.

The same EU report suggests that the commitment of marine industry for further reduction of environmental emissions is required and this could represent an opportunity for maritime equipment suppliers and shipyards to expand their market share.

In this scenario, the concept of green shipbuilding is attracting the attention of all the players of the sector. The purpose of green shipbuilding is to minimise the environmental emissions starting from the design phase, to manufacturing and service [9]. Green shipbuilding strongly relies on green

design, which is aimed at reducing the materials and energy waste during manufacturing and service, as well as increasing the share of recycling and reuse of parts during ships maintenance and disposal. In addition, shipyards should be based on a green philosophy too, in order to promote an efficient use of materials and manufacturing processes and methods with low environmental impact and minimum waste of resources.
Building techniques are also affected by green design and their improvement toward more sustainable solutions include a wider integration of modular concept which would improve the work efficiency.
One of the challenges for green shipbuilding and green ship design is the materials selection [9, 10], which should be based on the following key features:

- safety in production and use for people and environment;
- possible and convenient reuse and recycling;
- efficient materials manufacturing with high utilisation ratio;
- weight reduction to increase the ship loading capacity and ease the logistic issues.

The importance of material selection and ship recycling was assessed by the Hong Kong International Convention for the safe and environmentally sound recycling of ships in 2009, overseen by the International Maritime Organization (IMO). The Convention [11] addresses the design, construction, operation and preparation of ships, which should be aimed at facilitating a safe and environmentally sound recycling, without compromising the safety and operational efficiency of ships. In addition the Conventions promoted some guidelines to setup a mechanism for ship recycling, incorporating certification and reporting requirements.
The path to achieve a “green” status for the marine industry is paved with challenges and only a continuous commitment to research and innovation will produce successful results.

1.3 Lightweight structures in marine applications: challenges and sustainability

Weight saving and materials sustainability are attractive topics for marine field, since increasing attention is paid to energy efficiency and environmental issues in this area. The warning of the IEA [1] on emissions growth in the shipping sector, highlights the urgency for massive actions to limit emissions with all possible strategies. In this scenario, structural weight reduction could play a critical role since it produces displacement decrease with consequent resistance reduction and therefore fuel consumption decrement [12]. Lightweight structures adoption would also results in material use reduction, in possible increment of payload and in speed increase at a given power [12].

Marine structures lightening could benefit from the application of appropriate sandwich structures, whose selection and design need to consider specific criteria such as manufacturing feasibility for large structures, sustainability issues, safety requirements, economical boundaries and materials compatibility with the aggressive marine environment. Lightweight sandwich structures could also be advantageous for damping purposes [13, 14], which should be considered to ensure the functionality and comfort of marine vehicles and structures. Current applications of lightweight sandwich structure in marine industry include: hulls, overheads, decks, dividers, furnitures, partition walls, berths, masts, spars [15] [16].

When applied in marine industry, lightweight structures are often demanded to fulfil also crashworthiness requirement. Crashworthiness refers to the ability of a structure to protect its occupants during an impact. When replacing traditional structures with lightweight alternatives it is necessary to assess their energy absorption capabilities to ensure their safe application. Impact resistance should be guaranteed both for localised low-velocity impacts and for large collisions events. The former [17] are usually the result

of interactions with floating debris, other craft, docks or small accidents during manufacturing a assembly phases. Other localised and impact phenomena are those resulting from wave impact and slamming. The capability of lightweight structures energy absorption during similar events could be evaluated with small-scale experimental tests and numerical analysis, involving, when necessary, the interaction of fluid and structure [18].

Collisions events with other ships and large structures are more difficult to reproduce. The crashworthiness evaluation, for these cases is often based on numerical studies and seldom large-scale experimental investigations are performed [19]. In addition, crashworthiness is affected by corrosion and ageing of ship structures [20].

In the last decades ship collisions events increased, as a result of the growing marine traffic and of the development of the motorways of the sea. This produced severe consequences on shipping safety and on environmental issues. Serious accidents are often at the base of structural innovations in the marine industry: a striking example was the disaster of the 1989 caused by oil spilling from the Exxon Valdez, which led to the double hulls (or alternative designs ensuring the same level of protection against pollution in the event of a collision or stranding) being compulsory for tankers.

The European Maritime Safety Agency (EMSA) [21] registered in 2018 an increase of 14.5% in very serious casualties and of 2.5% in serious casualties, in relation to the average of the previous five years. On the other hand, according to the preliminary data of the EMSA [22], 2019 was a positive year with 9% reduction in the overall number of accidents and a 40% reduction in the number of fatalities, when compared with the average over the past six years.

Therefore, dealing with ship collisions events is necessary to guarantee both maritime safety, by ensuring ships integrity, and marine environment protection, by avoiding oil spills.

One of the solution to innovate and contribute successfully to ships safety

and environment protection could be the adoption of metal lightweight structures, with high energy absorption capabilities.

A wide variety of lightweight materials and sandwich structures are used in the marine industry, but the most common solution at the moment is represented by fibre reinforced plastic (FRP) [23]. The extensive presence of FRP laminates and sandwich panels in marine constructions, raises the issue of material sustainability. FRP disposal at the ships end of life, is troublesome requiring difficult and expensive procedures [24]. Consequently, alternative materials with good sustainability properties for lightweight marine structures would further support the improvement of this industry toward more environmental-friendly horizons.

Aluminium structures could represent one of the response to the quest for improved sustainability. Differently from most FRP-based materials, aluminium has a good recyclability [25], which is crucial to make this material sustainable. Indeed, the production of secondary (i.e. recycled) aluminium requires less than the 93% of the direct energy used for primary aluminium production [26]. This means that the path to the reduction of aluminium alloys environmental impact is strongly dependent on recycling. Hence, the more these materials are applied in a responsible and conscious way, the more their recycling cycle will improve, even though, as observed by Soo et al. [27] the recycling market is often driven by profit logic, rather than environmental outcomes.

In addition, aluminium recycling convenience is dependent on the efficiency of the recycling processes. Therefore, new and more efficient technologies are constantly searched and developed. An example was provided by Fogagnolo et al. [28], who suggested a method for recycling aluminium alloy and aluminium matrix composites chips by cold and hot pressing followed by hot extrusion. Their experimental investigation pointed out that the process was able to recycle aluminium chips, rather than aluminium pow-

der, and also to treat aluminium composite chips without the segregation of the reinforcement particles. Another solution was proposed by Ingarao et al.[29], who analysed Friction Stir Extrusion as a solid-state technology for aluminium alloys recycling. During such process metal chips or solid billet are transformed into wires and rods. The authors observed that for these products, the Friction Stir Extrusion results in a primary energy demand reduction with respect to other traditional processes. Behrens et al. [30] investigated the potentialities of recycling of cold pressed aluminum chips by a hot backward extrusion process. Despite the method has to be optimised, it showed the potential to produce semi-finished components from aluminium waste, resulting in a reduction of post-treatment necessity.
These are only few examples of the endless search for improving aluminium recycling efficiency, which, together with a wider and responsible use of this material, will promote a virtuous cycle of aluminium use and re-use.

1.4 Biomimetics and lightweight philosophy

Innovative alternatives for numerous engineering applications, including lightweight marine structures, may be suggested by the observation of solutions provided by nature, according to the principles of biomimetics. The term "biomimetcs" was coined in 1969 by Schmitt [31], referring to the transfer of solutions, concepts and ideas from biology to technology. Millions of years of natural selection led to the development of incredibly complex structures, evolved for multiple functions [32], which can inspire original engineering designs.
The application of biomimicry could offer a holistic perspective in the resolution approach of engineering problems. A complete and thorough observation of natural solutions and strategies is not limited to an isolated function or property, but involves also the relationship of the object with the environment throughout its entire life, considering also its production and disposal.

Therefore, biomimetic science can be addressed not only at improving an object performance, but also at rethinking its overall impact, aiming at imitating the natural processes in terms of use and reuse of resources. The Blue Economy philosophy [33], which is inspired by these biomimetic principles, will consequently acquire increasing importance in the engineering design.

The interest toward bio-inspired engineering solutions is rising also thanks to the growing accessibility to additive manufacturing techniques, which allow the production of complex design solutions, as bio-inspired structures may be [34]. However, for an effective imitation of natural structures, simple observation is not sufficient, but a deep investigation of their structure and its effect on properties is required [35]. Focusing the attention on weight reduction, nature represents an endless and promising source of inspiration, not only to optimise mechanical design from a structural perspective, but also to promote sustainable and resource-savings improvements [36], which are basic criteria for natural structures evolution, whereas engineering structures often underestimate their importance. Several examples of bio-inspired lightweight structures and design protocols exist in scientific literature, proving the growing interest toward the subject and the possibility to achieve promising results.

For instance, Zhao et al. [36] suggested a methodology for lightweight bionic design of mechanical structures, with the aim of providing a systematic approach for a rational selection of natural solutions to be used as models for engineering design. They proposed to base the bionic design on different stages and levels. The first point to assess is the technical purpose, such as the lightweight design of mechanical structures. Then it is necessary to determine what kind of biological solutions exist for the problem, such as minimising resources or maximising efficiency. In the third stage three selection factors (structure, loading and function) are used to detect similarities between the engineering structure and biological structures. In the

last phase, a classification based on structural principles, such as material distribution, type of load resistance and dominant mechanical property, is performed. The performed classification should support the design in the selection of the most significant similarities, which are processed through a fuzzy assessment method, and in the application of the related configuration principles, instead of taking inspiration only from a natural structure, chosen without a guided procedure.

Another interesting example which explores the synergy among biomimetic approach, lightweight design and 3D printing technology, was presented by Kaminski et al. [34].They took inspiration from the structure of the plant motherwort stems, which are organised, in the longitudinal direction, into hollow internodes and solid nodes with a squared shape. They prepared different CAD models based on plant structure measurements, with increasing degree of abstraction from the reference stem structure and they manufactured some sample with selective laser sintering process using polyamide powder. The specimens were tested under four-point bending and torsion conditions. In order to quantitatively assess the lightweight benefits obtained with the bio-inspired design, an efficiency ratio was evaluated. The results highlighted that the design which differed the most from the natural model was the most efficient one, with regard to flexural and torsional efficiency. Consequently, it was proved that a simple imitation of natural structure is not useful, if not supported by intelligent evaluations. Indeed, natural structures are optimised for multiple and coupled functions, hence their reproduction for structures addressed to one function only and manufactured with a homogenous and isotropic material could not be effective, without any additional adjustments.

Among numerous biological structures, eligible to be mimicked for lightweight purposes, Li et al. [37] selected the glass sponges, whose porous, light,

tough and strong skeleton was used as the archetype for two bionic tube-like lightweight structures. The observations with a super-depth-of-field microscope allowed an accurate identification of the cylindrical glass sponge structure, which consists of a fibrous network structure and octagon mesh, crossed by orthogonal diagonally-oriented struts which surrounds the main cylindrical structure in spirals. The first bio-inspired structure was shaped as a tube whose walls are made with an octagonal mesh; the second bionic structure adds to the octagonal mesh a double helix outer ridge surrounding the tube. The prototypes of the bio-inspired structures were manufactured with stereolithography 3D printing technology. They used lightweight numbers, defined as the ratio between the maximum load, in different testing conditions, and the weight, to assess the lightweight efficiency of each model, with respect to a tube whose walls were shaped with a common honeycomb mesh. The lightweight numbers of the bio-inspired structures demonstrated significant improvements in lightweight properties. Further advances were obtained by an optimisation procedure based on neural networks. The promising results endorsed the possibility to apply similar thin-walled tubular structures for aerospace, vehicles and ships applications.

One of the industry which could benefit from lightweight bio-inspired design is the marine one. An example was provided by Leidenfrost [38], who presented a concept for a bionic hull structure to be adopted in a 46 m yacht. The bio-inspired design was motivated by the necessity of integrating large glass windows into the sailing yacht and, in particular, in the areas where the highest global loads usually act. This required an unconventional approach to the design phase, and the exoskeletons of some planktonic organisms were taken as a source of inspiration. Several topology optimisation iterations were performed and the result was a bio-inspired hull structure with truss elements following the main load paths, which allow the presence of large windows in positions not possible with traditional design.

The above mentioned examples prove the endless potentialities of design solutions inspired by nature, which can contribute to chart the way towards ground-breaking innovations in structural design.

1.5 Objective of the thesis

The current thesis deals with the theme of marine structures weight reduction through the application of lightweight solutions.
The main objective and novelty of the thesis was to develop and design lightweight structures for marine applications, by applying metal sandwich structures in substitution to traditional solutions. The development of structural elements for marine applications, based sandwich concept followed some guiding principles: the necessity to guarantee lightweight properties, the crashworthiness capabilities, the importance of green design and the innovation achievable through biomimicry.
The thesis aims to promote a broader integration of lightweight sandwich structures in the marine industry, with particular attention to the aluminium sandwich structures (AHS). Indeed, these are able to combine low-density and excellent mechanical properties with good recyclability and sustainability.
Despite their advantages, the application of sandwich structures in the marine industry is often limited to non-structural components. Indeed the design of sandwich structural elements cannot be performed following the rules and criteria of traditional materials, bot in static and dynamic conditions. Therefore, an efficient integration of lightweight sandwich elements with structural functions, requires a reliable and safe design methodology, based on a significant amount of experimental evidences. The objective of the thesis is to contribute to such goal by combining experimental results with theoretical evaluations and critical considerations.
An extensive experimental investigation regarding low-velocity impact and

fatigue bending conditions was performed, with the aim of investigating some critical conditions for AHS applications and deriving some guidelines for design purposes.
In addition, it was suggested the possibility to apply biomimetic principles to find innovative lightweight solutions for the marine industry. Starting from observations on low-velocity impact response of bamboo, some bio-inspired structures were suggested and tested.
Finally, a comparison between aluminium honeycomb sandwich structures and glass-fibre reinforced plastics (GFRP) sandwich panels for marine applications was provided, in order to assess the feasibility and the benefits of AHS application. A case study regarding the possible substitution of a GFRP-based ship balcony overhang with an equivalent aluminium honeycomb sandwich structure was outlined and the results showed the benefits, in terms of weight saving and mechanical performance improvement, of AHS use.

1.6 Outline of the thesis

The thesis will be outlined as follows:

- Chapter 2 will discuss the basics of sandwich structures and the main theories for sandwich structures mechanics, with particular attention to bending, low-velocity impact and fatigue conditions. Then, the marine applications of sandwich structure, distinguished for the different material categories, were reviewed.

- Chapter 3 will deal with investigation on aluminium honeycomb sandwich structures. Two main loading conditions were investigated: low-velocity impact and fatigue. For the former, an extensive experimental analysis on single and double-layer honeycomb sandwich structures will be described and correlated to structures configurations. A theoretical

approach will be applied to single-layer structures to define contact parameters, useful for design purposes.

The fatigue analysis on AHS will be focused on three-point bending conditions. Collapse mechanism under fatigue conditions will be described and compared to static failure mechanism. An analytical model for fatigue collapse modes and limit loads prediction will be developed. A fatigue failure map describing the relationship between supports span, collapse modes and fatigue limit loads is introduced.

- Chapter 4 will propose the application of biomimetics to design innovative lightweight crashworthy structures for marine applications. An experimental analysis on low-velocity impact response of bamboo structures will be described, along with the main conclusions regarding the correlation between bamboo impact behaviour and its structure. Some bamboo-inspired structures were designed and tested and an analytical model was applied to predict their response.

- Chapter 5 will present a comparison between AHS and GFRP sandwich structures for marine applications. An equivalence parameter to guide the replacement of existing GFRP sandwich panels with AHS will be defined. Material charts for materials and sandwich structures selection will be drawn. A graphical approach for the identification of the main design variables will be introduced. In conclusion, a case study regarding the possible substitution of a GFRP-based ship balcony overhang with an equivalent aluminium honeycomb sandwich structure will be outlined.

- Chapter 6 will present the main conclusions.

2

Sandwich structures: basics, mechanics and applications

2.1 Basics

Sandwich structures consists of two thin and stiff facings (or skins) which enclose a tick and low density core. The basic principle of sandwich structures is to maintain a low weight, while ensuring a high bending stiffness, according to the same principle of I-beams. The facings sustain mainly bending and in-plane load, similarly to the flanges of an I-beam. The core acts as the web of an I-beam, carrying the shear load and improving the bending stiffness by separating the skins but, differently from an I-beam, it allows a regular supports to the skins, distributing the loads and producing a uniformly stiffened panel [39]. The core keeps two stiff facings separated,

increasing the distance from the neutral axis and therefore maximising the area moment of inertia I (or second moment of area) and the section modulus (W) to which is proportional the bending stiffness. Considering the lightweight properties of core, such increase in bending stiffness is generally achieved with a small weight increment. The so-called "sandwich effect" is illustrated in Figure 2.1, where the density of the skins was assumed to be 20 times higher than the core.

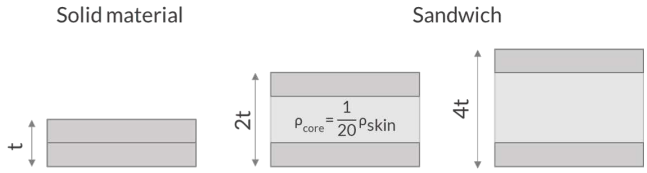

Area moment of Inertia *I* (facings)	1	7	37
Section modulus $W(I/d_{max\,neutral\,axis})$	1	3.5	9.2
Total weight	1	1.05	1.15

Figure 2.1. Example of "Sandwich effect".

The bond between core and skins is usually provided by an adhesive layer, which joins the parts in a rigid way so as to make the assembly to respond as a whole component. Depending on the materials, core and skins adhesion is also achievable via welding, blending or other techniques. In general the core-facings interface is a critical part of the sandwich panel.

Core material and structure are selected in order to provide a proper load distribution between the two skins and to resist compression maintaining the adequate distance between the face-sheets, whereas the facings act as a protection for the low-density core.

The peculiarity of sandwich structures lies in their properties versatility, depending on the infinite combinations of facings and core materials and configurations.

Despite countless sandwich structures with different properties are possible, some common advantages and disadvantages can be identified. The strengths of sandwich structures include [4], [40]:

- high stiffness/weight and strength/weight ratios;
- excellent crashworthiness;
- good damping properties;
- possibility to combine different properties within a single material construction, by a proper choice of the parts;
- reduction of parts number by integrating different functions in the sandwich design;
- improved quality of the parts due to prefabrication;
- time and costs saving for assembly;
- possibility to reduce the necessity of secondary stiffening and supporting elements, simplifying the architecture of components and increasing the available volume. For the structure of a ship, this is exemplified in Figure 2.2.

The potential benefits offered by sandwich structures are insufficient to guarantee a high degree of diffusion, since numerous questions to practical application are still open [4]; these include:

- difficult design, as a consequence of different materials combination and structure configurations, which produce also a wide range of failure modes;
- complex design and implementation of joining systems;

Figure 2.2. Comparison of traditional design and sandwich design for a ship.

- lack of standardised procedures for testing, inspection, safety, repair for all applications;
- possible long certification processes, as a result of complex mechanical response;
- lack of scientific information and data to support the design of sandwich structure-based components;
- necessity to develop and spread new approaches for design and production.

On the basis of the above considerations, it is straightforward that sandwich structures have incredible potentialities to be applied in numerous fields, improving and innovating countless systems. Nevertheless, an extensive application of sandwich structures needs to be by deeper knowledge on their behaviour in different conditions, in order to extend designers' confidence area and aid the development of adequate design procedures.

2.2 Classification of Sandwich Structures

Despite the wide variety of sandwich structures makes their classification difficult and susceptible to omissions, some key features can be considered to distinguish the main categories. The most significant classifications for sandwich structures are based on:

- material of skins and core;
- core configuration.

The material-based classification is summarised in Figure 2.3.
The core-based classification is presented in Figure 2.4.
Typical materials for all-metal sandwich structures are steel, aluminium and titanium alloys. Usually, skins and core of all-metal sandwich structures are made with the same material. Common core configurations for metallic sandwich structures are honeycomb, foam, corrugations, beams, lattice or truss.
Honeycomb cores, both metallic and non-metallic, is a one of the most interesting structure for its excellent stiffness and shear strength combined with lightweight properties. Honeycomb core, which are more expensive than other solutions, were developed to be used in high-performance applications such as aerospace and aeronautical, but their use is now spread in several fields, from naval to buildings.
Lattice core can have complex geometries and are difficult to obtain with traditional processes, but they are becoming increasingly wide-spread thanks to additive manufacturing techniques [41].

In composite sandwich structures, facings are commonly made with fibre-reinforced polymer (FRP) material, where fibres of different types (glass fibre, carbon fibre, natural fibre, etc,), with different possible forms and

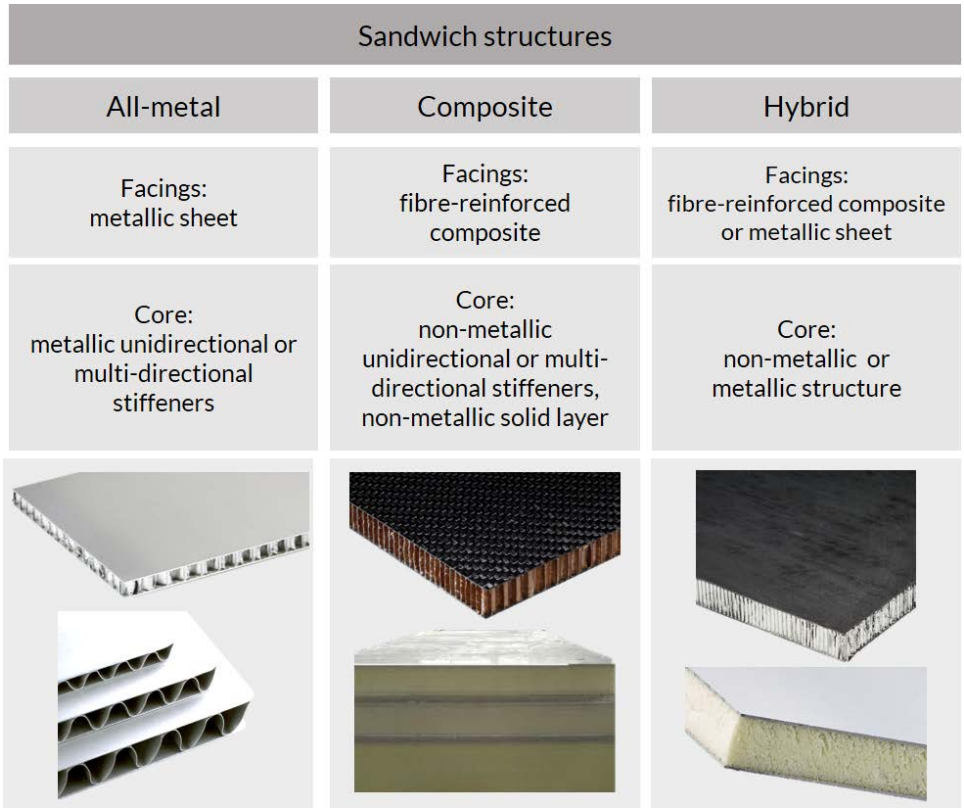

Figure 2.3. Materials-based sandwich structures classification.

arrangements (continuous, discrete, random, oriented), are dispersed in a polymeric matrix (termosetting such as epoxy or phenolic or thermoplastic such as polypropylene). FRP skins usually consists of a laminate made by a sequence of bonded plies, where each ply can have different fibres arrangements. Common cores for composite sandwich structures are polymeric foams, aramid paper or polymeric honeycomb, polymeric corrugated stiffeners, elastomers layers, wood layers (e.g. balsa).

Hybrid sandwich structures are made with both metallic and non-metallic

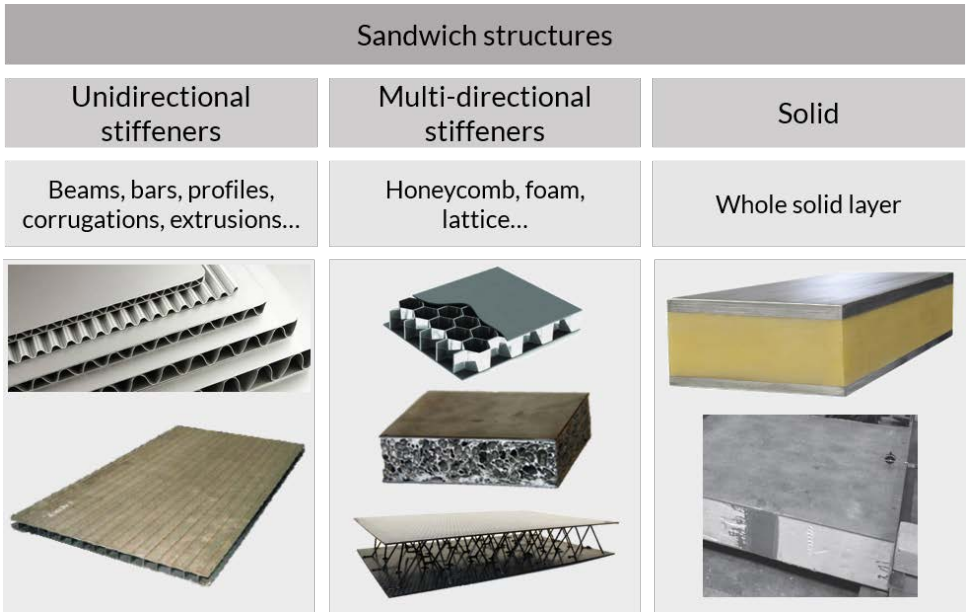

Figure 2.4. Core-based sandwich structures classification.

materials, with the aim of combining their properties and obtain an ideal integration of features of different material categories. Typical examples are sandwich panels with polymeric foam or aramid honeycomb core with metallic skins, often used for marine and aeronautical applications.

2.3 Sandwich structures basic mechanics

The following section aims at presenting some basic information on sandwich structures mechanics. The formulations and the theory described below, address some specific cases, which are functional to the activities developed in the following chapters. More general information can be found in the reference literature.

2.3.1 Sandwich beams under three-point bending

The theoretical analysis of sandwich beams is based on the Timoshenko beam theory, which takes into account shear stress and transverse shear deformations. The extension of the theory to sandwich structures was first developed by Plantema [42] and Allen [43] and was reviewed by many authors, like Zenkert [44].
Figure 2.5 is the illustration of the sandwich beam with its geometrical parameters, loading and boundary conditions, which will be used in the analytical formulations.

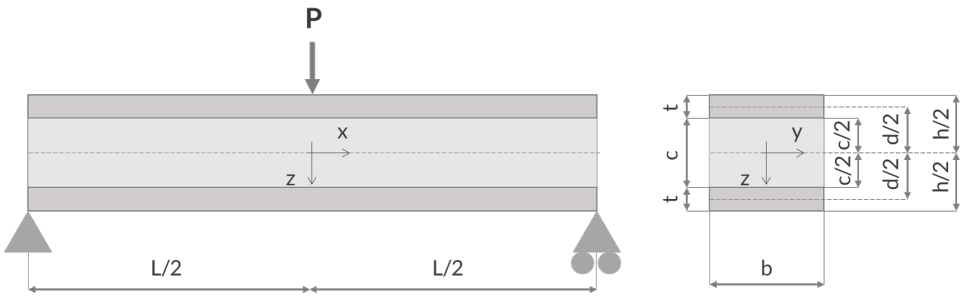

Figure 2.5. Sandwich beam scheme.

The assumptions made for the analysis are the following:

- the loading configuration is static
- the deflections are elastic;
- the skins are firmly bonded to the core;
- the materials of facings and core are isotropic;
- the stiffness of the skins material is significantly larger than the core;
- the beam is narrow, making the stress in the y direction negligible.

According to the considered assumptions, when a beam is loaded in bending with a point load, the curvature $(1/R_c)$ is proportional to the bending moment (M), according to equation 2.1:

$$\frac{M}{EI_x} = -\frac{1}{R_c}. \tag{2.1}$$

The quantity EI_x in an ordinary beam is the bending stiffness of the beam (D). A sandwich beam consists of two parts, the core and the facings, hence its flexural stiffness is the sum of the contributes from the two constituents, calculated about the neutral axis of the entire section. Naming E_f and E_c the modulus of elasticity of the facings and the core respectively, equation 2.2 expresses the bending rigidity for a sandwich beam:

$$D = E_f \frac{bt^3}{6} + E_f \frac{btd^2}{2} + E_c \frac{bc^3}{12}. \tag{2.2}$$

The first two terms represent the bending stiffness of the skins and the third term is the bending stiffness of the core, calculated about the neutral axis. In common sandwich panels, the second term is the dominant one. Indeed, if the conditions in equations 2.3 and 2.4 are satisfied, the first and third terms respectively are negligible, being their value less than 1% of the second term.

$$3\left(\frac{d}{t}\right)^2 > 100 \tag{2.3}$$

$$6\,\frac{E_f}{E_c}\,\frac{t}{c}\left(\frac{d}{c}\right)^2 > 100. \tag{2.4}$$

Under three point bending conditions, the maximum bending moment (M) is

at the beam midspan and the resulting strains and stresses in the face-sheets (ε_f, σ_f) and the core (ε_c, σ_c) are respectively:

$$\varepsilon_f = \frac{Mz}{D}; \qquad \sigma_f = \frac{Mz}{D}E_f \tag{2.5}$$

$$\varepsilon_c = \frac{Mz}{D}; \qquad \sigma_c = \frac{Mz}{D}E_c \tag{2.6}$$

where z is the coordinate measured respectively within the facing and the core. It is straightforward that the maximum stresses in the facing and in the core, are reached in the farthest sections from the neutral axis:

$$\sigma_f = \pm\frac{M}{D}\frac{h}{2}E_f \tag{2.7}$$

$$\sigma_c = \pm\frac{M}{D}\frac{c}{2}E_c. \tag{2.8}$$

The normal stress distribution is linear within each component, with a discontinuity at the interface between facings and core, due to different Young's modulus. If the skins material is considerably stronger than the core material (i.e. $E_f >> E_c$), which is a common situation, the elastic modulus of the core can be neglected ($E_c = 0$) and the normal stress in the core is assumed to be null. In addition, if the skins are thin ($c >> t$), hence the conditions 2.3 and 2.4 are both fulfilled, the normal stress distribution in the facings is approximated as constant:

$$\sigma_f = \pm\frac{M}{btd} \tag{2.9}$$

The normal stress distribution, at different level of approximation, is illustrated in Figure 2.6.

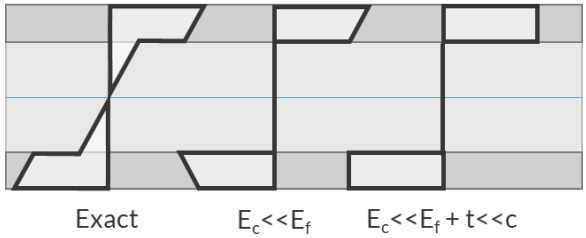

Figure 2.6. Normal stress in a sandwich beam under 3 point bending, according to different approximations.

In a homogenous beam, the shear stress τ in a section produced by a shear force T_z in that section is expressed by equation 2.10:

$$\tau_{xz} = \frac{T_z S_x(z)}{I_x b(z)} \tag{2.10}$$

where $S_x(z)$ is the first moment of area about the neutral axis in function of the coordinate z and b is the width of the section in function of the coordinate z. However, for a sandwich beam is necessary to take into consideration the presence of different parts and materials, thus equation 2.10 is modified into equation 2.11:

$$\tau_{xz} = \frac{T_z}{Db(z)} \sum S_x(z)_i E_i \tag{2.11}$$

where D is the bending stiffness of the entire section and $\sum S_x(z)_i E_i$ is the sum of the products of $S_x(z)$ and E for all sandwich components. The shear stress in the core τ_{xz_c} is equal to:

$$\tau_{xz_c} = \frac{T_z}{D(z)} \left[E_f \frac{td}{2} + \frac{E_c}{2} \left(\frac{c^2}{4} - z^2 \right) \right]. \tag{2.12}$$

Therefore, the maximum shear stress in the core is at the neutral axis, where $z = 0$ and the minimum shear stress in the core is at the interface with the core, where $z = \frac{c}{2}$, which corresponds to the maximum shear stress in the skins. Equation 2.13 shows the maximum and minimum values of τ_{xz_c}:

$$\begin{aligned} \tau_{xz_{c,max}} &= \frac{T_z}{D}\left(\frac{E_f t d}{2} + \frac{E_c c^2}{8}\right); \\ \tau_{xz_{c,min}} &= \tau_{xz_{f,max}} = \frac{T_z}{D}\left(\frac{E_f t d}{2}\right). \end{aligned} \tag{2.13}$$

Approximation to the above expressions can be considered in many practical cases, depending on the properties and the geometry of the core and skins. For instance, the ratio between $\tau_{xz_{c,max}}$ and $\tau_{xz_{c,min}}$ yields:

$$1 + \frac{1}{4}\,\frac{E_c}{E_f}\,\frac{c^2}{td}. \tag{2.14}$$

If the second part of expression 2.14 satisfies the following condition:

$$4\,\frac{E_f}{E_c}\,\frac{t}{c}\,\frac{d}{c} > 100 \tag{2.15}$$

therefore, the ratio between the maximum and minimum shear stress (eq. 2.14) is close to 1. Consequently, the shear stress in the core can be assumed to be constant. Considering that, for common sandwich structures, the ratio d/c assumes values near to 1, the conditions expressed in equations 2.15 and 2.4 are almost superimposable. Both assumption are satisfied if the facings elastic modulus is significantly higher than the core elastic modulus. The resulting deduction is that when the core is considerably weaker than the skins, its contribution to the sandwich structure bending stiffness is negli-

gible and the shear stress along the core is approximately constant. Hence, considering null the core elastic modulus ($E_c = 0$) the shear stress in the core can be expressed as:

$$\tau_c = \frac{T_z}{D} \frac{E_f t d}{2}. \tag{2.16}$$

Moreover, if also the bending stiffness of the facings with respect to their own centroid axes in negligible, i.e. the condition 2.3 is satisfied being the core thickness predominant on the facings thickness, the shear stress in the core is further simplified as:

$$\tau = \frac{T_z}{bd}. \tag{2.17}$$

The corresponding shear strain for this condition is the following:

$$\gamma = \frac{T_z}{G_c b d} \tag{2.18}$$

where G_c is the shear modulus of the core.

The shear stress distribution is represented in Figure 2.7, where different level of approximations are compared.

The deflection δ of a sandwich beam is the result of a bending (δ_b) and a shear contribute (δ_s), according to equation 2.19:

$$\delta = \delta_b + \delta_s = \frac{k_b P l^3}{D} + \frac{k_s P l}{A G_c} \tag{2.19}$$

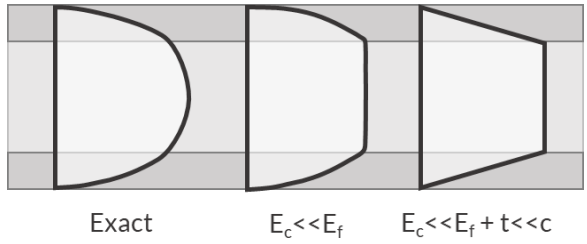

Figure 2.7. Shear stress in a sandwich beam under 3 point bending, according to different approximations.

where:

$$A = \frac{bd^2}{c}, \tag{2.20}$$

The product AG_c is known as the shear stiffness of the sandwich beam, k_b and k_s are deflection coefficients, relative to bending and shear respectively, dependent on boundary and loading conditions. For a simply-supported beam under three point bending loading, $k_b = \frac{1}{48}$ and $k_s = \frac{1}{4}$. The bending component produces a rotation of the beam sections, which made them remaining perpendicular to the neutral axis. The shear component produces an additional vertical displacement of the beam sections. The deflection of a simply-supported three-point bending sandwich beam is illustrated in Figure 2.8:

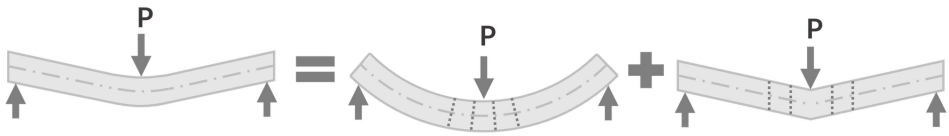

Figure 2.8. Deflection of a simply-supported sandwich beam under 3 point bending.

2.3.2 Sandwich plate under a uniformly distributed load

In practical applications, sandwich structures are often use in the form of plates, where the ratio between the width b and the length a of the panel is greater than 1/3. The sandwich plate geometrical parameters are illustrated in Figure 2.9.

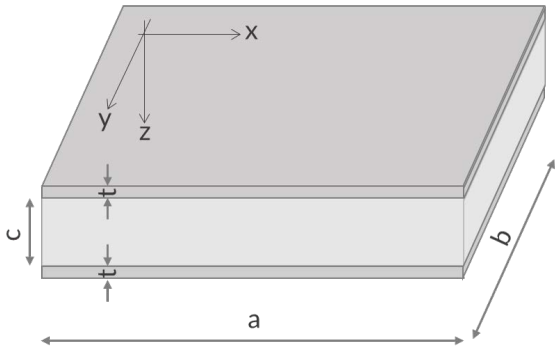

Figure 2.9. Sandwich plate.

In order to analyse the mechanics of a sandwich plate under a uniformly distributes normal load, simply-supported along all four edges, the following assumptions are considered:

- skins and core are isotropic;
- the deflections are small;
- stresses along the z axis are negligible both in the facings and in the core;
- the core elastic modulus in the $x-y$ plane is negligible in comparison to skins, hence the core does not contribute to sandwich bending stiffness and the core shear stresses are constant throughout the entire core;
- the facings are thin, thus their local bending stiffness is negligible and it is possible to assume $c = d$.

The maximum deflection for a simply-supported plate subjected to a normal load uniformly distributed, occurs at the centre of the panel ($x = a/2, y = b/2$) and it is expressed by equation 2.21:

$$\delta_p = \frac{qb^4}{D_p}(\beta_1 + \rho\beta_2) \tag{2.21}$$

where q is the load per unit area, D_p is the bending stiffness of the sandwich plate, which is equal to:

$$D_p = E_f \frac{td^2}{2(1-\nu_f^2)}, \tag{2.22}$$

ρ is a non dimensional parameter, which is function of the ratio between the flexural stiffness $E_f td^2/2(1-\nu_f^2)$ and the shear stiffness $G_c d$:

$$\rho = \frac{\pi^2}{b^2} \frac{E_f td}{2G_c(1-\nu_f^2)} \tag{2.23}$$

β_1 and β_2 are parameters function of ratio a/b whose expressions and graphical representations can be found in literature [43], [4], [44]. The maximum stresses are usually of interest for design purposes. In the facings, the normal stresses are maximum at the centre ($x = a/2; y = b/2$) and the shear stress at the corners ($x = 0, y = 0;\ x = a, y = 0;\ x = a, y = b;\ x = 0, y = b$). The corresponding expressions are reported below:

$$\sigma_x = \frac{qb^2}{dt}(\beta_3 + \nu_f\beta_4); \tag{2.24}$$

$$\sigma_y = \frac{qb^2}{dt}(\beta_4 + \nu_f\beta_5); \tag{2.25}$$

$$\tau_{xy} = \frac{qb^2}{dt}(1-\nu_f)\beta_5. \tag{2.26}$$

In the core, the shear stress τ_{zx} is maximum at the middle section of the

edges of length b ($x = 0, y = b/2$; $x = a, y = b/2$) and the shear stress τ_{yz} is maximum at the middle section of the sided of length a ($x = a/2, y = 0$; $x = a/2, y = b$). The expressions for the maximum stresses in the core are the following:

$$\tau_{zx} = \frac{qb}{d}\beta_6; \tag{2.27}$$

$$\tau_{yz} = \frac{qb}{d}\beta_7. \tag{2.28}$$

In equations 2.24-2.28 β_{3-7} are parameters depending on the ratio a/b.

2.3.3 Impact on sandwich structures

Impact loading consists of dynamic contact between a mass, with different possible shapes, and a target object. Depending on the speed at which the event occurs, it is common to distinguish:

- low-velocity impact: $\leq 10\,\mathrm{m/s}$;
- high-velocity impact: $> 10\,\mathrm{m/s}$.

Impact is a dynamic event which usually produces non-linear responses on the target element. Several analytical models were developed for impact description, with different levels of approximations, depending on the required accuracy. A thorough review of impact modelling and sandwich structures impact response was provided by Abrate [45], which will be the main reference for the current section.
Two fundamental models will be addressed in the following description, considering that they are widely applied in scientific literature and have proved their effectiveness:

- the spring-mass model;
- the energy-balance model.

One of the most common and effective solution is to model the structure as an equivalent spring-mass system, as first proposed by [46]. Such analysis provides an accurate description of impact phenomenon in some cases, especially during small-size laboratory tests. In the most general version, the spring-mass model allows the description of impact behaviour even when the structure experiences large deformations, introducing geometrical non-linearities and possible membrane stiffening effects. The equivalent system of is displayed in Figure 2.10.

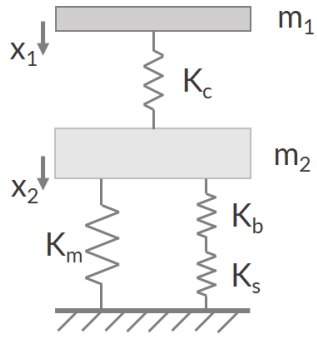

Figure 2.10. Spring-mass model.

The model, which has two degree of freedom, consists of:

- two linear springs in series, which account for the linear stiffness of the structure correlated to the effect of bending (K_b) and shear (K_s) deformation; the spring series can be replaced by a single spring for both effects (K_{bs});
- a spring for the non-linear membrane stiffness (K_m);
- a mass m_1, which is the projectile mass;
- a mass m_2, which represents the real mass of the sandwich structure;
- a spring representing the non-linear contact stiffness (K_c).

The motion of the system, for both the degrees of freedom, is described by equations 2.29:

$$\begin{cases} m_1\ddot{x}_1 + P = 0 \\ m_2\ddot{x}_2 + K_{bs}x_2 + K_m{x_2}^3 - P = 0 \end{cases} \tag{2.29}$$

where P is the contact force. The model can be simplified when geometrical non-linearities are negligible and the indentation is small compared to the global deformation of the structure. In similar cases, a single degree of freedom equivalent system is acceptable: assuming that the mass of the structure is negligible and the impactor and the structure move together immediately after contact, the resulting equation of motion is:

$$m_1\ddot{x} + K_{bs}x = 0. \tag{2.30}$$

The general solution for equation 2.30 yields:

$$x = A\sin\omega t + B\cos\omega t \tag{2.31}$$

where A and B are constant dependent on the initial conditions and ω^2 is equal to:

$$\omega^2 = \frac{K_{bs}}{m_1} \tag{2.32}$$

Naming v the impact velocity, the initial conditions are:

$$\ddot{x}(t=0) = v, \quad x(t=0) = 0 \tag{2.33}$$

leading to the following solution for equation 2.31:

$$x = \frac{v}{\omega}\sin\omega t. \tag{2.34}$$

According to the previous assumptions, the contact force equals the force in the linear spring, therefore the contact force history is:

$$P = K_{bs}x = v(K_{bs}m_1)^{\frac{1}{2}} \sin \omega t. \tag{2.35}$$

From equation 2.35, it is clear that the maximum contact force is directly proportional to the impact velocity and to the square root of the impacting mass and the structure stiffness K_{bs}. The application of spring-mass models to impact problems, allow contact force history evaluation, giving that the structure stiffness is known.

Impact phenomena can be analysed from another perspective referring to the balance of energy involved in the event. The underlying principle is to consider that the kinetic energy of the impacting mass is spent to deform the target structure. If a quasi-static approximation is acceptable to describe the behaviour of the impacted structure, it follows that when the maximum deflection of the structure is achieved, the velocity of the impacting mass becomes zero and the entire kinetic energy was used to deform the structure. When the damage caused by an impact event is negligible, and so is the energy required to cause it, the energy-balance includes only the energy amount spent for bending (E_b), shear (E_{sh}) and membrane (E_m) deformations and for indentation in the contact region (E_{cn}). The energy-balance is thus described by equation 2.36:

$$\frac{1}{2}m_1v^2 = E_b + E_{sh} + E_m + E_{cn} \tag{2.36}$$

where m_1 is the impacting mass and v its speed. Referring to the spring-mass model, the relation between contact force and deflection at impact point (w_b) equals to:

$$P = K_{bs}w_b + K_m w^3. \tag{2.37}$$

Therefore, the energy contributions for bending, shear and membrane effects can be expresses as:

$$E_b + E_{sh} + E_m = \frac{1}{2} K_{bs} w_{b\ max}^2 + \frac{1}{4} K_m w_{b\ max}^4. \tag{2.38}$$

In order to explicit the energy related to contact phenomenon, it is required a contact law, which expresses the relationship between the contact force and the indentation (α), defined as the relative displacement between the indentor and the target. A common contact law, often applied in impact problems, is the Meyer contact law, whose formulation is reported in equation 2.39:

$$P = K_c \alpha^n \tag{2.39}$$

where n is a non-dimensional parameter. Meyer's contact law refers to static contact conditions; therefore, its application to impact events is subjected to some limitations. In general, the impact response of sandwich panels is dependent on wave propagation effects, especially through the core thickness [47]. Nonetheless, it was demonstrated [48] that when the impactor mass is large, compared to the target panel, and when the impact velocities are low, compared to the wave velocity in the target medium, quasi-static approximations yield adequately accurate results. The energy absorbed in contact effects is obtained integrating Meyer contact law, between 0 and the maximum indentation (α_{max}), obtaining the following result:

$$E_{cn} = \int_0^{\alpha_{max}} P \, \mathrm{d}\alpha = \frac{P_{max}^{1+\frac{1}{n}}}{(n+1) K_c^{\frac{1}{n}}}. \tag{2.40}$$

Neglecting the membrane effects ($K_m = 0$) and combining equations 2.37, 2.38 and 2.40, the initial kinetic energy in equation 2.36 can be expressed

as:

$$\frac{1}{2}mv^2 = E_b + E_{sh} + E_{cn} = \frac{1}{2}\frac{P_{max}^2}{K_{bs}} + \frac{P_{max}^{1+\frac{1}{n}}}{(n+1)K_c^{\frac{1}{n}}}. \tag{2.41}$$

The energy balance model allow the evaluation of the maximum contact force, provided that the required structure properties are known.

2.3.4 Fatigue behaviour of sandwich structures

In numerous real applications, repetitive dynamic loads act on sandwich structures, which may lead to fatigue phenomena. Fatigue response and fatigue life prediction is a complex and troublesome subject even for traditional materials but it gets even more challenging for sandwich structures, where infinite combinations of skin and core materials are possible and numerous damage mechanisms may arise, interacting with each other and affecting in different ways the fatigue response.
Unlike other loading conditions, sandwich structures fatigue behaviour cannot be analysed with a standard procedure nor univocal fatigue life prediction is viable. Therefore, the issue of sandwich structure fatigue response will be examined by presenting some approaches applied in scientific literature, which cannot be exhaustive for all possible combinations and conditions but provide useful insight on the topic.

An overall review of the main approaches for the evaluation of fatigue behaviour of foam and honeycomb sandwich structures was provided by Sharma et al. [49], who highlighted that the majority of scientific works focus on fatigue response of laminates rather than sandwich structures. When it comes to all-metal sandwich structures, the fatigue-related scientific works are even fewer. A common approach to investigate fatigue life is based on S-N curves, which are derived from experimental tests. Kanny and Mahfuz [50] tested

sandwich panels with GFR skins and PVC foam core, under three-point fatigue bending. They fitted the experimental points with a logarithmic function, of the type:

$$\log \Delta\sigma = -\frac{1}{m} \log N + \frac{\log C}{m} \tag{2.42}$$

where $\Delta\sigma$ is the stress range and C and m are empirical constants. Thus the obtained expression can provide a prediction for fatigue life for sandwich panels and conditions similar to the investigated ones.

Burman and Zenkert [51] introduced another data-fitting method, based on a two parameter Weibull function. They investigated sandwich structures with polymeric (PVC and PMI) foam core and fibre-reinforced facings under four-point fatigue bending. They observed that the failure mode for the applied load was core shear and they expressed the fitting Weibull function in terms of shear stress, as follows:

$$\tau(N) = \tau_{th} + (\hat{\tau} - \tau_{th})\, \mathrm{e}^{-\log\left(\frac{N}{a}\right)^b} \tag{2.43}$$

where τ_{th} is the endurance limit, $\hat{\tau}$ is the static stress level, a and b are fitting parameters for the curve, obtained by a quadratic error minimisation procedure. As for the previous case, the Weibull function can be used for fatigue life evaluation, provided that the required structure parameters are known after an extensive experimental campaign.

The Weibull fitting function was applied by the same authors [52] also for undamaged and damaged sandwich panels made of Nomex honeycomb core and carbon fibre epoxy prepegs skins. In order to account for the defects presence, a static strength reduction factor was suggested.

The same approach was extended by Belingardi et al. [53] to sandwich panels with aluminium honeycomb core and carbon-fibre reinforced facings, subjected to four-point fatigue bending. They proved that Burman's [52]

method for fatigue life prediction of damaged specimens does not yield acceptable results. The main reason for this conclusion lies probably in the significant difference of collapse modes for non-defected and defected specimens.
This proves that theoretical considerations for sandwich structures cannot be easily generalised and need to be supported by experimental evidence.

Other procedures developed for sandwich structures fatigue life assessment, evaluate the strength or the stiffness degradation. For both methods, the evaluation of parameters involved in strength ad stiffness degradations is complex and requires to be calibrated for each structure type. In addition, stiffness degradation is not registered for all kinds of sandwich structures.

Another perspective on sandwich structures fatigue response was offered by Harte et al. [54], who analysed the fatigue strength of all-aluminium sandwich structures with foam core under four-point fatigue bending. For each failure mode experienced by specimens in the considered conditions, they adapted the known formulations for static collapse strength by replacing the static strength of core and facing with their endurance strengths. This approach allowed the identification of fatigue failure maps, which were in good accordance with experimental results and therefore provide an effective tool for sandwich design.

2.3.5 Failure modes of sandwich structures

A thorough knowledge of sandwich failure modes is required to properly design them, by a correct prediction of their strength, and to aid an intelligent selection of the constituent materials. Scientific literature has widely investigated sandwich structures collapse [55], [56], which is produced by the failure of one of their constitutive parts: skins, core or bonding layer. For each component, failure can occur with different modes, depending on

the boundary conditions and on the characteristics of the parts. The main failure modes for sandwich skins and core are summarised below.

- *Face yielding.* Skins can fail when the axial stress σ_x in one of the skins equals the in-plane strength σ_{fy} of the face material

$$\sigma_x = \sigma_{fy}. \tag{2.44}$$

  In three-point bending conditions, for instance, one of the skin is subjected to tension and the other to compression. Depending on the material, tension and compression may produce different risk level: e.g. for composite facings, compression is more critical whereas for metal skins, tension is more likely to produce the failure.

- *Face wrinkling.* A compression loading acting in the in-plane direction of one of the skins can produce a local buckling of the facings with a wavelength grater than the cell width, when the core has a cellular structure. Buckling deformation can be directed both in towards the core or outwards, depending on the bonding strength and on the core stiffness in compression. The simplest solution for the critical wrinkling stress, was derived by Allen [43], by modelling the facing as an infinitely long strut attached to an elastic foundation extended to infinity on one side of the strut.In similar conditions, the critical compressive stress for wrinkling σ_{fw} is:

$$\sigma_{fw} = \frac{3}{[12(3-\nu_{cxz})^2(1+\nu_{cxz})^2]^{\frac{1}{3}}} E_f^{\frac{1}{3}} E_3^{\frac{2}{3}} \tag{2.45}$$

  where ν_{cxz} is the out-of-plane Poisson's ratio of the core and E_3 is the out-of plane Young's modulus of the core.

- *Intra-cell dimpling.* When the core has a cellular structure, like a honeycomb, compression acting in-plane on the skins may result in

buckling where the facing is unsupported by the core cells walls. The critical in-plane stress in the skin for intra-cell dimpling σ_{fi} is:

$$\sigma_{fi} = \frac{2E_{fx}}{1-\nu_{fxy}^2}\left(\frac{2t}{s}\right)^2 \tag{2.46}$$

where ν_{fxy} is the Poisson's ratio of the skin in the axial direction and s is the core cell size.

- *Core shear.* One of the most common failure mode observed in sandwich structures is produced by shear in the core. As observed in section 2.3.1, in a sandwich beam subjected to three-point bending, the shear stress along the core thickness is constant, if the facings are significantly stiffer and thinner than the core. In this case, the mean shear τ_{cxz} stress in the core is expressed by equation 2.17. Core shear failure occurs when the applied stress τ_{cxz} equals the shear strength of the core τ_{cs}:

$$\tau_{cxz} = \tau_{cs} \tag{2.47}$$

- *Local indentation.* The action of a loading element with a small contact surface compared to the core thickness, may provoke the local indentation of the sandwich panel, after core crushing under the indenter. An empirical approach used to predict the failure for local indentation, assumes that, when the indenter is a cylinder, such as during a three-point bending test, the compressive stress in the core σ_z is the ratio between the applied load P and the contact length l. Consequently, the local indentation occurs when the compressive stress in the core equals the out-of-plane compressive strength σ_{cc} of the core:

$$\sigma_z = \sigma_{cc} \tag{2.48}$$

The described failure modes are schematised in Figure 2.11.

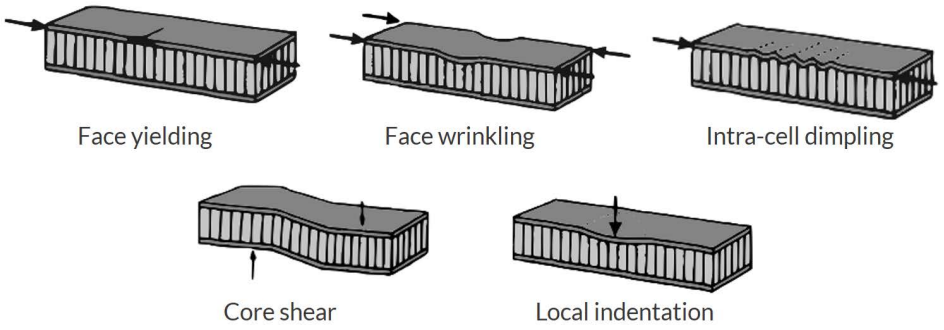

Figure 2.11. Sandwich structures failure modes [56].

2.4 Applications of sandwich structures

The demand for sandwich structures is increasing in all fields, due to the growing need of high-performance lightweight materials.

Sandwich structures were first used for military purposes during World War II: the Mosquito aircraft of the Royal Air Force is recognised as the first example of sandwich construction structural application [57], with the majority of its components made with plywood-based sandwich structures.

Since then, sandwich structures concept spread in all sectors: marine, automotive, railway, aeronautical, aerospace, buildings, energy production, packaging, furniture, are only some examples of fields which make large use of sandwich structures to cope with different requirements, ranging from weight reduction to temperature resistance, from acoustic insulation to chemical compatibility.

A general and exhaustive review of all possible sandwich structures applications lies outside the scope of the current thesis. On the other hand, an insight of lightweight sandwich structures applications in the marine field is

required to focus the main objective of the thesis and to give an overview of the state of the art.

2.4.1 Sandwich structures for marine applications

The marine field is one of the most promising for applications of innovative lightweight sandwich structures. Design of marine structures is often subjected to a double constraint: providing excellent structural performance and reducing weight. Lightness is an essential feature for marine structures and materials for several reasons [23], such as reduce fuel consumption and environmental emissions, increase the payload for a given ship size, increase the achievable speed or lighten the upper decks to reduce the centre of gravity and improve stability.
Numerous boats and ships components are eligible to be manufactured with sandwich panels; the most common are listed below, along with the main advantages that are achievable with a proper materials and configuration choice:

- deck: low weight, good bending, shear and compression strength;
- hull bottom: good impact and slamming resistance, fatigue and compression strength, high stiffness, corrosion resistance, fire resistance;
- hull side: low weight, impact and slamming resistance, high stiffness, good bending strength, corrosion resistance;
- superstructures: low weight, high stiffness, good compression and bending strength;
- interiors: low-weight, high stiffness, good compression and bending strength, good fire resistance.

Marine applications use all three main categories of sandwich structures: all-metal, composite and hybrid (see section 2.2). Some marine applications

for each of the three category will be presented in the following sections, with the aim of assessing the valuable role played by sandwich structures in the marine industry and the critical issues and improvements required to further promote their use.

2.4.1.1 Marine applications of composite sandwich structures

Historically, the main input for sandwich structures use in marine applications derived from the Royal Institute of Technology (KTH) in Stockholm, which, starting from the sixties, pioneered the research about sandwich structures, under the leadership of Karl-Axel Olsson [57].The efforts made at KTH led to the design and manufacturing of the first small Naval vessels based on fibreglass sandwich structures. Since then, composite sandwich structures gained a primary role in ship hulls building, especially for small vessels. The acquired know-how eventually led to the ground-breaking design and building of the 72 m long Visby class corvette [58] (see Figure 2.12) by the Swedish Navy, whose hull is entirely sandwich-based, with PVC foam core and carbon fibre reinforced facings.

The success of sandwich structures for military applications, conveyed their use for other types of marine constructions.

Composite sandwich structures have become probably the most common solution in the marine industry. Their main advantage lies in the possibility to be manufactured with complex geometries and shapes, which are required by most vessels parts. In addition, numerous manufacturing techniques are available, such as hand lay-up, resin transfer moulding, vacuum infusion or prepeg consolidation [4]: this makes their preparation feasible at different scale levels, from small boats to large vessels.

Composite sandwich structures are typically applied in numerous part of pleasure boats, which require lightness, high mechanical performance and

Figure 2.12. The Visby corvette of the Swedish Navy.

possibility to be easily manufactured with semi-handmade processes by small shipbuilders. Composite sandwich structures are used for decks, hulls, interiors, bulkheads, stringers, rudder, foils, canopies.

The use of composite sandwich structures for the deck and the reinforcing elements of a pleasure boat is reported in Ref. [59], which deals with sandwich structures made with PVC foam core and GFR facings. They compared the three-point bending properties of reinforcement elements bonded to the deck with two different joining techniques: a traditional over-lamination method and a structural methacrylate adhesive. They proved the mechanical reliability of structural adhesive, which offers additional advantages, such as time saving during production or easy refitting.

Indeed, one of the critical issue for composite sandwich structure in marine applications, regards the design and technology of joints, between sandwich parts or between a sandwich panel and a metal component. An example of the latter problem was investigated by Kharghani and Guedes Soares [60]. They evaluated the shear and bending performance of a balcony overhang, for cruise ships applications, composed of a steel support and a FRP-balsa sandwich panel, displayed in Figure 2.13.

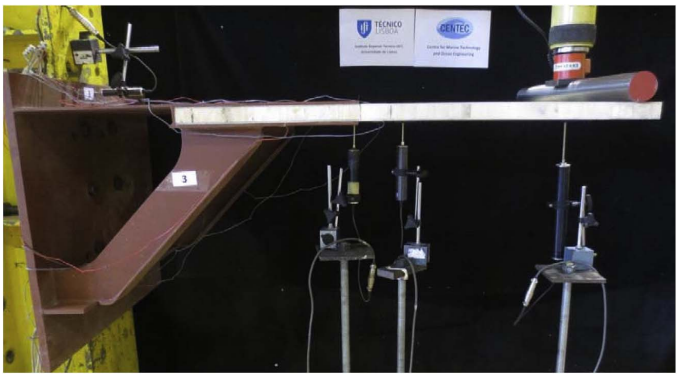

Figure 2.13. Balcony overhang made with a hybrid steel-composite sandwich configuration, reprinted from [60] with permission from Elsevier.

The adhesion between the steel frame, the facings and the core was obtained during the manufacturing process with vinylester resin. The stiffness mismatch between the metal and the composite part was addressed as one of the crucial points in the hybrid structure design. The experimental investigation demonstrated that under both bending and shear, the interface between the steel frame and the upper sandwich facings is the weakest section, causing core shear to happen earlier than steel yielding. The ultimate strength of the assembly was still significant, attesting the effectiveness of the hybrid steel-sandwich solutions, which can provide considerable weight savings.
The concept of a hybrid steel-composite sandwich assembly was developed also for an entire ship hull in Refs [61], [62] and [63]. In the cited papers, a 142 m ship hull was designed and a 6 m scaled model was manufactured in order to perform experimental analysis. A section of the scaled model, showing the steel frame with only one sandwich panel placed in the deck position, is displayed in Figure 2.14.
Bonding between steel trusses and sandwich panels was obtained with a

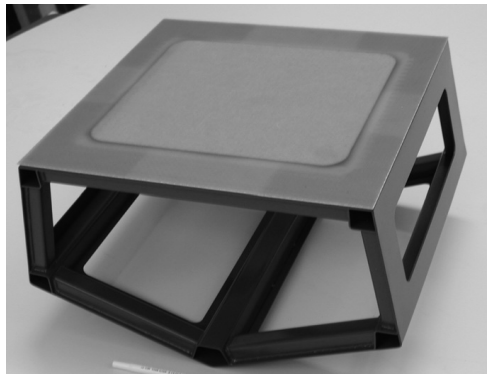

Figure 2.14. Section of the hybrid hull concept, reprinted from [62] with permission from Elsevier.

structural adhesive and with a peculiar shaping of both elements at the interfaces. Sagging and hogging conditions were investigated and the obtained results endorsed the possibility to successfully use a metal-sandwich hybrid concept for lightweight ship hulls.

Composite sandwich structures are also used for ships superstructures from the sixties. The main advantages for using composite sandwich solutions in ships superstructures are the corrosion resistance and the lightening of ships topside. A full replacement of a steel superstructure with a sandwich composite panels assemblies is reported to provide a weight saving of about 40% without significant cost construction increase [64], even though the costs are strongly dependent on the material selected for sandwich panels. The possible economical drawbacks during constructions due topside structures made with composite sandwich panels are becoming widely accepted, because of the potential costs savings during ships life [64], deriving from reduced repair and maintenance costs. A classic example of composite sandwich superstructure is offered by the La Fayette frigate of the French Navy, which was the first large warship to introduce the composite sandwich concept for part of its topside structure. The superstructure section made with sandwich panels

is 38 m long, 15 m wide and 6.5-8.5 m high [64] The sandwich panels for La Fayette frigate were made with GRP facings and balsa wood core and they were joined to a steel hull [65]. Another ship component often designed as a composite sandwich part is represented by mast. If compared to steel masts, the benefits of composite sandwich are: weight saving, corrosion resistance, fatigue strength, good damping properties, improved signature, possibility to embed within the sandwich structures the main antennas, sensors and electronic equipment improving their performance and reducing installation time. As for other parts, the connection between the composite sandwich part and adjacent metallic components, if present, needs to be carefully analysed. An experimental and numerical analysis of a similar problem was presented by Gaiotti et al. [66]. They investigated a hybrid connection between a composite mast and a steel deck, consisting of both bonding and bolted joints. They selected a representative portion of the connection to be subjected to full-scale tests, which is displayed in Figure 2.15 along with the 3D model of the mast and the joint area.

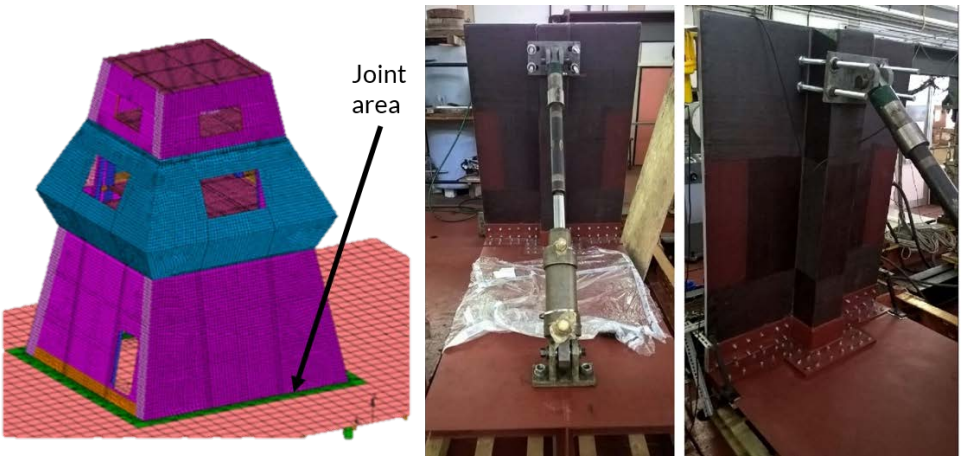

Figure 2.15. Hybrid joint area and large-scale experimental setup of ref.[66], reprinted with permission from Elsevier.

The sandwich wall consisted fibreglass-epoxy skins with a PVC core stiffened by carbon fibre-based elements with an omega shape. They found that numerical analysis allowed the prediction of the first structure failure, but it was not able to accurately predict the progressive collapse of the bolted-bonded joint. Therefore the importance of large-scale investigation was highlighted.

A major drawback in composite sandwich structures application is their disposal, which was thoroughly analysed by Summerscales et al. [67]. Most of the marine composite sandwich structures are based on thermoset matrix, which require a great effort to be treated, but difficulties arise also for thermoplastic composites. Separation of plies and fibres is not feasible for both cases and the main approach is to cut composite panels in order to be transferred to dedicated plants, where they are reduced in small parts. The processes required for composites grinding, fragmentation and crushing are expensive both economically and energetically. This is partly the result of fibres presence which makes the material tough. In addition, the fibres and the coatings often applied on the hulls surface further contaminate the materials, limiting their possible reuse. For thermoplastic composites, a possible recycling solution is the extrusion or injection of the granulated material, even though the residual fibres are source of abrasion and worsen the mechanical properties. Some methods for fibres recovery were also suggested, such as incineration, pyrolysis, catalytic degradation or acid digestion, but they all have some critical points and it is not always possible to treat all composites types in the same process. Therefore, the disposal of composites sandwich panel is still an open question and requires to be seriously considered starting from the design phase.

2.4.1.2 Marine applications of hybrid sandwich structures

Hybrid sandwich structures combine metallic and non-metallic constituents, in order to exploit the advantages of both material categories. Hybrid solu-

tions can be successfully exploited in marine structures, especially in parts such as decks or hulls where high mechanical properties are required together with large-scale manufacturing feasibility, but weight reduction is also essential. In addition, a combination of traditional metallic structures with polymeric or composite parts could improve the performance of existing structures in order to meet specific demands.

An example of mechanical improvement of a marine steel sandwich structure through a hybrid configurations is described by Romanoff et al. [68]. They observed that in I-core sandwich panels, where the core stiffeners are unidirectional, the shear stiffness orthotropy induce normal stresses in the facings and in the web plates which can become critical. As a result, they suggested to fill the core with a PVC foam, with the aim of improving the shear stiffness of the sandwich structure. They performed both experimental and numerical analysis, using foams of different densities. They proved that foam-filling results in reduced deflection, shear-induced normal stress in the facings and in the laser welds. The collapse mode under four-point bending changes from plastic hinge formation at laser-weld to filling foam shear failure and the residual strength increases. Moreover, the weight increase with foam filling was only between 6% and 15%.
A hybrid sandwich structure which is eligible for marine and offshore applications is the steel-concrete-steel (SCS) sandwich, which consists of a concrete core enclosed in two steel facings. The main advantages of similar structures lie in the possibility to avoid stiffeners and in cost savings, considering the comparison between shipbuilding grade steel and concrete. The bonding between the concrete core and the steel skins is crucial in order to make similar sandwich structures reliable. Apart from adhesives at the interfaces, some mechanical shear connectors are needed. Several solutions can be found literature, but for marine and offshore structures, the mechanical performances should meet also weight requirements, which, for SCS systems, are strongly

dependent on core thickness and weight. Grafton and Weitzenböck [69] selected two marine applications to compare the original steel structure with a SCS alternative: a deck of RoRo ship and a process deck for a floating production, storage and offloading unit (FPSO). The SCS structure considered in the evaluation consisted of a lightweight concrete core and two steel facings with vertical studs crossing the core, whose function is to provide an adequate stress distribution between the skins, avoid early failure of concrete under compression or shear loading and preventing facings wrinkling. For the RoRo ship scenario, two different configurations for SCS sandwich panels in the main deck were suggested, as visible in Figure 2.16.

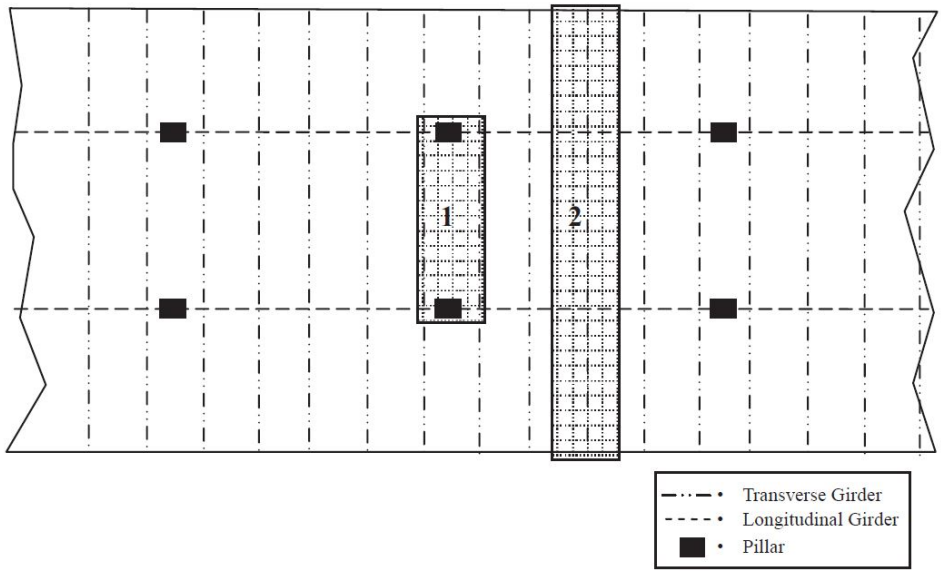

Figure 2.16. Possible configurations for SCS in a RoRo deck [69].

The main benefits of SCS use in a RoRo deck derive from elimination of stiffeners and some girders, decrease of deck depth, energy absorption improvements, reduction of welding time and easier maintenance. However, it

was estimated an increase in materials costs and weight. Thus, the suggested solution is not competitive for weight sensitive applications. For the FPSO process deck with SCS, economical advantages were detected, along with improved performance in case of explosion, thermal insulation and adaptability for equipment location. On the other hand, total weight increased.

The SCS weight issue was targeted by Sohel et al. [70], who suggested some innovative shear connectors, with the aim of reducing the weight of SCS sandwich structures and making them suitable for marine and offshore constructions. They analysed experimentally and numerically the mechanical response of SCS structures with J-hook and U connectors with interlinked cables, which are displayed in Figure 2.17.

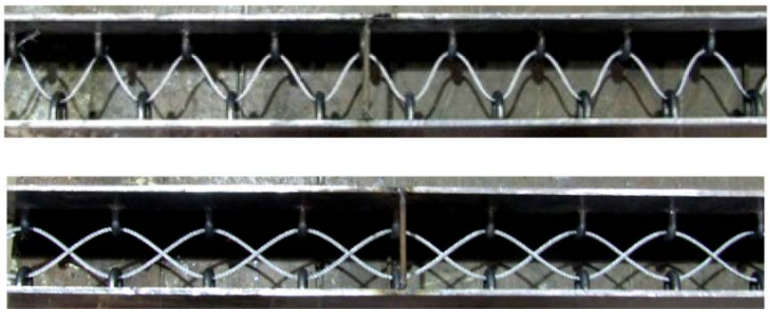

Figure 2.17. U connectors with interlinked cables tested in Ref. [70], reprinted with permission from Elsevier.

In addition, they evaluated the use of ultra-lightweight composite cement instead of lightweight aggregate, in order to improve the weight reduction potentialities of the structures. They concluded that the U cable connectors, increase the vertical shear strength and improve the interfacial bond between the facings and the core. In addition, the ultra-lightweight cement had similar ultimate strength than the lightweight aggregate.

The use of sandwich structures for RoRo decks was also investigated by Sujiatanti et al. [71]. They proposed a sandwich structure made of two steel facings and a synthetic resin core. The structural performance of the hybrid sandwich structure was investigated via numerical analysis, according to which the sandwich structure allowed a stress reduction in comparison to a traditional deck structure. In addition, a weight reduction of about 15% was estimated.

An optimal material combination in hybrid sandwich structures could offer solutions hardly feasible with a single material typology. This concept was adopted by Niklas and Kozak [72], who proposed a steel-concrete-polymer sandwich structure to be integrated in ship tank as a crashworthy barrier during grounding and collisions events. Their design consists in a sandwich made with a steel outer layer, which is the external surface of the ship, a lightweight concrete core and a hyperlastic polyurethane layer, whose aim is to keep water tightness preventing oil spills. Therefore, the intended applications are the bottom or the side shell of fuel tanks or other applications where water tightness is crucial. Their idea of the protective barrier is displayed in Figure 2.18.

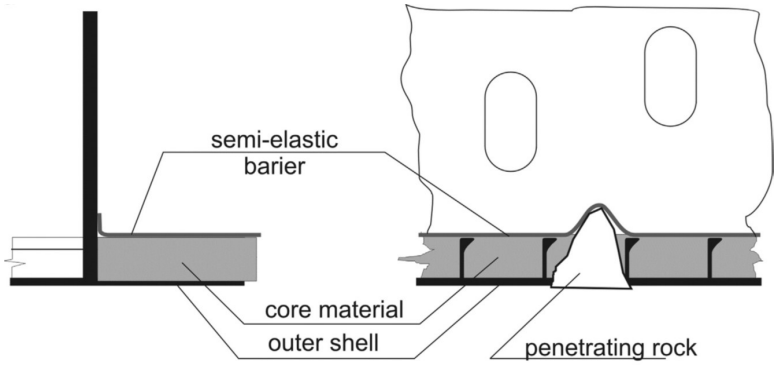

Figure 2.18. Sandwich barrier concept, reprinted from [72] with permission from Elsevier.

They performed both large-scale experimental investigations and numerical analysis. They experimentally demonstrated that the tightness was kept for a penetration depth up to 5 times higher than a standard steel construction. Indentation force and failure indentation depth for steel increased. The major drawback of their solutions was a significant weight increase (about 103%), which makes the design suitable only for offshore structures or ships where weight is not a critical issue.

2.4.1.3 Marine applications of all-metal sandwich structures

All-metal sandwich structures for marine applications are usually made of steel or aluminium alloys. The connection between facings and core is obtained via welding, mechanical joints, such as riveting, or adhesive bonding. In general, aluminium sandwich structures have good lightweight properties, are resistant to corrosion and to flames, but they are expensive. Steel sandwich structures are cheaper than aluminium ones but their weight saving is lower as well as their corrosion and fire resistance. All-metal sandwich structures guarantee a high accuracy level, since they are pre-manufactured in controlled environments, leading to improved quality, reduced working time at the shipyard and reduced production costs.

Some typical applications of all-metal sandwich structures are reviewed in Ref. [4]. Among those, it is worth mentioning the steel sandwich panels with the core made of a repetition of I-beams as unidirectional stiffeners, laser-welded to the facings. They are mainly applied as staircase landing in cruise ships, as deck houses or as ships deck. An example of their use in a deck is showed in Figure 2.19.
The same sandwich structure type was considered by Kortenoeven et al. [73] for possible applications superstructures of dredging ships. They performed

Figure 2.19. I-core™ deck, reproduced from [4].

a thorough feasibility analysis for different applications of steel I-core sandwich structures in dredging ships of different types. According to their preliminary evaluation concerning the application of steel sandwich panels for a superstructure, they observed that structural weight saving is significant only for large ships, but the production costs are reduced and steel building hours and throughput time are estimated to be reduced up to 50%. What is more, the flat surfaces of sandwich panels produce a decrease of insulation work costs up to 22%. In addition they observed that the full potential of sandwich structures advantages, in terms of mechanical performance, costs and weight, can be achieved only by modifying the design concept instead of proceeding with conventional structural design. They presented a comparison between traditional and sandwich-driven design approaches, which is summarised in Figure 2.20.

The evaluations in Ref. [73] pointed out also that sandwich structures undergo larger deflections than traditional structures but the stresses are reduced. Their evaluations lead to the manufacturing by IHD Dredgers of a real switch board room, of a 6000 m^3 trailing suction hopper dredger, based

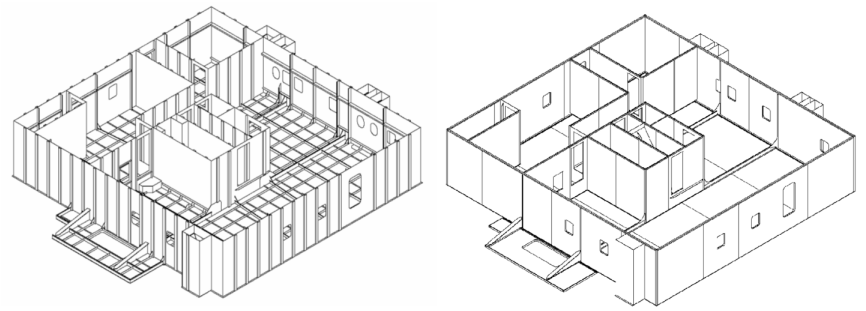

Figure 2.20. Comparison between conventional and sandwich-driven design approaches by [73].

on steel sandwich panels. According to the evaluations made in a preliminary phase and during the structure manufacturing, the total costs are reduced of 34%, the weight reduction is of 20% and the savings on production throughput time are equal to 71%.

All-metal sandwich structures can be successfully applied for RoRo decks, both fixed and hoistable, in order to save weight, increase volume and cargo load and simplify the manufacturing procedures. Ref [4] reports the application of a stainless steel sandwich structure for RoRo decks. The considered sandwich panel, shown in Figure 2.21 was developed by MacGregor Ltd and has the commercial name of COREX ™: it consists of steel facings and a core with trusses arranged in a pyramidal geometry.
Another all-metal sandwich structure analysed in Ref. [4] is the CORALDEC™, a sandwich panel entirely made of aluminium AA 5059 with a core shaped in a triangular-corrugated fashion, which is reported to be used in the mega yacht Athena, built by Royal Huisman shipyard in 2004.

The benefits of all-metal sandwich structures were analysed by Kujala and Klanac by means of a case study regarding the optimisation of a steel sand-

Figure 2.21. COREX™ RoRo deck, reproduced from [4].

wich hoistable car deck [40]. They consider two alternatives to replace the traditional structure with steel sandwich panels having I-beam core: a sandwich structure supported by a grillage or a sandwich structure with only C girder along the perimeter. The traditional design and the two alternative solutions are schematised in Figure 2.22. The authors used an optimisation procedure based on a genetic algorithm, whose constraints were the set according to the possible failure modes of the car deck elements. Two objective functions were considered separately: the weight and the production cost. The performed optimisation procedure was considered as an efficient alternative to numerical analysis in the preliminary design stage, in order to save time and encourage the evaluation of new design solutions. The obtained results showed that the variant with sandwich supported by the grillage offered the minimum possible weight, whereas the solution with the sandwich panel and the C girders was the cheapest.

One of the concerns for all-metal sandwich structures regards their production process and the possibility to join different metals, both within the sandwich structure itself and with other ship elements. The issue was addressed by Mueller and Volpone [74], which investigated the feasibility of manufacturing steel-aluminium sandwich panels, assembled with mixed laser welding

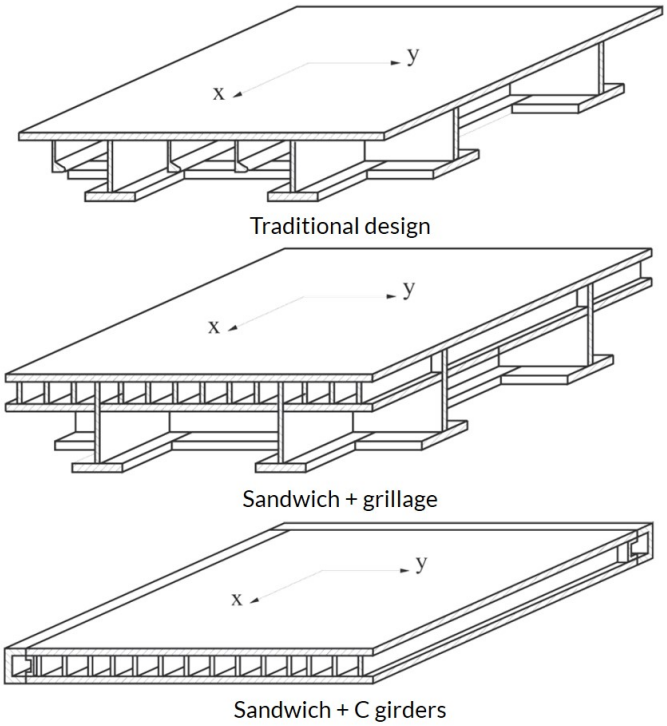

Figure 2.22. Traditional design of a hoistable car deck and two alternatives with steel sandwich structures suggested in Ref.[40].

and friction stir welding technology. The main advantage of an all-metal hybrid sandwich structure is to ensure the possibility to be connected to both steel and aluminium components. In the investigated structure, the core and one skin were made of steel, whereas for the other facing an aluminium alloy was used. They demonstrated the possibility to effectively manufacture an all-metal hybrid sandwich structure, opening up a path to new solutions for lightweight sandwich structures applications in marine industry.

Among all-metal sandwich structures, a special role is played by honeycomb sandwich structures. All-metal honeycomb sandwich panels are commonly

made with aluminium alloys, which improve their lightweight properties and make them suitable for high-performance applications. All-metal honeycomb sandwich structures are used in different marine applications, thanks to their exceptional strength to weight ratio. For example, in 1973 the first hydroplane to use aluminium honeycomb panels as structural elements for bulkheads, decks and the hull, was built by Pay 'n Pak [75]. The design solution was successful since the racing boat, shown in Figure 2.23, won several races, thanks also to its stiffness and lightness.

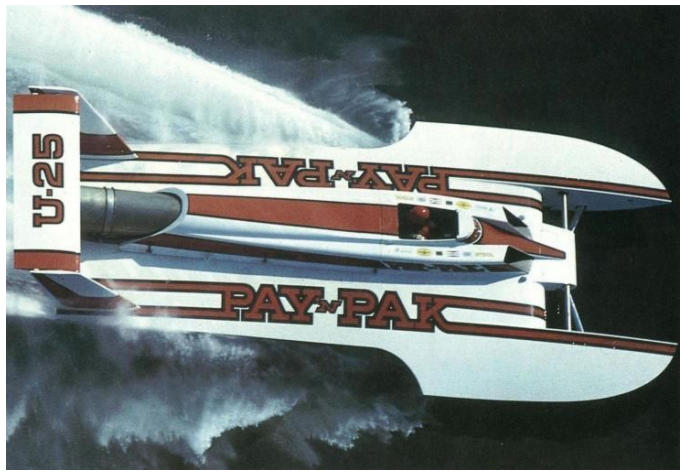

Figure 2.23. The first hydroplane by Pay 'n Pak to include aluminium honeycomb sandwich parts in its structure.

Sandwich panels with honeycomb core are also used for military ships bulkheads, to reduce ship weight above the waterline, hence improving the stability and manoeuvrability of the ship [76]. Honeycomb panels combine low weight with high stiffness and also with exceptional compression [18] and energy absorption properties [77]. Such features allowed honeycomb sandwich panels to be widely used for several structural and semi-structural elements of large ships, such as cruise ships, where weight reduction is a crucial issue.

The main elements of large ships that are commonly made with honeycomb sandwich structures are: decks, overheads, partition walls, dividers, berths, cabinets. A clarifying representation of actual honeycomb sandwich applications is shown in Figure 2.24, by Plascore Inc.® [15].

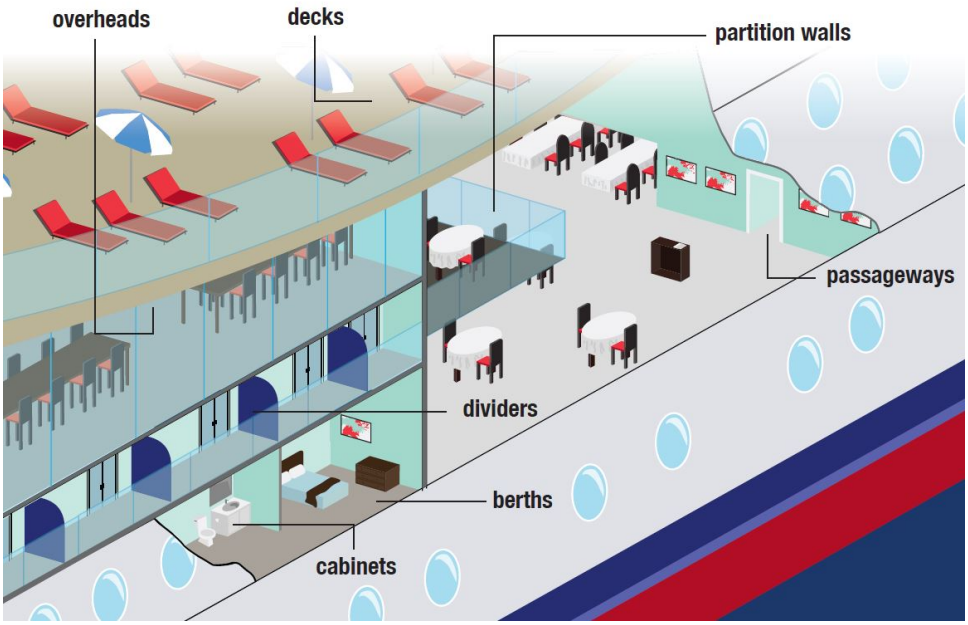

Figure 2.24. Aluminium honeycomb sandwich structures applications in large ships [15].

As visible from Figure 2.24, one of the advantage of aluminium honeycomb sandwich panels, is the possibility to be effectively applied not only for structural applications, but also for decorative elements: by applying an external layer with the desired aspect (wood, marble, textile, mirrors, etc.), it is possible to obtain aesthetically pleasant architectural elements with good mechanical and lightweight properties.

3

Aluminium honeycomb sandwich structures: a lightweight solution to discover

Honeycomb sandwich structures includes a central core made of a cellular material, whose cells resemble the honeycomb of the bees. Commonly, honeycomb structures have prismatic hexagonal cells, but other shapes are possible, such as squared or triangular cells. The main attractivenesses of honeycomb sandwich structures lie in their low density, which is a consequence of the core structure, in their energy absorbing capabilities and in their high stiffness to weight and strength to weight ratios, which make them suitable for structural applications where weight reduction is a primary concern, such as marine, aerospace, automotive or aeronautic industries [76].

A typical honeycomb structure consists of an array of hexagonal cells, whose geometry is characterised by the following parameters, shown in Figure 3.1:

- the cell wall lengths l and l_1;
- the angle between two cell walls θ, also known as expanding angle;
- the cell wall thickness f;
- the cell size which, for a regular hexagonal cell, is equal to the diameter of the inscribed circle s.

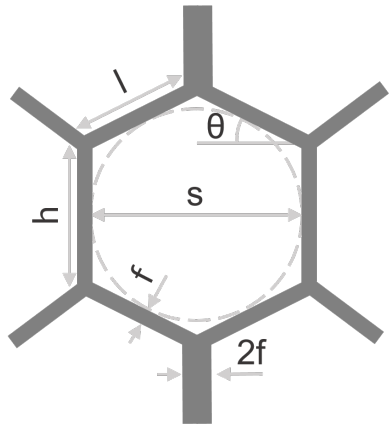

Figure 3.1. Honeycomb cell geometrical parameters.

Honeycomb sandwich structures are available in a wide range of materials, including aluminium, steel, aramid paper, carbon-fibre composites, polypropylene. The selection of sandwich structures base materials is strongly dependent on the final applications, and it is function of several aspects, such as the required mechanical performance, economical constraints, compatibility with surroundings structures and environment or technological limitations. However, concerns about materials sustainability are attracting the attention of customers and hence institutions and builders, even in the marine

field. These issues should be addressed right from the start of the design phase with an intelligent selection of materials, but which must also comply with the structural and weight constraints.
Almost exclusively, marine applications use fibre reinforced plastic (FRP) polymeric foam-cored sandwich structures, with some use of honeycomb cores in the high-performance/racing vessel sector of the industry. Further, a very high percentage of the FRP used in marine sandwich skins is glass reinforced polyester resin, commonly referred to as GFRP (glass fibre reinforced plastic). However, a major drawback of composite sandwich panels is the difficulty of disposing of them at end of life (and of the waste disposable products of the production process, e.g. vauum bags, breathers, peel-plies etc), as observed in section 2.4.1.1.

An attractive alternative to composites materials in marine applications is that of all-metal sandwich structures, and in particular that of aluminium sandwich structures with cellular cores. Aluminium is recognised as a sustainable and versatile material [25] due to its recyclability. In addition, aluminium recycling offers promising perspectives considering that the direct energy use in the production of recycled (secondary) aluminium is decreased by 93% in comparison to that required to produce primary aluminium [26].

A broader integration of aluminium sandwich components in marine structures requires a deeper knowledge of their mechanical response under complex loading conditions, reliable guidelines to support their design and effective procedures for their selection, and comparisons with better-known "traditional" alternatives. In this scenario, research plays a primary role both in improving the experimental and theoretical knowledge, and in organising the available data into practical tools for design purposes.

An overall description of the mechanics of honeycombs was provided by Gibson and Ashby [55] in their pioneering work on cellular structures. Several other studies in the last few decades have thoroughly investigated the main

aspects of honeycomb mechanics, such as out-of-plane compression [18, 78–80], in-plane compression [78, 81–83], bending [81, 84–87] and shear [88–91].

More critical loading conditions occur when dynamic events are considered. However, the designation "dynamic" can be referred to two different conditions:

- a single highly dynamic event, such as an impact;
- a cyclic loading which repeats over time, also referenced as fatigue loading.

Both conditions need to be thoroughly investigated, since they can be responsible for sudden failures difficult to predict or for severe damage which can compromise a structure functionality. In the case of marine structures design, both aspects are of great importance and their relevance is even higher when referred to sandwich structures. Indeed, being sandwich structures used only for limited applications in the marine industry at present, their response to the most critical conditions require to be carefully analysed, in order to provide designers with valuable information and data.

In view of the above considerations, the current chapter is focused on the investigation of low-velocity impact and fatigue response of aluminium honeycomb sandwich structures, with the aim of analysing the main aspects involved in their response to the considered dynamic conditions and of providing useful information for design purposes. The obtained results were published in two scientific papers [92, 93].

3.1 Honeycomb sandwich panels under impact loading

One of the peculiarity of honeycomb structures is their high energy absorption capability [94], especially when load is applied in the out-of- plane

direction, since this loading condition produces the buckling of the cells walls [55], which is a collapse mode able to absorb large amount of energy. The impact response of honeycomb sandwich structures was described by Abrate [45] with an energy-balance-model, according to which the energy of the impacting mass equates the energy spent in shear, bending and contact phenomena. The applicability of this theoretical model was verified in several studies [77, 95–99]. The parameters involved in the energy balance model are commonly determined in literature from quasi-static indentation tests, but an alternative measurement procedure which uses tomographic images to obtain the desired information directly from the impacted specimens was developed by Crupi et al.[95–98].

In recent years, the necessity to improve energy absorption cap- abilities of honeycomb sandwich structures has led to the design and the analysis of some multi-layer honeycomb structures. Yasui [100] experimentally investigated the quasi-static and dynamic crushing behaviour of multi-layer honeycomb sandwich structures, with layers arranged both in a uniform and in a pyramidal way. It was found that the pyramidal assemblies had a higher energy absorption capability. Fazilati and Alisadeghi [101] performed a crashworthiness optimisation of multi-layer honeycomb energy absorbers with a genetic algorithm. The optimised multi-layer configurations, if compared to a mono-layer sandwich with equivalent volume, height and cell characteristics, are able to damp the shock levels and reduce the stopping distance of the impacting mass. Wang et al. [102] investigated the axial response of tandem honeycombs constituted by three honeycomb layers and two separators, with various cell dimensions and core arrangements. They found that tandem structures yield a more stable force-compression history and that different core arrangements influence the collapsing order. Single and multi-layer corrugated sandwich panels were studied by Cao et al. [103] with a large-scale impact Hopkinson bar. They investigated different layer

orientations and found that the configuration with parallel layers enhances the energy absorbing capabilities of the structure, as a result of the inter-layer bending. A crucial point in multi-layer sandwich structures design is the core arrangement, which has a considerable influence on the deformation mode of the composite structure, as demonstrated by Shiqiang et al. [104] in a study on sandwich panels with triple layered graded aluminium honeycomb cores under blast loading. They observed that if the first core layer has a smaller cell dimension, the deformation mode tends to be a localised failure. Kılıçaslan et al. [105] investigated the deformation mechanism of single and double-layer aluminium corrugated-core sandwich under quasi-static and dynamic loadings, considering also the effect of fin imperfections. They conducted both experimental and numerical analysis and found that loading rate influences the deformation mechanism and the sensitivity to fin imperfections. In particular, for the double-layer structures they observed that the deformation mode changes from shearing of interlayer sheet to fin buckling when loading rate is increased.

As evidenced by the literature review above, an effective design of honeycomb energy absorbers requires extensive knowledge of their mechanical response under impact loading conditions. Therefore, the starting point of the analysis on aluminium honeycomb sandwich structures was the experimental investigation of their low-velocity impact response.

3.1.1 Investigation on single and double-layer honeycomb sandwich structures

Single and double-layer aluminium honeycomb sandwich panels were analysed under low-velocity impact conditions. Double-layer aluminium honeycomb sandwich structures were assembled arranging two types of mono-layer sandwich panels in four different ways.
The low-velocity impact response of both mono-layer and double-layer struc-

tures was evaluated experimentally.
The mono-layer experimental results were applied to the energy-balance model and the obtained parameters were compared to previous studies conducted both on small-scale [95] and large-scale [106] panels. The comparison allowed the preliminary identification of a size effect for the definition of the impact parameters. The performance of mono-layer and double-layer honeycomb sandwich structures was compared to other structures reported in literature, in order to verify the advantage of multi-layer assembly for energy absorption purposes.
Six different aluminium honeycomb sandwich structures were tested:

- Type 1: single-layer honeycomb sandwich with hexagonal cells of 3 mm diameter;
- Type 2: single-layer honeycomb sandwich with hexagonal cells of 6 mm diameter;
- Type 3: double-layer honeycomb sandwich structure, made of two layers of Type 1 sandwich;
- Type 4: double-layer honeycomb sandwich structure, made of two layers of Type 2 sandwich;
- Type 5: hybrid double-layer honeycomb sandwich structure, whose upper layer is made of Type 1 sandwich and the bottom layer is made of Type 2 sandwich;
- Type 6: hybrid double-layer honeycomb sandwich structure, whose upper layer is made of Type 2 sandwich and the bottom layer is made of Type 1 sandwich.

Type 5 and Type 6 structures are equivalent, but they differ for the layer arrangement during the low-velocity impact tests. The main characteristics of the tested structures are summarised in Table 3.1.

Table 3.1. Characteristics of the investigated honeycomb structures

	Type 1	**Type 2**	**Type 3**	**Type 4**	**Type 5 and 6**
Material designation	1/8-5052-0.002	1/4-5052-0.0025	Double-layer of 1/8-5052-0.002	Double-layer of 1/4-5052-0.0025	Double-layer of 1/8-5052-0.002 + 1/4-5052-0.0025
Cell diameter (s) [mm]	3	6	3	6	3 and 6
Core thickness (c) [mm]	9	9	9+9	9+9	9+9
Facesheet thickness (t) [mm]	1	1	1	1	1
Foil thickness (f) [mm]	0.05	0.06	0.05	0.06	0.050 and 0.060
Core alloy	AA5052	AA5052	AA5052	AA5052	AA5052
Skin alloy	AA5754-H32	AA5754-H32	AA5754-H32	AA5754-H32	AA5754-H32
Honeycomb density (ρ_c) [kg/m^3]	130	80	130	80	130 and 80
Average sandwich density (ρ_p) [kg/m^3]	654	579	666	639	727
Adhesive between core and skin	Epoxy resin	Epoxy resin	Epoxy resin	Epoxy resin	Epoxy resin

The transversal section of the tested sandwich structures are shown in Figure 3.2

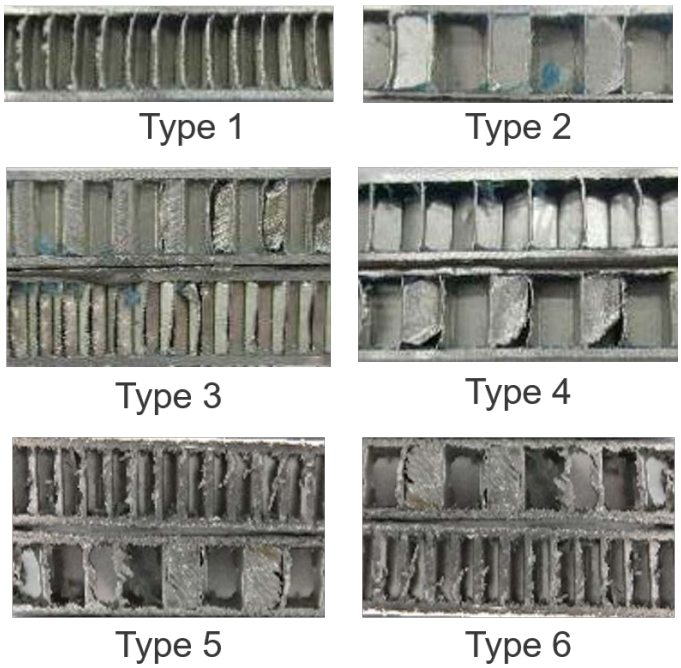

Figure 3.2. Tested sandwich structures.

The double-layered structures were assembled by bonding two single-layer sandwich panels with a commercial bi-component epoxy adhesive.

The low-velocity tests were performed with a Ceast Fractovis Plus drop test machine, equipped with a system for the elimination of multiple impacts. Impact energy can be varied by adjusting the impactor mass and the drop height. The machine is provided with a spring system, which is automatically activated when the tower height is insufficient to obtain the requested potential energy.

The impactor used for the tests has a hemispherical tip with a diameter di equal to 20 mm and it hits the centre of the specimen. The tests were performed with an impacting mass of 6.5 kg and different impact energies ranging from 14 to 265 J. The impact velocity ranged from 2.08 to 9.03 m/s. The specimens were simply supported on a rigid metallic ring with an internal diameter of 40 mm and an external diameter of 95 mm.
Some impact tests were recorded with a synchronised Phantom V711 high speed camera at 6000 fps, with the aim of correlating the load trend to the striker location in the specimens.

The impacted specimens were analysed with a 3D Computed Tomography System Y.CT Vario, which provides a three-dimensional reconstruction of the object. The tomographic models were used to detect and measure the damaged area, which is often not visible externally, without altering the tested objects. Such non-destructive measurements were useful to obtain the parameters involved in the energy-balance model. The inspection of the tested materials was conducted with 250 µm focal spot size, with the X-ray tube set at a voltage of 190 kV and a current of 1 mA. The sample rotation of 2π advanced with steps of 0.0087 rad/s. The total projections acquired and used for 3D reconstruction were 1440. The voxels have cubic shape with edge length of about 0.05 mm and the image size is 1088×1088 pixels. The integration time was equal to 250 ms. A copper filter with thickness equal to 0.5 mm was applied to the source. The parameters chosen for the analysis are the result of a balance between good quality of the images and reasonable scan and reconstruction time.

3.1.1.1 Low velocity impact tests

All the investigated sandwich structures were subjected to low-velocity impact tests. Table 3.2 reports specimens geometrical characteristics, testing

parameters and the results of the experimental tests in terms of contact peak force and entity of damage. When the test performed were more than one, the results refer to the average value.

Table 3.2. Performed tests and results.

Sandwich structure type	**Impact energy [J]**	**Impact velocity [m/s]**	**Specimen dimensions [mm]**	**Number of tests**	**Peak Force [N]**	**Damage**
1	14	2.08	75×50×11	1	5261	Indentation
	32	3.14	75×50×11	1	7895	Indentation
	56	4.15	75×50×11	1	10306	Indentation
	81	5	75×50×11	1	11319	Upper skin fracture
	117	6	60×60×11	1	10979	Perforation
2	14	2.08	100×100×11	1	4875	Indentation
	32	3.14	100×100×11	1	7193	Indentation
	56	4.15	100×100×11	1	9282	Indentation
	81	5	100×100×11	2	10002	Upper skin fracture
	117	6	100×100×11	2	8284	Complete penetration
3	14	2.08	60×60×22	1	5683	Indentation
	32	3.14	60×60×22	1	8433	Indentation
	56	4.15	60×60×22	3	11602	Upper skin fracture
	81	5	60×60×22	2	12577	Damage progression in bottom layer
	117	6	60×60×22	1	14216	Damage progression in bottom layer
	159	7	60×60×22	1	15368	Upper core detachment
	210	8.04	60×60×22	4	15878	Intermediate skins failure
	265	9.03	60×60×22	1	17077	Perforation

Continued on next page

Sandwich structure type	Impact energy [J]	Impact velocity [m/s]	Specimen dimensions [mm]	Number of tests	Peak Force [N]	Damage
4	14	2.08	60×60×22	1	4770	Indentation
	32	3.14	60×60×22	1	7450	Indentation
	56	4.15	60×60×22	1	9896	Upper skin fracture
	81	5	60×60×22	2	9542	Damage progression in bottom layer
	117	6	60×60×22	1	11968	Damage progression in bottom layer
	159	7	60×60×22	1	12946	Upper core detachment
	210	8.04	60×60×22	1	14982	Intermediate skins failure
	265	9.03	60×60×22	1	17411	Perforation
5	14	2.08	60×60×22	1	5648	Indentation
	32	3.14	60×60×22	1	8363	Indentation
	56	4.15	60×60×22	1	10090	Upper skin fracture
	81	5	60×60×22	1	11079	Damage progression in bottom layer
	117	6	60×60×22	1	11120	Damage progression in bottom layer
	159	7	60×60×22	1	12489	Upper core detachment
	210	8.04	60×60×22	1	16545	Intermediate skins failure
	265	9.03	60×60×22	1	15837	Perforation

Continued on next page

Sandwich structure type	**Impact energy [J]**	**Impact velocity [m/s]**	**Specimen dimensions [mm]**	**Number of tests**	**Peak Force [N]**	**Damage**
6	14	2.08	60×60×22	1	4811	Indentation
	32	3.14	60×60×22	1	7977	Indentation
	56	4.15	60×60×22	1	11161	Upper skin fracture + damage initiation in bottom layer
	81	5	60×60×22	1	10505	Damage progression in bottom layer
	117	6	60×60×22	1	13156	Damage progression in bottom layer
	159	7	60×60×22	1	15685	Intermediate skins failure+ Upper core detachment
	210	8.04	60×60 x× 22	2	16044	Global damage progression
	265	9.03	60×60×22	1	16287	Complete penetration

The entity of damage, described in 3.2 was deduced both from visual inspection and from CT images. The term *perforation* refers to the striker piercing the sandwich structure and causing a fracture on the bottom skin, without the complete passage through the bottom skin; the definition of *complete penetration* applies to the cases in which the striker pierces the whole sandwich structure, including the bottom skin. Sandwich structures Type 1, 3, 4 and 5 experienced perforation at the maximum impact energy, with visible cracks on specimens back face. For sandwich structures Type 2 and 6, the maximum impact energy applied during the tests, generated the complete penetration of the panels.

For the Type 2 structure, larger specimens were preferred because smaller specimens experienced a significant deformation under high impact energies,

which do not allow a correct evaluation of the out-of-plane deformation.

The effect of the number of cells in the exposed area and the effect of specimens dimensions were investigated.

In order to analyse the effect of specimens dimensions, low velocity impact tests were performed on Type 1 and Type 2 specimens with dimensions equal to 60×60×11 mm. The effect of the number of cells included within the internal diameter of the supporting ring was also investigated. A different supporting ring with an internal diameter of 125 mm and an external diameter of 160 mm was used. Specimens of Type 2 structure with dimensions equal to 160×160×11 mm were subjected to low velocity impact tests in a simply supported configuration on the larger supporting ring. The specimens with different dimension and the different supporting rings are shown in Figure 3.3.

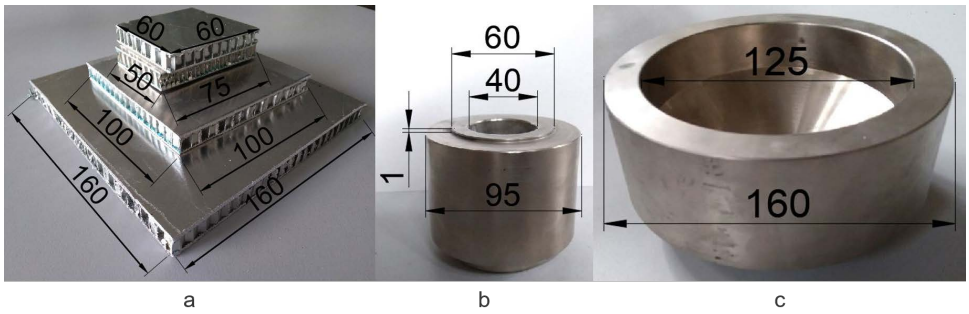

Figure 3.3. a) Different specimen dimensions; b) smaller supporting ring; c) larger supporting ring.

The results of impact tests performed with different specimen size and with different supporting ring are compared in Table 3.3.

According to the results reported in Table 3.3, specimen geometry does not significantly influence test results.

Table 3.3. Results of the impact tests performed to verify the influence of specimen geometry and supporting ring dimensions.

Sandwich structure type	Specimen dimensions [mm]	Support internal diameter [mm]	Impact energy [J]	Peak Force [N]	Number of tests	Damage
1	75×50×11	40	32	7895	1	Indentation
			56	10306	1	Indentation
			56	10306	1	Indentation
			81	11319	1	Upper skin fracture
1	60 x 60 x 11	40	32	7930	1	Indentation
			56	10323	1	Indentation
			81	11704	1	Upper skin fracture
2	100 x 100 x11	40	32	7193	1	Indentation
			56	9282	1	Indentation
			81	10002	2	Upper skin fracture
2	60 x 60 x 11	40	32	6735	2	Indentation
			56	8737	2	Indentation
			81	10616	2	Upper skin fracture
2	160 x 160 x11	125	32	6250	1	Indentation
			56	7902	2	Indentation
			81	9595	1	Indentation

For what concerns the effect of the supporting ring dimension, the obtained results show a slight reduction in the peak force, which may be the consequence of the larger number of cells free to deform in the out-of-plane direction, but also of the lower area sustained by the ring. Indeed, the considered configuration affect specimens stiffness which is directly correlated to the peak force.

The load-displacements curves for all the sandwich typologies described in Table 3 at different impact energies are shown in Figure 3.4.

The load-displacements curves show an initial linear trend whose slope is independent from the impact energy, but is distinctive of each structure.

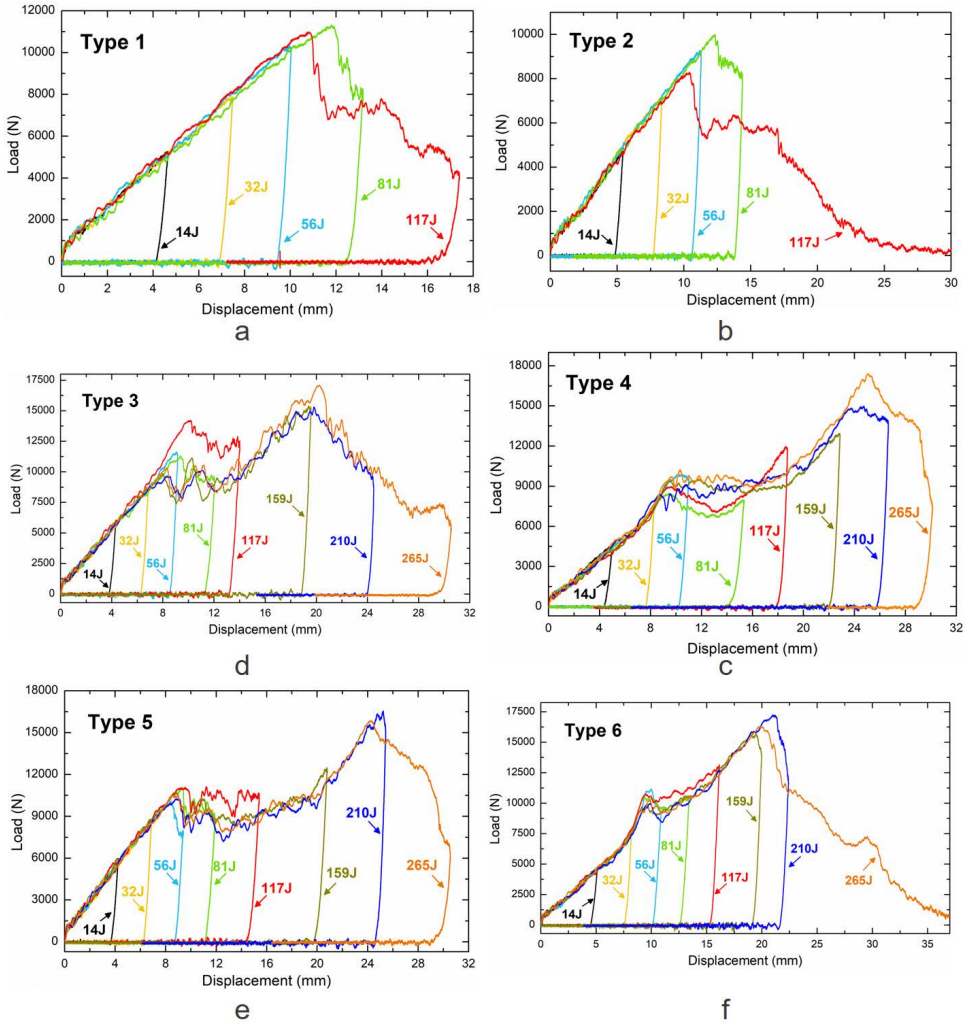

Figure 3.4. Load-displacement curves for Type a)1, b)2, c)3, d)4, e)5 and f)6 sandwich panels.

The same behaviour was observed in previous studies performed on the same single layer materials, but on clamped specimens instead of simply supported [95].

The curves for both single-layer and double-layer sandwich structures show a single load peak for impact energy within 56 J. The load-displacement curves for higher impact energies present two or three load peaks. In order to understand the source of different load peaks, some impact tests were recorded with a synchronised high speed camera (Phantom V711) at 6000 fps. The captured frames were compared with the load-displacement curves with the aim of verifying the position of the impactor when the peaks are registered. Figure 3.5 reports the load-displacement curve for a Type 3 specimen impacted at 210 J with the frames corresponding to the load peaks. Geometrical and dimensional references on the striker allowed the recognition of its location inside the specimen.

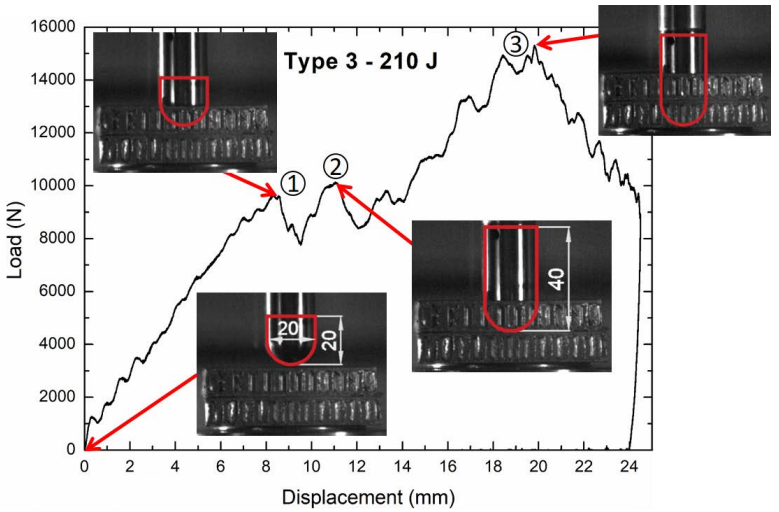

Figure 3.5. Frames from high speed video of the impact event corresponding to load peaks for a Type 3 specimen tested at 210 J.

The images acquired with the high speed camera led to the identification of

the following phenomena during the impact event:

- load increases linearly with the displacement, with some local peaks which can be correlated to progressive buckling of core walls, until the striker reaches a penetration of about 8 mm, corresponding to the load peak 1;
- a sudden load fall is registered, which may be dependent on the upper skin fracture and the subsequent resistance reduction to the striker penetration;
- shortly afterwards, the impacting mass contacts the intermediate skins and load peak 2 is registered;
- as the striker continues the penetration, load has a short fall and then increases; some local peaks, resulting from buckling of core walls, are registered;
- when the striker hits the lower skin, load peak 3 is registered;
- the striker causes an out-of-plane deformation of the lower skin until the whole impact energy is absorbed; if the impact energy is sufficient, the striker could induce perforation or complete penetration of the structure.

The highest peak force at the maximum impact energy considered in the study (265 J) was recorded for the double-layer hybrid structures with the larger cell size in both layers (Type 4). Some curves have at the highest impact energy a lower peak load, in comparison to the previous impact energy, even though the striker did not cause complete penetration but only perforation. This can be explained considering that the effect of skin fracture on the peak force is comparable to those of complete penetration, since after the fracture the sandwich is no more able to bear load.

The different impact behaviour of the tested materials, which results in different load-displacement curves, is deducible from the visual inspection of the impacted specimens. The top, later and bottom views of some damaged specimens, of all the typologies, are reported in Figure 3.6.

Figure 3.6. Lateral, top and bottom views of impacted specimens.

As visible in Figure 3.6, the perforation, or the complete penetration, of each sandwich structure occurred at different impact energies. According to the results reported in Table 3.2, the impact energy required to produce the perforation or the complete penetration of the sandwich structures is between 81 J and 117 J for monolayer sandwich panels and between 210 J and 265 J for double-layer and hybrid structures.

The inspection of the impacted double-layer specimens provides evidence of a different absorbing-energy mechanism depending on the cell size and on core arrangement.

For double-layer structures with the smaller cell size (Type 3) in the upper core the damaged area is strongly localised around the impacting objects, assuming an aspect similar to that obtained with static indentation tests or with clamped conditions. In the double-layer sandwich panels Type 4 the damaged area is wider, especially for lower energies. In both cases, an increase in impact energy and velocity leads to a localisation of the deformed area.

In double-layer Type 3, impact energy is mainly absorbed by the local collapse of the cells in the first layer in the area corresponding to the impacting object, whereas the second-layer cells are not involved in the energy absorption, except for high energies, which cause sandwich penetration. Double-layer structure Type 4, shows a differential energy absorption mechanism between the two layers. The upper layer undergoes a deformation similar to that observed for the single-layer structure, with a significant indentation and an extended damaged zone. The bottom layer acts as an energy absorber subjected to a crash: it is possible to observe an almost uniform buckling of all the cells, not only in the impacted area, which allows a significant energy absorption and avoids an excessive out-of-plane deformation. The detected behaviour proves that impact energy is transmitted across the first layer and distributed, through the two bonded skins, to the second layer in a uniform way.

The deformation mechanism of the hybrid structures is different depending on the side exposed to the impactor. The specimens with the bigger cell size in the upper layer (Type 6) are subjected to a localised damage in the impact area, similarly to the structure Type 3. The specimens with the bigger cell size in the lower layer (Type 5), exhibit a differential deformation mechanism between the two layers: in the upper one the damage is limited to the impact area, whereas the lower one is almost uniformly crushed, as observed for Type 4 sandwich panels.

Similar failure modes were observed by Cao et al. [103] in a multilayer structure with corrugated core sandwich panels, even though they performed the test with a direct impact Hopkinson bar.

The collapse sequence among the layers, is influenced also by the geometry of the multi-layer structures, as reported in Ref. [100], where a three-layer uniform honeycomb sandwich structure was compared to a three-layer pyramid structure. In the uniform structure, the first layer to collapse was the top one, followed by the bottom layer and at the end the middle one; for the pyramid structure, the collapse occurred with regularity from the top panel to the bottom panel.

The effect of the honeycomb cell dimension on the localisation of the damage, observed in the present study, is in good agreement with the conclusion of Shiqiang et al. [104], although the test conditions are completely different.

The different energy absorption mechanisms between the layers, suggest that multilayer honeycomb sandwich structures may be designed in order to have convenient deformations among the layers and prevent damage to structures or people, in different fields of application.

3.1.1.2 Comparison on Specific Absorbed Energy

The total energy absorption (TEA) is the amount of energy absorbed by the structure during the impact. The TEA is equal to the area under the

force-displacement curve, according to equation 3.1:

$$TEA = \int P \, \mathrm{d}s. \tag{3.1}$$

Specimens which do not undergo a complete failure, absorb all the impact energy: as a result, they have a TEA equal to the impact energy set for the test. The specific energy absorption (SEA) is calculated by dividing the TEA for the density ρ_p of each specimen (reported in Table 3.1), as described in equation 3.2:

$$SEA = \frac{\int P \, \mathrm{d}s}{\rho_p}. \tag{3.2}$$

The energy required for the complete failure (perforation or complete penetration) of the sandwich panels (which is equal to 117 J for mono-layer structures and 265 J for double-layer structures) was not considered in the evaluation of the SEA.

In order to evaluate the effectiveness of the investigated structures in terms of energy absorption capabilities, the values of the maximum specific energies which do not cause the complete failure of the structures, were compared to the maximum specific energy absorption of other structures reported in literature. The structures included in the comparison are described in Table 3.4.

Table 3.4. Structures considered in the SEA comparison.

Structure description	**Ref.**	**Specimens dimensions [mm]**	**Test type and conditions**	**Max. impact energy [J]**	**Max. impact velocity [m/s]**	**Density [kg/m^3]**
Aluminium foam sandwich panels (AFS Alulight) with skins bonded to the core with an epoxy adhesive	[96]	60×60×11	Low-velocity impact test; clamped configuration; hemispherical indenter	127	6	906
Aluminium foam sandwich panels (AFS Schunk) with integral skins	[96]	60×60×11	Low-velocity impact test; clamped configuration; hemispherical indenter	88	5	674
AFS Alulight with skins reinforced by glass fibre reinforced epoxy matrix (GFR-AFS Alulight)	[97]	75×50×17.5	Low-velocity impact test; clamped configuration; hemispherical indenter	225	8	1066
AFS Schunk with skins reinforced by glass fibre reinforced epoxy matrix (GFR-AFS Schunk)	[97]	75×50×17.5	Low-velocity impact test; clamped configuration; hemispherical indenter	225	8	1032

Continued on next page

Structure description	**Ref.**	**Specimens dimensions [mm]**	**Test type and conditions**	**Max. impact energy [J]**	**Max. impact velocity [m/s]**	**Density [kg/m^3]**
Aluminium honeycomb sandwich structures of Type 1 tested in clamped conditions (AHS T1 clamped)	[96]	60×60×11	Low-velocity impact test; clamped configuration; hemispherical indenter	88	5	674
Aluminium honeycomb sandwich structures of Type 2 tested in clamped conditions (AHS T2 clamped)	[96]	60×60×11	Low-velocity impact test; clamped configuration; hemispherical indenter	88	5	639
AHS Type1 with skins reinforced by glass fibre reinforced epoxy matrix (GFR-AHS T1)	[98]	75×50×17.5	Low-velocity impact test; clamped configuration; hemispherical indenter	225	8	926
AHS Type2 with skins reinforced by glass fibre reinforced epoxy matrix (GFR-AHS T2)	[98]	75×50×17.5	Low-velocity impact test; clamped configuration; hemispherical indenter	285	9	910
Single-layer corrugated aluminium sandwich (CAS)	[103]	55×55×12	Direct impact Hopkinson bar test	N.A	9	N.A.

Continued on next page

Structure description	**Ref.**	**Specimens dimensions [mm]**	**Test type and conditions**	**Max. impact energy [J]**	**Max. impact velocity [m/s]**	**Density [kg/m^3]**
Four-layer corrugated aluminium sandwich structures (4L-CAS)	[103]	55×55×45.5	Direct impact Hopkinson bar test	N.A.	9	N.A.
Seven-layer trapezoidal corrugated aluminium sandwich structures, with 0°/0° oriented fins (7L-TCAS 0°/0°)	[107]	100×100×70	Low-velocity impact test; clamped configuration; hemispherical indenter	284	6	370
Seven-layer trapezoidal corrugated aluminium sandwich structures, with 0°/90° oriented fins (7L-TCAS 0°/90°)	[107]	100×100×70	Low-velocity impact test; clamped configuration; hemispherical indenter	284	6	370
Bio-inspired aluminium honeycomb sandwich structures with CFRP panels (AH-CFRP)	[108]	80×80×21.2	Low-velocity impact test; clamped configuration; hemispherical indenter	27	1.6	N.A.
Sandwich structures with glass fibre reinforced plastic (GFRP) skins and Ti64 body centred cubic (BCC) micro lattice cores (GFRP-BCC)	[109]	52.5×52.5×9.5	Low-velocity impact test; simply supported configuration; hemispherical indenter	81	5	825

The structures studied in Ref. [103] are tested with a direct Hopkinson bar, in complete different conditions from those applied for the current investigation. Nevertheless, they are considered in the comparison in order to include information about multi-layer sandwich structures, which are rarely reported in literature. The structures in Ref. [107] were not tested until complete penetration, as a result the reported SEA is intended to be useful for comparing the energy absorption capabilities at similar impact energies. The results of the comparison are reported in Table 3.5.

Table 3.5. Comparison of maximum SEA.

Structure	**Maximum SEA [Jm^3/kg]**
AFS Alulight [96]	0.14
AFS Schunk [96]	0.131
GFR-AFS Alulight [97]	0.211
GFR-AFS Schunk [97]	0.218
AHS T1 clamped [96]	0.131
AHS T2 clamped [96]	0.138
GFR-AHS T1 [98]	0.243
GFR-AHS T2 [98]	0.313
AHS Type 1	0.126
AHS Type 2	0.14
AHS Type 3	0.312
AHS Type 4	0.328
AHS Type 5	0.288
AHS Type 6	0.289
CAS [103]	0.063
4L-CAS [103]	0.219
7L-TCAS 0°/0° [107]	0.811
7L-TCAS 0°/90° [107]	0.797
AH-CFRP [108]	0.14
GFRP-BCC [109]	0.098

Among the tested structures in the current study, the structure Type 4

has the maximum specific energy absorption. The comparison confirms the excellent performance of the double-layer sandwich panels with the bigger cells (AHS Type 4), even though the highest value of SEA belongs to the 7L-TCAS 0°/0° structure [107]. Nonetheless, it is necessary to observe that the structure considered in Ref. [107] consists of seven layers, which allow a significant improvement in energy absorption capabilities at the cost of a substantial volume increase.
High SEA values were yielded also by the tested hybrid structures, which represent a promising solution to develop efficient energy absorbers with controlled deformation.

3.1.1.3 Computed tomography analysis on impacted specimens

All the tested structures were subjected to CT investigation in order to observe and analyse the consequences of impacts and the deformation mechanism.
The CT images of the sandwich structures tested at the impact energy previous to the overall collapse, are reported in Figure 3.7.
The tomographic analysis validates the conclusions drawn from visual inspection and gives a deeper understanding of the failure mechanisms.
The behaviour observed for the mono-layer structures is consistent with that experimented in clamped conditions [95]: the specimens experience the deformation of the upper facesheet and the buckling of the honeycomb cells, which is clearly visible in the tomographic images.
The CT investigation confirms the influence of the cell size on the collapsing. In particular, for both single-layer and double-layer structures with the smaller cell size, the collapsed cells are located in the area subjected to impact, while the rest of the panel is nearly intact. Under the same impact energy, in the specimens with cell size equal to 6 mm, the deformation is more extended.

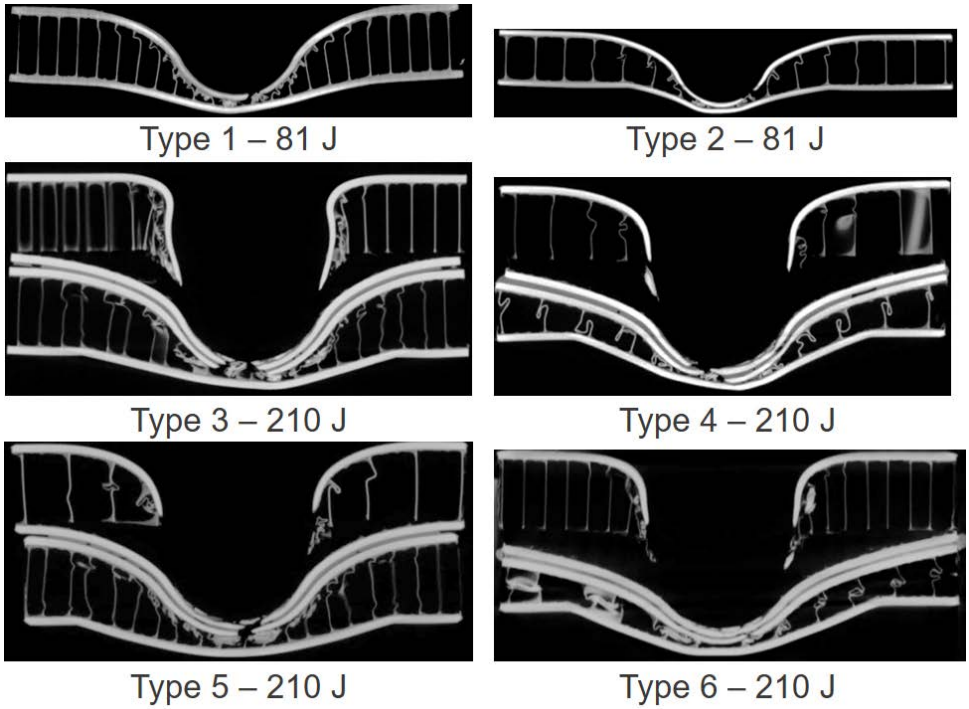

Figure 3.7. CT images of impacted honeycomb sandwich structures.

Through the CT images, it is possible to observe the failure of the top and the intermediate skins. Both the monolayer sandwich panels experience the top facesheet failure at 81 J. The top skin of the double-layer structure Type 3 fails at 81 J, whereas in the double-layer structure with cell size equal to 6 mm (Type 4), the failure of the top skin is delayed by the global deformation of the specimen and it occurs at 159 J. The intermediate skins failure was observed at 210 J for all the double-layer structures.

The investigated single-layer honeycomb sandwich panels under low-velocity impact failed after upper skin fracture and core piercing. For double-layer structures, the behaviour of the bottom layer was analogous to that observed in the single-layer panels; in the upper layer, high impact energies produced

a significant local deformation around the impactor, which was impossible for the upper core to follow and resulted in the debonding of the upper core from the lower skin, as visible from CT images.
CT investigation allowed also the identification of progressive cells walls buckling, testified by walls folds, which is induced during core crushing and is reported in Figure 3.8.

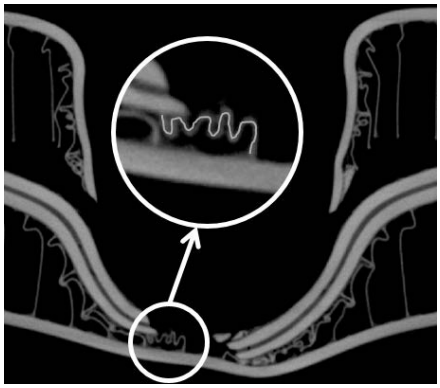

Figure 3.8. Progressive cells walls buckling.

Direct measurements of the maximum out-of-plane displacement w_b of the core at the lower facesheet were performed on the CT scans. The measured values on the specimens tested at the impact energy previous to the overall collapse are reported in Table 3.6
Among the double-layer sandwich panels, the highest value of out-of-plane displacement belongs to structure Type 4 and the lowest to structure Type 3. The out-of-plane displacement is an essential parameter in the design of crashworthy structures, which may require limited displacements, in order to protect people or objects during an impact event.
According to the experimental evidences, a proper choice of cell dimension and layers arrangement leads to controlled out-of-plane displacement and energy absorption.

Table 3.6. Out-of-plane displacement w_b measured on CT images.

Sandwich structure	**Impact energy [J]**	**w_b [mm]**
Type1	81	5.02
Type2	81	5
Type3	210	4.55
Type4	210	7.2
Type 5	210	6.08
Type 6	210	5.28

3.1.1.4 Theoretical analysis for small and large-size single-layer panels

The theoretical description of low-velocity impact events can refer to the energy-balance model [45]. This theoretical approach is based on statistically determined contact laws, whose application is acceptable for low-velocity impacts on common sandwich structures because the strain rate and wave propagation effects have proven to be negligible [45]. The description of the energy balance model is reported in section 2.3.3.

In order to deduce the parameters required by the theoretical model, CT images were used to measure the out-of-plane displacement w_b of the core at the lower facesheet and the impactor displacement w_i. The measures were taken on the specimens which did not undergo perforation or complete penetration. The same technique was applied with reliable outcomes in [95–97].

According to the spring-mass model, the impact load and the corresponding global displacement are correlated by a linear relationship, whose proportionality constant is the stiffness K_{bs}, which does not change with the impact velocity. The linear relation between the impact force and the global displacement is expressed in equation 2.35

In the current study, the K_{bs} stiffness of the simply supported mono-layer

structures was evaluated plotting the peak loads P_{max}, at different impact velocity, against the corresponding deflection measured in the middle plane. A linear regression was performed to interpolate the experimental results and find the value of the stiffness K_{bs}.

The plots of peak load against global deflection for mono-layer sandwich panels, with the equations obtained through linear regression, are displayed in Figure 3.9. The slope of the linear function is equal to the K_{bs} stiffness.

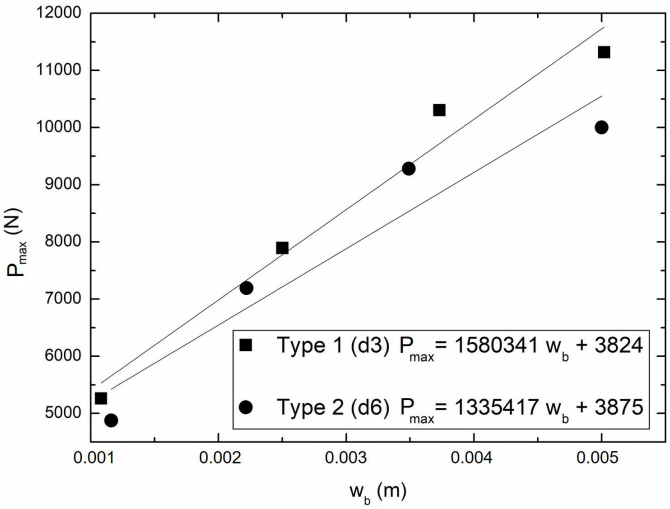

Figure 3.9. Peak load vs sandwich deflection.

Both linear functions correlating the peak load and the global deflection do not pass from the origin of the axes: this means that a significant out-of-plane displacement occurs only when the peak force is higher that a threshold value, which is equal to the constant term of the linear function. The same deduction was made for clamped specimens [95].

Once calculated the K_{bs} stiffness, the energy absorbed in bending and shear effects E_{bs} (which is equal to $E_b + E_{sh}$) was evaluated through equation 2.38, neglecting the membrane effects. Therefore, the contact energy E_{cn} was

calculated subtracting the values of E_{bs} from the values of the total absorbed energy E_t (or TEA), obtained as the area under the load-displacement curve. In order to obtain the dynamic parameters of the tested materials, it is possible to express equation 2.40 in bilogarithmic form, obtaining equation 3.3:

$$\log E_{cn} = \left(1 + \frac{1}{n}\right) \log P_{max} - \left[\log (n+1) + \frac{1}{n} \log K_c\right]. \tag{3.3}$$

The values of the contact energy E_{cn} were represented, in a bilogarithmic plot against the corresponding peak load P_{max}, as displayed in Figure 3.10.

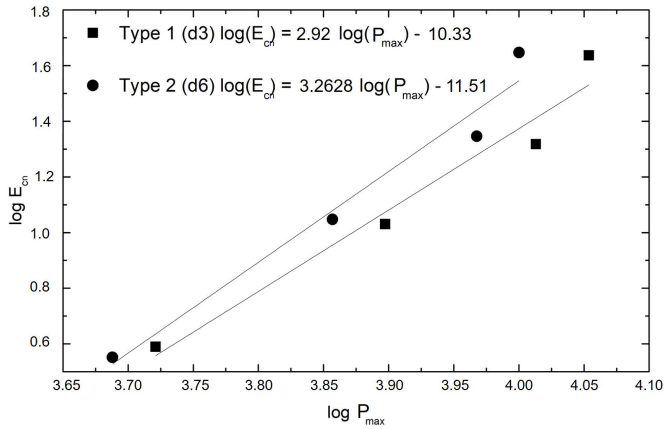

Figure 3.10. Contact energy vs peak load.

A linear regression performed on the experimental data, allowed the evaluation of the contact parameter n and K_c, whose values are reported in Table 3.7.

Hertz's contact theory predicts for the parameter n a value of 3/2, in the case of contact between two homogeneous isotropic solids [110]. The investigated materials are not homogeneous and isotropic, and, as a result, the calculated

Table 3.7. Calculated values of n and K_c.

Sandwich structure	**n**	**K_c [N/m^n]**
Type 1	0.67	465321
Type 2	0.44	103353

values of n differ significantly from the hertzian prediction.

3.1.1.5 Boundary conditions and size effect

Further details about honeycomb sandwich impact response were obtained from the comparison of the results of the current study, with simply supported configuration, with those found in Ref. [95]. for the same materials in clamped conditions. The visual aspect of the single-layer impacted specimen is slightly different from that observed for the same structures in clamped configuration. Simply supported specimens are free to deform around the impacting objects: as a result, under the same impacting conditions, a higher percentage of energy is absorbed by specimen global deformation, delaying the initiation of upper skin failure. For the single-layer sandwich panels with the smaller cell size in clamped configuration, an impact energy of 56 J is sufficient to produce the failure of the upper facesheet and a significant out-of-plane deformation. In simply supported configuration an impact energy of 81 J is necessary to achieve the failure of the upper skin.

For the single-layer sandwich structure with cell size equal to 6 mm, the failure of the upper skin is observed for an impact energy of 81 J for both boundary conditions. On the other hand, the shape of the fracture is different: the simply supported configuration causes a circular crack around the impactor tip, whereas in the clamped configuration the skin tears under the impactor mass with a large X-shaped crack.

According to the results reported in Table 3.6, the boundary conditions

affect also the maximum SEA. The mono-layer sandwich structure Type 1 tested in clamped configurations present a higher specific absorbed energy. The same behaviour was observed by Minak et al. [111], who compared the low-velocity impact response of simply supported and clamped circular plates made of carbon fibre reinforced polymers (CFRP). They observed that the boundary conditions affect the specimen stiffness and, consequently its impact response. They detected a lower stiffness for the supported plates, which results in a greater displacement and a lower energy absorption, whose consequence is a reduction in damage extension.
A further comparison between simply supported and clamped configuration regarded the evaluated stiffness. The percentage difference between the results obtained in clamped and in simply supported conditions was calculated as shown in equation 3.4:

$$\%diff. = \frac{K_{bs\ simply\ supported} - K_{bs\ clamped}}{K_{bs\ clamped}} 100. \tag{3.4}$$

The values, reported in Table 3.8 , prove that the conclusions drawn in Ref. [111] are pertinent with the results presented in this section.

Table 3.8. Influence of the boundary conditions on K_{bs} values.

Sandwich structure	**Boundary condition**	**K_{bs} [N/m]**	**% difference**
Type 1	simply supported clamped	1580341 2060000	-23%
Type 2	simply supported clamped	1335417 1470000	-9%

The simply supported configuration produces a reduction in stiffness for both sandwich panels, but the effect of the boundary conditions is more

evident for Type 1 panels. This could be a consequence of the dimensional characteristics of Type 1 panels (s=3 mm), which limit significantly the possible deformation in clamped conditions. The result is a considerably higher stiffness for Type 1 clamped panels, in comparison to the simply supported configuration.

According to the energy-balance model, the contact parameters n and K_c are correlated to the stiffness K_{bs}. Consequently, it is reasonable to expect that the boundary conditions will also affect the values of the contact parameters.

In order to deepen the evaluation of boundary conditions effect on contact parameters, a further comparison was performed among the results obtained for structures Type 1 and 2 in simply supported conditions, the results reported in Ref. [95] for structures Type 1 and 2 in clamped configuration and the results reported in Ref. [106] for a large aluminium honeycomb sandwich panel.

As previously mentioned, contact parameters are often calculated in literature by means of small-scale quasi-static indentation test [77, 99] and this approach was applied also in Ref. [106]. The quasi-static indentation test described in [106], was conducted at the CERISI Laboratories of the University of Messina, on a large aluminium honeycomb sandwich panel (800×1000×82 mm), with cell diameter equal to 19 mm, in clamped conditions. The test was performed with a portal for large structures provided with a 100 kN actuator and a cylindrical indenter with a diameter d_i equal to 200 mm, as visible in Figure 3.11.

Although the characteristics of the aluminium honeycomb sandwich subjected to the full-scale test are significantly different from the structures described in section 3.1.1, a comparison of their contact parameters was considered useful to evaluate the size effect and the difference between the quasi-static approach and the method based on CT measurements, used for the investigated structures.

Figure 3.11. Setup for full-scale indentation test, used in [106].

Hence, the values of n and K_c obtained in the current study are compared to those obtained in clamped conditions and to those found for a large-structure. The results of the comparison are reported in Table 3.9, together with the ratio between the the cell size s and the core thickness c and the ratio between s and the indenter diameter d_i.

The percentage differences in Table 3.9, were calculated as described in equation 3.4 for the stiffness K_{bs}.

The experimental results prove that considering the contact parameters exclusively a function of the material could lead to significant inaccuracies, unless the experimental configuration is able to minimise the effect of the

Table 3.9. Comparison of contact parameters.

Sandwich structure	**s/t**	**s/d_i**	**Boundary condition**	**n**	**n % diff.**	**K_c [N/m^n]**	**K_c % diff.**
Type 1	0.33	0.15	simply supported	0.67	-19%	465321	-31%
			clamped	0.83		677000	
Type 2	0.67	0.3	simply supported	0.44	-31%	103353	-44%
			clamped	0.64		185000	
Large-scale sandwich [106]	0.24	0.09	clamped	0.82	-	677522	-

boundary conditions.

Despite the substantial differences between the large structure of Ref. [106] and structure Type 1, giving the same boundary condition (i.e. clamped conditions), their contact parameters have almost the same values. This finding could be explained considering the existence of a size effect. The large panel and the Type 1 sandwich structure have similar values of the ratio between the cell diameter s and the core thickness c. In addition, the ratio between the cell diameter s and the indenter diameter d_i for Type 1 structure is close to the same ratio calculated for the large panel.

The considered dimensional relations may influence the deformation mode and the energy absorption mechanism of the honeycomb sandwich panels and affect the interaction between the indenter and the sandwich. As a result, the similarities found in the geometrical proportions, may explain the analogous values of n and K_c.

The detected dependence of contact parameters on the dimensional ratios identified above, could be a hint of the existence of a size effect.

The conclusions here drawn represent a preliminary phase in the identifica-

tion of a size effect. Further experimental investigations are required for a full understanding of the influence parameters on scale effect. Future findings regarding size effect could lead to the development of guidelines to support the design of large-scale structures on the basis of small-scale results.

The observed similarities confirm also the possibility to obtain the contact parameters directly from impacted specimens.

Figure 3.12 displays the peak value of the contact force for a specific impact energy for the honeycomb sandwich panels Type 1 and 2 tested in simply supported and clamped conditions.

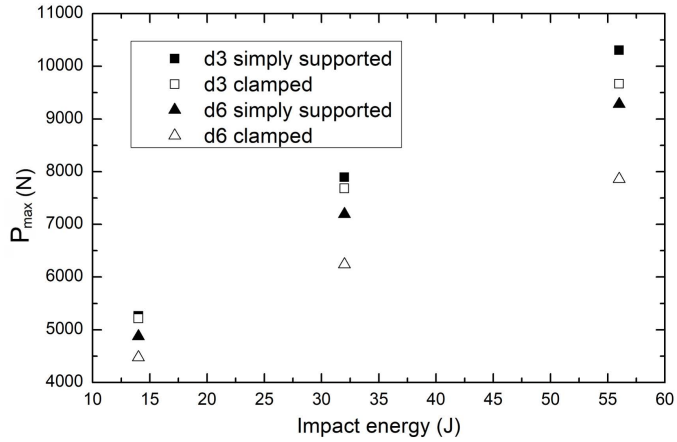

Figure 3.12. Effect of the boundary conditions on the maximum contact force.

The maximum value of the contact force recorded during the impact was less affected by the experimental configuration. The peak force for the honeycomb with the smaller cell size was almost independent from the boundary conditions, whereas for the bigger cell size a higher dispersion of the results was observed, even though the difference between the peak values for a certain impact energy was always less than 1500 N.

3.1.1.6 Final remarks

The experimental analysis performed on aluminium honeycomb sandwich structures subjected to impact loading confirmed their excellent energy absorption properties.
Further improvement to their crashworthiness was achieved with the introduction of double-layer sandwich structures with different cells dimensions and core arrangement.
The impact tests on double-layer structures highlighted a differential energy absorption mechanism between the two layers depending on cells dimension and on layer position. In particular, the structures whose bottom layer had the larger cell size, experienced an almost uniform compression of the lower core, whereas other structures presented a localised deformation around the impacting object. As a consequence, a proper core arrangement could allow the development of progressive energy-absorbers, which may be applied as impact-protective structures in marine applications.

The comparison of the specific energy absorption of the tested AHS with other lightweight sandwich structures, highlighted the high energy absorption capabilities of double-layer structures: in particular, the double-layer panels with the larger cell size (Type 4) presented the highest SEA among the tested structures, being also the lightest and cheapest of the analysed double-layer structures. However, the same structure produced the highest peak force and showed an out-of-plane displacement about 60% higher than Type 3 structures. Such parameters need to be considered according to the final application.

The non-destructive analysis, performed by means of 3D Computed Tomography on impacted specimens, allowed the observation of skins fractures and cell walls buckling, which is the mechanism responsible for the exceptional energy absorption properties of honeycomb structures. Out-of-plane dis-

placement of the core of each structure was measured on the CT images. Among the double-layer structures, the lowest displacement belongs to the sandwich whose both layers have the smaller cells (Type 3).

The application of a theoretical approach, based on the energy-balance model, to the mono-layer structures allowed the deduction of the parameters for the analytical description of the low-velocity impact phenomena. The obtained values, compared with those derived from a different testing configuration, showed the effect of the boundary conditions on the impact response of honeycomb sandwich structures. In addition, they could be applied to support the design of impact-resistant components.
The comparison of the contact parameters obtained for the small-scale panels with those resulting from tests on a large honeycomb sandwich, allowed the identification of a size effect, dependent on dimensional relations between the honeycomb and the indenter. Such findings may give useful information in the design phase of large structures, which is often the case for marine applications.

The experimental and analytical study introduced the possibility to obtain efficient energy absorber combining honeycomb sandwich with different characteristics, in order to induce controlled mechanism deformation and impact resistance.

3.2 Honeycomb sandwich panels under fatigue bending loading

A relatively few number of studies are concerned on the fatigue response of honeycomb sandwich structures, as reported in section 2.3.4. Nevertheless, cyclic loads are typical of numerous applications and the knowledge of honeycomb sandwich structures fatigue response is crucial for their effective and

reliable use.

Focusing on marine applications, fatigue phenomena may originate from several sources such as wave action, vibrations induced by vortex, machinery or propeller, wind effect, diving and resurfacing cycles [112, 113].

Some insight into fatigue bending response of honeycomb sandwich structures was provided by Belingardi et al. [53]. They experimentally investigated the four-point bending fatigue response of honeycomb sandwich beams, with and without adhesion defect between the aluminium core and the carbon-fibre skin. They compared the failure mechanisms of damaged and undamaged specimens and found that the undamaged specimens fail because of local buckling of the compressed face, whereas the damaged specimens experience crack propagation in the core, where the facesheet is not bonded.

Jen and Chang [114] studied the fatigue behaviour of aluminium honeycomb sandwich beams under four-point bending conditions, with three different relative densities. They suggested several global and local parameters, the latter derived from numerical simulations, to describe the fatigue life of the beams. They concluded that local parameters allow a better correlation with experimental results since they are based on the failure mechanisms.

Belouettar et al. [115] investigated four-point bending behaviour of honeycomb sandwiches with aramide or aluminium core and aluminium skins, under static and fatigue loading. They experimentally investigated the effect of core densities and cell orientation. Shear was responsible for aramid panels failure, which experienced a crack propagation through the core thickness, independently from cell orientation. Aluminium sandwich structures always failed after cracking in the lower facesheet.

Jen et al. [116] studied experimentally and analytically the two-stage cumulative fatigue response of aluminium honeycomb sandwich panels subjected

to four-point bending conditions. They observed that load sequence affects the fatigue life of the specimens. In order to take into account such effect, they applied a non-linear damage rule to predict the residual life. The non-linear model was based on specimens stiffness degradation and it yielded more accurate results in comparison to Miner's rule. Another critical point in honeycomb sandwich panels application is the effectiveness of joining systems with other sandwich structures or with metal parts.
Demelio et al. [117] investigated the static and fatigue behaviour of sandwich panels with nomex honeycomb core joined by fasteners and found a substantial effect of skin material and core thickness on joints fatigue strength.

The examples above highlight the complex phenomena involved in fatigue response of honeycomb sandwich structures, which is often difficult to analyse and predict. In addition all-aluminium honeycomb sandwich structures are seldom studied in scientific papers concerned with fatigue problems.
As a consequence, fatigue behaviour of aluminium honeycomb sandwich panels needs to be deeply investigated, in order to support the design of honeycomb-based marine structures and predict their durability.

3.2.1 Investigation on honeycomb sandwich structures under fatigue bending loading

Three-point fatigue bending conditions were applied, since they are poorly considered in existing literature on the subject, and particular attention was paid to failure mechanisms and boundary conditions effect.
Similar information are required to extend all aluminium honeycomb sandwich panels applications for structural purposes. As a result, specific fatigue analysis on such structures are essential, since it is not possible to deduce their fatigue behaviour from static information or from data regarding structures with different constituent materials.

The experimental investigation was conducted on one of the same commercial aluminium honeycomb sandwich structures investigated in section 3.1.1. In particular, the analysis were performed on structure Type 1, whose main characteristics are reported in Table 3.1.

The experimental procedure included a preliminary quasi-static investigation followed by fatigue analysis. Static tests were performed both under three and four point bending conditions, to assess the static bending strength and the crashworthiness performance.

The specimens for bending tests had the dimensions of 200×45×11 mm.

Bending tests were performed with an Italsigma servo-hydraulic testing machine equipped with a 12.5 kN load cell. Rigid cylinders with 20 mm diameter were used to support the specimen and to apply the load.

Static tests were performed at room temperature in displacement control mode. Three and four-point bending tests were performed at several displacement rates ranging from 2 to 50 mm/min.

Fatigue analysis were conducted under three-point bending and the effect of boundary conditions on collapse mechanisms under cyclic loading was investigated by considering different supports span. Fatigue tests were performed in load control mode. The cycling load varied with a sinusoidal shape at a frequency fr of 5 or 10 Hz and a load ratio R equal to 0.1. Runout threshold was set at $2 \cdot 10^6$ cycles. Fatigue tests were performed with different supports spans in order to analyse the effect of boundary conditions .

A 3D Computed Tomography System Y.CT Vario was used to perform non-destructive analysis to investigate the phenomena involved in AHS static bending response. The tomographic investigation was conducted with a X-ray tube voltage of 180 kV, a current of 1 mA, and a focal spot size of 250 µm. A 0.5 mm copper filter was applied to the source. 1440 projections were acquired for 3D model reconstruction during a specimen rotation of 2π at 0.0087 rad/s.

An analytical model was introduced to evaluate the effect of boundary conditions on fatigue collapse modes and to predict the fatigue limit loads and a failure map for the prediction of fatigue collapse modes and limit loads was obtained.

3.2.1.1 Crashworthiness evaluation

One of the main advantage of honeycomb structures is their capability of absorbing significant amount of energy [87] while being lightweight. In order to quantify energy absorption properties of the investigated honeycomb sandwich panels under bending conditions, the following parameters were evaluated:

- maximum bending moment (M_{max}), which is the maximum moment value registered during bending tests;
- total energy absorption (TEA), which, in this case, is the energy amount absorbed up to the maximum rotation of the specimen (θ_{max}); for bending tests, the TEA is obtained by integrating the moment-rotation curve, according to equation 3.5:

$$TEA = \int_0^{\theta_{max}} M(\theta)\,\mathrm{d}\theta; \tag{3.5}$$

- specific energy absorption (SEA), which is the ratio between TEA and the material density, according to equation 3.6:

$$SEA = \frac{TEA}{\rho_p} = \frac{\int_0^{\theta_{max}} M(\theta)\,\mathrm{d}\theta}{\rho_p}; \tag{3.6}$$

- average moment (M_{avg}), which can be obtained by the ratio between the energy absorption and the maximum rotation, as reported in equa-

tion 3.7:

$$M_{avg} = \frac{TEA}{\theta_{max}} = \frac{\int_0^{\theta_{max}} M(\theta)\,\mathrm{d}\theta}{\theta_{max}}; \tag{3.7}$$

- energy efficiency (η), which is the ratio between the measured TEA and the energy absorbed by an ideal absorber, according to equation 3.8:

$$\eta = \frac{TEA}{E_i} = \frac{\int_0^{\theta_{max}} M(\theta)\,\mathrm{d}\theta}{M_{max}\theta_{max}}. \tag{3.8}$$

3.2.1.2 Preliminary quasi-static bending tests

Three and four-point bending static tests were performed in order to obtain information on the static bending strength of the investigated structures and on the strain rate influence.
The specimens were tested at the following displacement rates: 2, 5, 10, 20, 30, 40, 50 mm/min.
The supports span for the three-point bending configuration was equal to 130 mm. For the four-point bending configuration, the outer supports span was equal to 110 mm and the inner supports span was equal to 40 mm. The test configurations are schematised in 3.13. Supports distances for four-point bending tests were selected in order to obtain almost the same flexural stiffness for the panels.
The obtained bending moment-displacement curves at each displacement rates are reported in Figure 3.14, in terms of maximum bending moment M_{max} against specimen rotation angle θ:
Experimental curves, for both configurations, are almost overlapped: it follows that quasi-static bending response of the investigated structures is independent on the displacement rate. Neither collapse modes were affected

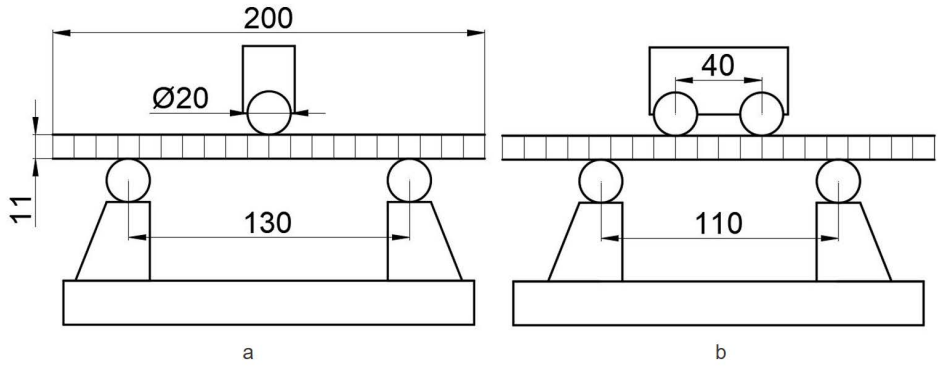

Figure 3.13. Test configuration for a) three and b) four-point bending configurations.

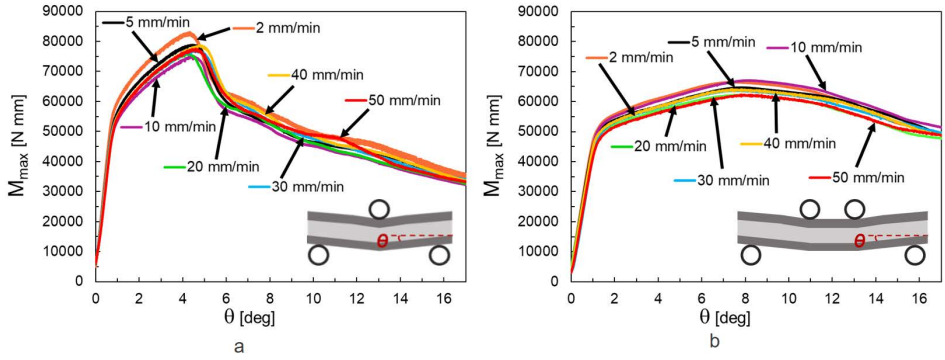

Figure 3.14. Maximum bending moment-rotation angle curves at different displacement rates for a) three and b) four-point bending conditions.

by displacement rates. The same consideration is valid for crashworthiness evaluation. The calculated crashworthiness parameters and the static bending strength are reported in Table 3.10, which contains also a comparison with the results derived from a previous study [98] on the same honeycomb sandwich structure, subjected to three-point bending, reinforced by means of two additional glass fibre reinforced skins. In order to have an adequate comparison, the crashworthiness parameters were evaluated considering the

Table 3.10. Results of the crashworthiness evaluation

	Disp. rate [mm/min]	**M_{max} [Nmm]**	**Static bending strength [MPa]**	**TEA [J]**	**SEA [Jm^3/kg]**	**M_{avg} [Nmm]**	**η**
3-point bending	2	83098	91.6	16	0.02	54853	0.66
	5	78828	86.9	15	0.02	52083	0.66
	10	75083	82.7	15	0.02	49588	0.66
	20	75826	83.6	15	0.02	50474	0.67
	30	76881	84.7	15	0.02	52090	0.68
	40	78693	86.7	16	0.02	52768	0.67
	50	77584	85.5	15	0.02	52031	0.67
4-point bending	2	66542	73.3	17	0.03	58373	0.88
	5	64685	71.3	17	0.03	57269	0.89
	10	67080	73.9	17	0.03	58756	0.88
	20	62232	68.6	16	0.02	55013	0.88
	30	63688	70.2	17	0.03	56178	0.88
	40	64125	70.7	17	0.03	56694	0.88
	50	62290	68.6	16	0.02	54775	0.88
GFR-AHS [98]	2	162305	N.A.	25	0.04	83970	0.52

same maximum rotation for each test, equal to 17°.

Energy absorption characteristics are dependent on the loading configuration. Four-point bending crashworthiness parameters are higher than those obtained under three-point bending conditions, except for the maximum bending moment (M_{max}). The comparison with sandwich reinforced by GFRP skins highlights the significant skin involvement in energy absorption, though the energy efficiency is lower.

According to literature results [118] crashworthiness parameters depends also on other features, such as cell size and foil thickness.

For each M_{max}–θ curve, four regions can be distinguished, as shown in Figure 3.15, which refers to 2 mm/min tests. After a steep linear trend (zone 1), a sudden slope decrease is registered (zone 2), which is maintained up to the maximum moment value, after which the moment drops (zone 3); the de-

creasing trend continues with a lower slope (zone 4) until the test is stopped.

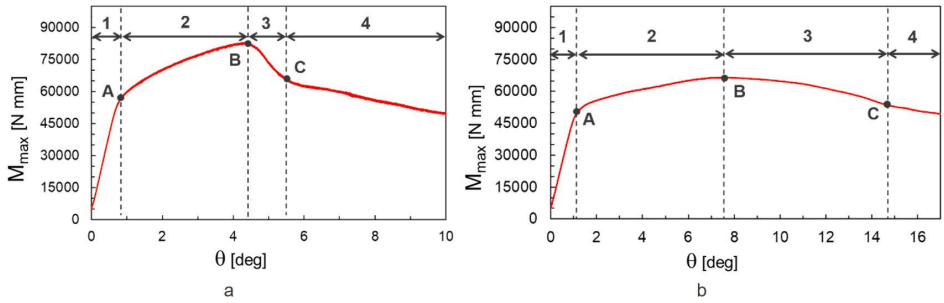

Figure 3.15. Regions of $M_{max}\theta$ curves for a) three and b) four-point bending conditions.

In order to understand the phenomena responsible for the trending changes in the $M_{max}\theta$ curves, some bending tests were repeated and interrupted immediately after the points of interest (A, B and C) indicated in Figure 3.15. At each interruption a tomographic analysis was performed on the specimen. Such procedure allowed the non-destructive identification of the deformation mechanisms which cause the variation in the curve trend and influence the load carrying capabilities of honeycomb sandwich structures under bending conditions. The tomographic images obtained at the three critical points are displayed in Figure 3.16, which refer to the same displacement rate of Figure 3.15 (2 mm/min).

The tomographic images obtained after the first slope variation (point A), show the honeycomb sandwich structure perfectly intact, without any sign of permanent damage. Such observation proves that the first slope variation might depend on an elastic event, probably linked to cell wall buckling. It is consequently realistic to consider the first two regions (1 and 2, up to point B) related to the panel elastic response. Such behaviour is comparable to what was observed by Zhang and Ashby [119] in low-density honeycomb under simple compression conditions.

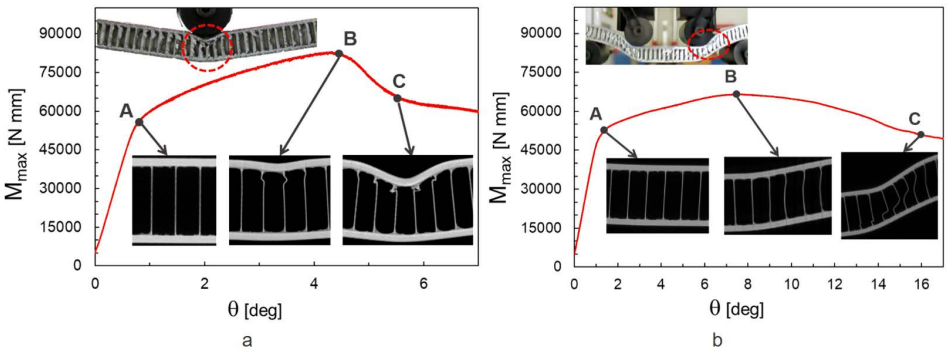

Figure 3.16. Tomographic images showing the deformation mechanisms at the critical points of the bending curves for a) three-point and b)four point bending conditions.

After reaching the maximum moment value, the tomographic images show the typical buckling deformation in the cell walls nearest to the load application section. The sudden load decrease registered at this point, may be attributed to the initiation of plastic buckling in the cell walls, probably accompanied by the formation of a plastic hinge in the load application section.

In the tomographic images obtained after point C, the propagation of buckling collapse to a higher number of cells is evident. In addition, the specimens show a significant indentation of the upper facesheet. The subsequent decreasing trend (region 4) is the result of the cells walls progressive buckling, together with indentation intensification. Buckling plays a crucial role in honeycomb mechanical response, similarly to what was observed for other sandwich structures with corrugated core [105, 120].

Under three-point bending conditions, none of the tested specimens showed any sign of skin or core fracture; only the partial debonding of two adjacent cell walls was observed, as visible in Figure 3.17a. The recorded collapse mode with L=130 mm was indentation, visible in Figure 3.17, combined

with the rotation of the two halves of the sample around the mid-plane and with the formation of 4 plastic hinges. The scheme for the observed failure mechanism is reported in Figure 3.17b.

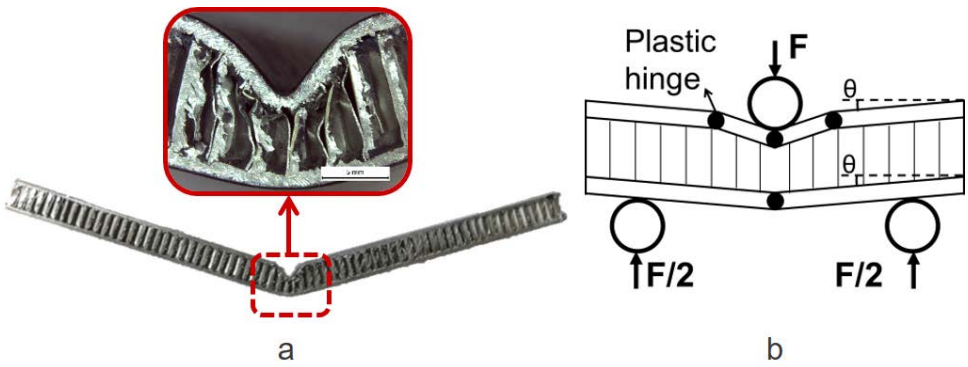

Figure 3.17. Indentation collapse mode: a) specimen; b) theoretical model.

The described mechanism confirms the observations made in a previous study on the same honeycomb panels [95], in which the same collapse mode, called Mode I, was observed for specimens with a supports span higher than 70 mm, whereas specimens with a supports span lower than 70 mm were subjected to the so-called Mode II, which mainly involved core shear.

The collapse mechanism registered under four-point bending conditions is displayed in Figure 3.18.

As visible from Figure 3.18, neither four-point bending loading produced skin fracture. On the other hand, four plastic hinges were formed on each facesheet, core shear was observed and it produced cell walls rotation and fracture, together with debonding between core and facesheets in the load application section.

The observed failure mechanisms are strictly correlated to honeycomb core properties, facesheet characteristics and interfacial mechanisms between them.

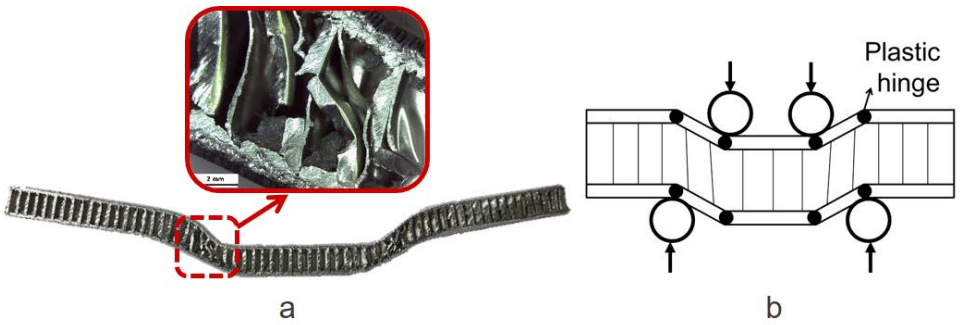

Figure 3.18. Collapse mode for four-point bending conditions: a)specimen; b)theoretical model.

3.2.1.3 Three-point bending fatigue tests

Three-point bending fatigue tests were performed with a double purpose:

- obtaining information on aluminium honeycomb sandwich panels fatigue resistance;
- finding the collapse mechanisms under fatigue conditions and comparing them to the static ones.

Aluminium honeycomb sandwich panels were subjected to fatigue tests with different supports spans L in order to analyse the effect of the boundary conditions on the failure mechanisms. The considered supports span are: 130, 100, 85, 70 and 55 mm. The applied testing conditions are summarised in Table 3.11.
The S-N curve was defined only for the larger supports span (L=130 mm) and it is reported in Figure 3.19 together with the equation obtained by means of linear regression.
The collapse mechanism observed for L=130 mm was identified as skin failure and it is described with more details in section 3.2.1.4.

Table 3.11. Applied conditions for three-point bending fatigue tests.

Supports span L [mm]	**Max. load P_{max} [N]**	**Max. moment M_{max} [Nmm]**	**σ_{max} [MPa]**	**$\Delta\sigma$ [MPa]**	**General result**
130	2000	65000	72	64	Failure
	1700	55250	61	55	Failure
	1500	48750	54	48	Failure
	1300	42250	47	42	Run-out
	1200	39000	43	39	Run-out
100	2500	62500	69	62	Failure
	2000	50000	55	50	Run-out
85	2500	53125	59	53	Failure
	2300	48875	54	48	Failure
70	2800	49000	54	49	Failure
55	3200	44000	48	44	Failure
	3000	41250	45	41	Failure
	2800	38500	42	38	Failure
	2700	37125	41	37	Run-out
	2500	34375	38	34	Run-out
	2300	32490	36	32	Run-out
	2000	37500	30	27	Run-out

Such failure mode consists mainly in a rapid crack propagation in the lower skin. For such reason, the experimental fatigue results were compared to literature data regarding skins base material [121] subjected to fatigue tension tests with R=0.1. From the S-N curve reported in Ref. [121], it was obtained an exponent of the linear regression curve equal to 0.15, which is the same value found in the current study. This endorses the hypothesis that for L=130 mm the fatigue bending response of the honeycomb sandwich structure depends mainly on the skin characteristics.

According to the experimental data, the fatigue limit in the considered con-

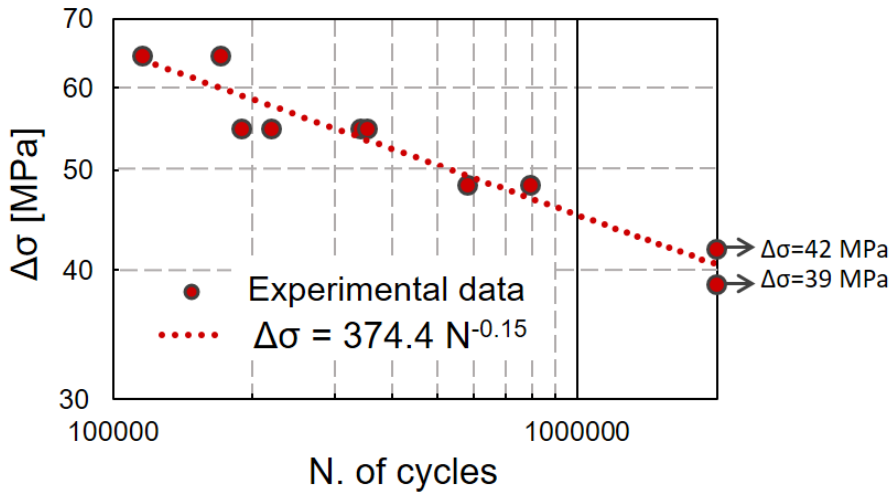

Figure 3.19. S-N curve for aluminium honeycomb sandwich panels under three-point bending with L=130 mm.

ditions (L=130 mm) was found for $\Delta\sigma$ equal to 42 MPa. Though, from the obtained results it is clear that the stress range included in the high-cycle fatigue region is narrow and this may lead to a high dispersion of the results and a difficult prediction of the fatigue life.

The experimental results obtained with different supports span are reported in Figure 3.20.

Despite a significant dispersion in the experimental data, a general trend with the supports span variation can be identified: in particular, it is evident that, for a given $\Delta\sigma$, supports span reduction causes a decrease in the number of cycles to failure. In other words, the bending stiffness increase, obtained by shortening the supports span, produces a reduction in fatigue life.

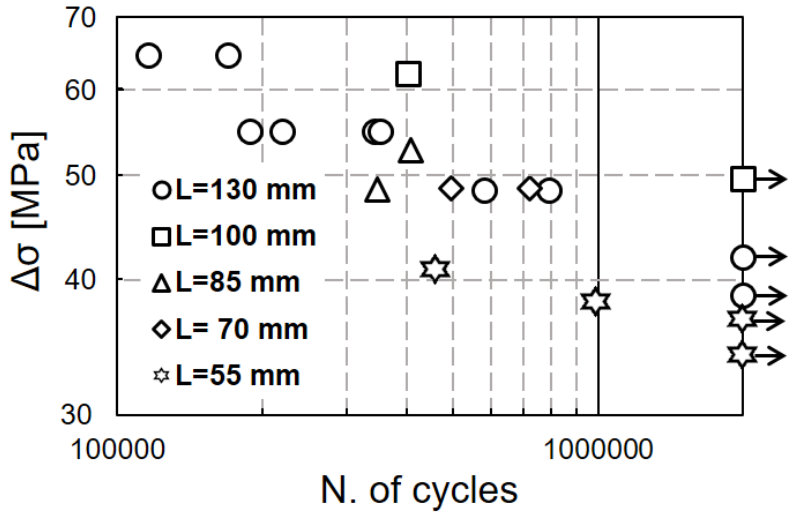

Figure 3.20. Fatigue tests experimental results with different supports span.

3.2.1.4 Collapse modes under three-point bending fatigue conditions

Different supports span did not produce only a variation in fatigue life, but also in failure modes.
The collapse mechanisms identified during three-point bending fatigue tests on aluminium honeycomb sandwich panels are dependent on the supports span, similarly to what was reported under quasi-static conditions for the same sandwich panels [95].
Two different fatigue failure modes were recognised:

- Skin failure after a sudden crack propagation, followed by core fracture on the same plane;
- Core shear with the formation of two plastic hinges for each facesheet and a consequent debonding between core and skins.

Skin failure was observed for supports span equal to 130 and 100 mm,

whereas core shear was registered in the other cases. The observed collapse modes and their schematisation are displayed in Figure 3.21.

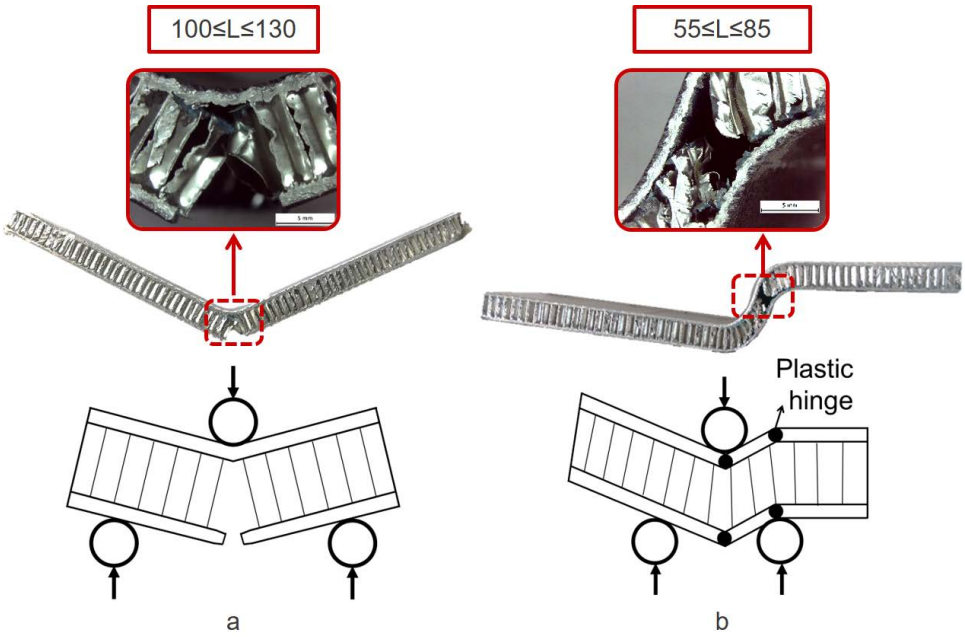

Figure 3.21. Fatigue tests experimental results with different supports span.

The collapse mode observed under fatigue loading with supports span equal to 130 and 100 mm differs significantly from what was observed in static conditions. Indeed, static loading produced only indentation and plastic hinges formation, whereas fatigue collapse mode is mainly driven by the tensioned facesheet failure, without any sign of core crush. Under service conditions, this fatigue failure mode may introduce severe risk for the structure functionality and integrity, since it produces a sudden failure, hardly predictable or detectable with monitoring techniques.

Core shear observed for L≤85 mm is an asymmetrical failure mode, in which half of the specimen entirely deforms by shearing whereas the other half de-

forms by shearing only between the load application point and the support since it is subjected to the formation of two plastic hinges near the support. The same failure mode was already reported for metallic foam core sandwich beams by Kesler and Gibson [122], who observed that such collapse mechanism is intermediate between core shear mode A and core shear mode B, traditionally considered in literature for sandwich structures [123]. Similar observations were also made in static conditions for the same honeycomb sandwich panels with a supports span lower than 70 mm [95], even though under fatigue loading the core compression was not evident.

The failure modes observed for all aluminium honeycomb sandwich panels are different from what is reported in literature for hybrid sandwich panels with aluminium core and composite skins. For instance, Belingardi et al. [53] tested sandwich panels with aluminium honeycomb core and carbon fibre reinforced skins, both with and without defects. They observed that all the undamaged specimens failed after local buckling of the compressed face, whereas such mechanism was not observed in all-aluminium panels.

In order to explain the mechanisms involved in failure and the relationship between the fatigue collapse modes and the boundary conditions, the analytical description of foam-cored sandwich panels failure modes, developed by Ashby et al. [123], was applied. According to this theory, the main failure modes for sandwich panels subjected to bending are face yield, indentation and core shear. The analytical formulations of the limit loads for each failure mechanism depend on the geometrical configuration, on the boundary conditions and on the mechanical properties of the skins material and of the core. Such analytical models were adapted to the current problem by introducing in their formulation the fatigue strength of the sandwich panels components. The feasibility of a similar approach was verified in Refs. [54] and [124] and it allowed the prediction of both the fatigue limit loads and

the failure collapse modes at different supports span.
The limit loads were derived from Refs. [122] and [123] for the following failure modes: facesheet failure, local indentation and core shear mixed mode AB. The sandwich panel failure mechanism is expected to be the one triggered by the lowest limit load.
Since the model was applied to fatigue conditions, during which the load varies between a minimum and a maximum value, the fatigue limit loads considered in the model referred to the maximum load.
Skin failure in fatigue bending occurs when the maximum stress in the tensioned facesheet reaches the fatigue tensile strength of the skin $\sigma_{s,f}$. Therefore, the fatigue limit load for skin failure $P_{s,f\ max}$ was derived equating the maximum bending moment in the sandwich beam to the collapse moment of the section:

$$P_{s,f\ max} = \frac{4bt(c+t)}{L}\sigma_{s,f}. \tag{3.9}$$

Local indentation failure is characterised by the formation of three plastic hinges in the top skin and the local compressive collapse of the core. The fatigue limit load for indentation $P_{i,f\ max}$ is reported in equation 3.10:

$$P_{i,f\ max} = 2bt\sqrt{\sigma_{s,f}\sigma_{c,f}} \tag{3.10}$$

where $\sigma_{c,f}$ is the fatigue compressive strength of the core.
Failure after core shear mixed mode AB [122] consists in an intermediate mode between core shear mode A and core shear mode B [123], in which one plastic hinge for each skin form at the load point, half of the specimen entirely deforms by shearing and in the other half one plastic hinge for each facesheet forms near the support, as a result shear deformation occurs only between the load application point and the plastic hinges. The fatigue limit

load for core shear mode AB $P_{AB,f\ max}$ is obtained considering the formation of two plastic hinges for each facesheet and the shear failure of the core, excluding one of the overhang length. The resulting expression is reported in equation 3.11:

$$P_{AB,f\ max} = \frac{2bt^2}{L}\sigma_{s,f} + 2bc\tau_{c,f}\left(1 + \frac{H}{L}\right) \tag{3.11}$$

where H is the overhang length on one side of the specimen and $\tau_{c,f}$ is the fatigue shear strength of the core.
The fatigue properties of the skins and core of the tested structures, were derived from Jen et al. [124], who experimentally evaluated them for an aluminium honeycomb sandwich structure similar to the panels here investigated. The power-law equations for the S-N curves at 25°C reported in [124], were applied to evaluate the fatigue strengths at $2 \cdot 10^6$ cycles. The obtained properties are reported in Table 3.12.

Table 3.12. Fatigue properties of the sandwich structures components [124]

Skin fatigue tensile strength ($\sigma_{s,f}$) [MPa]	**Core compressive fatigue strength ($\sigma_{c,f}$) [MPa]**	**Core shear fatigue strength ($\tau_{c,f}$) [MPa]**
113	1.5	1.7

Equations 3.9-3.11 were applied, with the properties stated in Table 3.12, at different supports span. The results of the analytical models are displayed in Figure 3.22.
As visible in Figure 3.22, at small supports span the lowest limit load is produced by core shear AB, whereas for higher supports span the lowest fatigue limit load is yielded by face failure. Local indentation is not expected to be observed, since the predicted limit load is significantly higher than the other

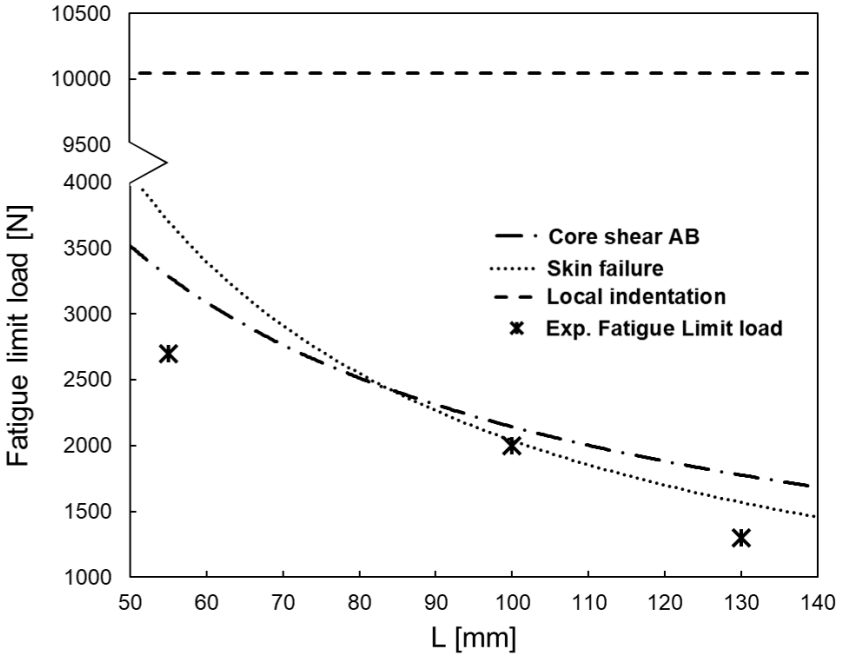

Figure 3.22. Analytical and experimental fatigue failure load for different collapse modes against supports span.

mechanisms. This explain also the difference between static collapse mode, which involved local indentation for the considered condition (L=130 mm) and fatigue failure mechanisms.

The analytical model results allowed the definition of a failure map, which is showed in Figure 3.23.

From the failure map it is evident that for supports span lower than 85 mm the predicted collapse mode is core shear mixed mode AB since it produces the lowest limit load. For higher supports span face skin failure is expected to occur. The transition between the two mechanisms occurs when they produce the same limit load, which happens for L almost equal to 85 mm. Figures 3.22 and 3.23 display also the experimental fatigue limit loads for

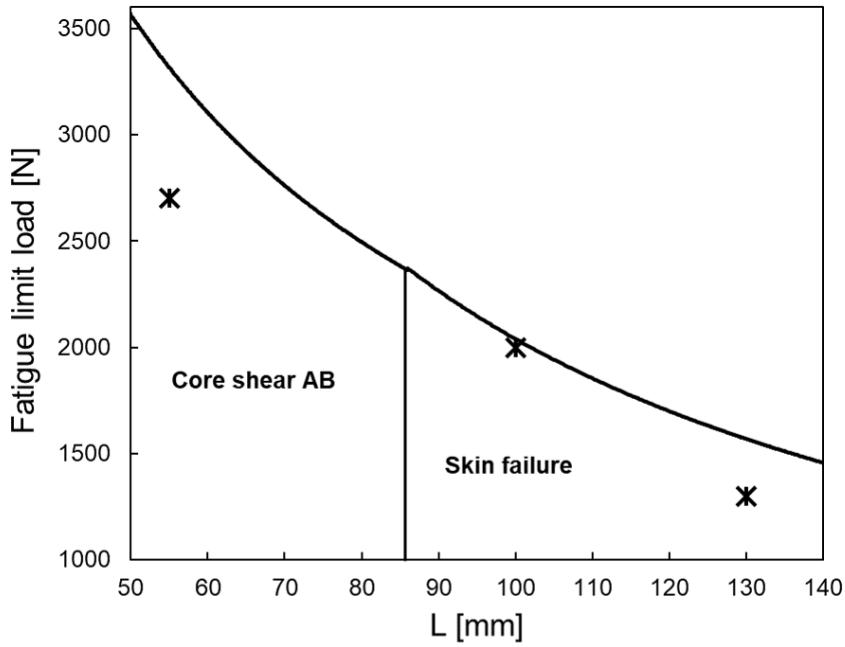

Figure 3.23. Failure map for fatigue collapse modes and limit load prediction.

supports span equal to 55, 100 and 130 mm, since, for the other conditions, tests with run-out result were not performed. Experimental and analytical results are in good accordance, both for the expected collapse mode and for the limit load. It can be concluded that the considered analytical formulations, in which fatigue properties of the investigated structures were introduced, are able to predict the honeycomb sandwich panels fatigue collapse modes and to theoretically describe the phenomena responsible for failure.

The good correspondence between experimental and analytical evaluations confirms the effectiveness of the proposed procedure, which could be applied to support aluminium honeycomb sandwich design for marine applications.

3.2.1.5 Final remarks

The performed experimental research allowed the identification of differences and analogies between static and fatigue behaviour of aluminium honeycomb sandwich structures.

The quasi-static three and four-point bending tests highlighted that the bending behaviour of aluminium honeycomb sandwich structure is independent on strain rate. The evaluated crashworthiness parameters confirmed the excellent energy absorbing properties of the investigated structures, which are mainly dependent on the progressive cell wall buckling.

Quasi-static failure mechanisms were analysed both for three and four-point bending conditions and the mechanisms involved in the bending response were identified, in a non-destructive way, by combining mechanical tests with computed tomography technique. The performed analysis pointed out the significant effect that cell wall buckling has on load carrying capability of honeycomb sandwich structures.

Three-point bending fatigue tests were performed with supports span ranging from 55 mm to 130 mm. Supports span affect the collapse mechanisms: in particular, for $L \leq 85$ mm core shear mixed mode AB was responsible for panels failure; for $L > 85$ mm skin failure caused specimen collapse.

The S-N curve obtained for L=130 mm highlighted a small stress range for high cycle fatigue region and a high scatter in experimental results.

Reducing the supports span resulted in a decrease in fatigue life, for a given $\Delta\sigma$.

An analytical model, involving the fatigue properties of the sandwich structure, was applied to predict the collapse mechanisms and the fatigue limit loads. The good accordance between experimental and analytical results confirms the effectiveness of the considered model, which may represents an useful tool for sandwich structures design in several applications.

The observed collapse mechanisms under fatigue loading, in particular the skin failure, highlighted the critical conditions that might occur during ser-

vice conditions. As a result, the application of aluminium honeycomb sandwich structures should consider carefully the presence of fatigue loading and the applied boundary conditions.

4

Biomimetics and lightweight concept: a proposal for marine applications

Design of marine structures is often subjected to a double constraint: providing excellent structural performance and reducing weight.

As observed in section 2.4.1, the benefits for marine structures deriving from weight reduction include fuel consumption limitation, speed increase, payload increment and stability improvement [23].

Low-velocity impact resistance is one of the structural requirements that marine structures have to provide. Indeed, low-speed collisions occur as a result of ordinary in-service events [17]: impact with floating and submerged objects, tools and equipment falling onto a deck, low-velocity collisions with docks or other vessels.

In order to merge the necessity of impact resistance with weight reduction, a proper selection of materials and structures is required.

An innovative perspective on the problem could be offered by the application of biomimetics principles.
Natural structures, as mentioned in section 1.4, could be the source of inspirations to solve several engineering problems, including the demand of marine industry for lightweight and impact-resistant structures.

Countless cases of bio-inspired materials and structures, with lightweight and impact-resistance properties, can be found in the literature. One among the numerous cases of bio-inspired structures is the one developed by Gu et al. [125], who took inspiration from seashells crossed-lamellar structure [126] made of different layers, to develop a biomimetic structure, produced via additive manufacturing. Their design consists of a multilayer polymeric structure, in which each level is made of a cellular structure with different cell orientation. Their experimental and numerical results proved an effective imitation of the conch shell crack-arresting mechanism under impact loading.
Tran et al. [127] suggested another example of bio-inspired crashworthy structures, highlighting also the increased potentialities for biomimetic structures applications deriving from additive manufacturing development. They designed and manufactured a composite structure inspired to the nacre's multilayer and staggered tablet architecture. An algorithm was developed to generate the nacre-inspired pattern, adapt it to complex structures and manufacture it with dual-material fused deposition modelling technique. Finally they used a numerical model to assess the effectiveness of the nacre-inspired structure against blast loading and found that it was able to minimise the damages by mitigate and absorbing the shockwave energy.
A common feature of many natural materials is the presence of a hierarchical organization, which affects their functions and properties [128]. Zhang et al.

[129] exploited this concept, combining it with the well-known energy absorption capabilities of honeycomb structures, to develop crashworthy bio-inspired hierarchical honeycombs. Numerical analysis were performed on honeycomb structures with different hierarchical levels, but constant mass, subjected to an out-of-plane crushing load. The results showed enhanced energy absorption performance at increasing hierarchical levels. This finding was attributed to the material concentration at the vertices of the base hexagons, which was responsible for local strengthening. A subsequent parametrical analysis allowed the identification of the optimum cell dimensions, for a given material. In addition, the effect of wall thickness on crashworthiness properties was investigated and an increase in specific energy absorption was found when thickening the second order cells.

Some cautious steps toward biomimetics application for marine structures were made in the last few years.

For instance, a bio-inspired composite structure destined for marine structures subjected to underwater impulsive loading were developed by Tran et al. [130]. They designed a composite panel inspired to nacre structure and in particular to the arrangement of its wavy layers and to the resulting interlocking mechanism. They performed a numerical analysis to compare the performance of a traditional composite panel and the bio-inspired panel during underwater impulsive loading. The results demonstrated that the nacre-inspired structure is able to reduce the stress concentration and the failure for inter-laminar debonding.

One lightweight natural structure which drew scientists' attention was bamboo. Bamboo stems have the structure of hollow tubes with transversal septa at regular intervals. Their constitutive structure [131] can be regarded as a fibre-reinforced cellular material with fibres oriented along the longitudinal direction. In the radial direction, bamboo has a graded cellular microstructure, with decreasing density from the outside to the inside. Bamboo's

hollow structure combined with its graded organisation allows a significant enhancement of specific flexural stiffness, which make bamboo suitable for many structural applications. Bamboo properties have been investigated from several points of view. For instance, Keogh et al. [132] studied the fatigue phenomena in bamboo under compression both in axial and diametral directions. They observed that fatigue does not occur on axially loaded specimens, which fail at the first cycle or do not fail at all. On the other hand, samples subjected to diametral fatigue compression fail after longitudinal crack propagation in different stages.

Some bamboo-inspired structures can also be found in the literature. Fu et al. [133] mimicked the bamboo structure to develop some thin-walled energy-absorbing systems. They introduced a tubular structure, with the outer and inner walls connected by longitudinal elements, arranged in different shapes. Their preliminary numerical analysis highlighted the excellent performance of tubes with "X" shaped reinforcements under axial crushing. Further numerical investigations were focused on optimising other parameters, such as wall thickness.

Bamboo has attracted also the attention of the marine industry thanks to its mechanical properties, its wide availability and its fast growing rate. Though, except for some simple structures, such as rafts [134], the main marine applications currently available for bamboo are limited to composite structures based on bamboo fibres [135, 136].

In view of the above considerations, the biomimetic approach could yield interesting alternatives and innovative ideas for engineering applications, including the marine industry. Thus, the current chapter was aimed at introducing the biomimetic ideas in the design of lightweight marine structures with crashworthiness properties.

This part of the thesis was mainly developed during a research period at the Trinity College of Dublin under the supervision of Professor David Taylor,

and the obtained results were published in a scientific paper [137].
The natural structure of bamboo was selected and examined. Its low-velocity impact response was investigated, with specific attention to the structure-property relationship. The analysis of its properties and their functions provided data to support engineering design based on bamboo structure imitation. In particular, the obtained results suggested some potential bio-inspired designs for lightweight impact-resistant structures, with possible applications in the marine industry.

4.1 Low-velocity impact investigation on bamboo structure

The experimental investigation of bamboo structure was performed on samples of a bamboo called Moso (Phyllostachys Pubescens), which is one of the most common bamboo species for structural applications. Bamboo culms were obtained from a local supplier (Bamboo Suppliers of Ireland, Dublin). Because bamboo is a hollow tubular structure, energy absorption in the longitudinal direction was the main impact property investigated in the literature [138, 139]. Nevertheless, bamboo stems are subjected also to low-velocity impacts in the radial direction, for instance as a consequence of collision events with other bamboo stems. The graded structure of bamboo may affect the energy absorption in the radial direction, thus more information on such behaviour is required.
As a result, low-velocity impact tests were performed both on the inside and on the outside of the bamboo structure. Tubular samples of bamboo, in an air-dried condition suitable for structural applications, were obtained from bamboo culms avoiding the nodes. Each tube was sectioned in the longitudinal direction to obtain semi-circular samples. In order to obtain similar conditions during the two types of impact tests, a rigid support, with the same shape of samples, was provided under the specimens tested both

on the inside and on the outside, with the aim of providing a full support to the specimens. In addition, whole cylindrical sections of the bamboo culms were subjected to low-velocity impact tests in the radial direction, with the aim of analysing the impact properties of the entire structure, as it actually responds in its natural environment.
Tests on the inside and outside of bamboo structures were performed also on specimens whose outside surface had been abraded to remove the outer layer for about a thickness of 0.1 mm.
The impactor was a rounded-ended steel cylinder of mass 1.325 kg, whose impact energy was varied by causing it to fall from different heights. The applied device allowed a maximum impact energy of 9.4 J. The test setup is schematised in Figure 4.1.

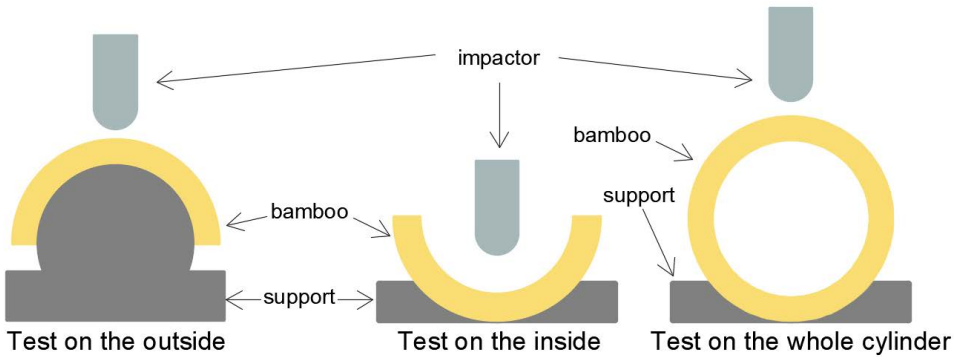

Figure 4.1. Impact test setup.

Information obtained from impact tests was analysed with statistical tools: the data normality was verified with Anderson-Darling test; ANOVA with least significant difference post-hoc test and t-tests were carried out to verify the statistical significance of differences between groups. In all statistical tests a confidence level of p=0.05 was used.
Visual inspection, optical microscopy and micro-tomographic analysis were applied to observe the damaged area. Micro-computed tomography (µCT)

investigation was performed with a Scanco µCT 40 device, with a voltage equal to 70 kV and a current of 114 µA.

4.1.1 Impact tests on the outside and inside of bamboo samples

Low-velocity impact tests on bamboo specimens revealed a different response to impact loading between the inside and the outside of the bamboo structure. 72 impact tests were performed. Specimens were divided on the basis of their thickness t_b into two groups:

- 3 mm $\leq t_b \leq$ 6 mm;
- 6 mm $< t_b \leq$ 10 mm.

Each group was tested at different impact energies, in order to assess the critical energy E_{cr} required to produce a visible crack. A typical dataset of experimental results is displayed in Figure 4.2, which refers to specimens with thickness between 6 and 10 mm, impacted on the inside.

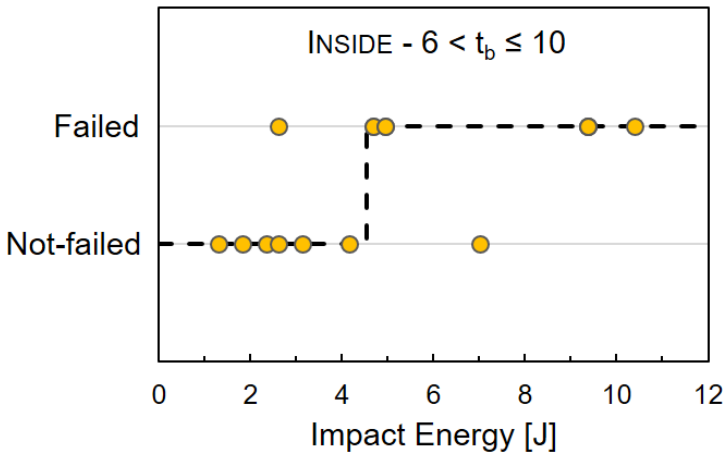

Figure 4.2. Experimental results for bamboo structure with 6 mm $\leq t_b \leq$ 10 mm impacted on the inside.

Above a certain impact energy, all the tested specimens experienced crack formation and propagation; below a certain energy no cracks formed, but there was a certain overlap region between these limits. The critical energy E_{cr} for each thickness group and impact side was identified by defining a step function, which describes the transition from not-failure to failure. Figure 4.2 shows the step function as a dashed line. The protocol applied for E_{cr} identification is the same used in ref. [140] - where impact properties of limpet shells were studied – and it is described below. Experimental points fitting exactly the function have an error equal to zero; points not fitting the function have an error e_i defined as:

$$e_i = E_i - E_{cr} \tag{4.1}$$

where E_i is the impact energy for a given test. Critical energy E_{cr} was evaluated by minimising the sum of all errors e_i.

The standard deviation (s.d.) of all e_i represents an indication of the E_{cr} uncertainty, due to scattered experimental results. Such definition of the s.d. is sensitive to the number of tests performed at energy values much higher or smaller than E_{cr}, which all fail or not-fail respectively. To prevent incorrect results, in the evaluation of s.d. only the e_i values obtained in a range of $\pm 20\%$ of E_{cr} were included.

The average thickness of each group and the corresponding critical energy E_{cr}, with error bars representing the s.d, evaluated as described above, are reported in Figure 4.3.

It is evident that both from inside and outside impacted specimens, critical energy increases with the thickness. The relationship between the critical energy and the thickness was analysed in order to find a normalised energy E_n able to provide an energetic comparison among experimental data. For this purpose, a fitting function including the ratio between critical energy

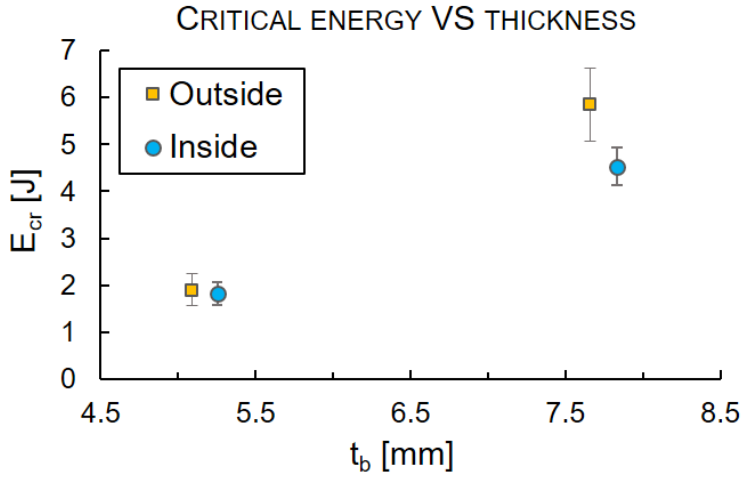

Figure 4.3. Critical energy E_{cr}against thickness t_b.

and thickness was searched. For specimens impacted on the outside the best results were obtained with equation 4.2:

$$E_{n,outside} = \frac{E_{cr}}{t^{2.7}} \tag{4.2}$$

For specimens impacted on the inside the best results were obtained with Equation 4.3:

$$E_{n,inside} = \frac{E_{cr}}{t^{2.3}} \tag{4.3}$$

Table 4.1 reports the values of the average thickness for each group and the corresponding critical energy E_{cr}±s.d. and normalised energy E_n±s.d.. Within each impact group E_n is almost constant, but the two different impact side affect its value. It could be deduced that the normalised energy

Table 4.1. Critical and normalised energies.

Impact side	**Average thickness t_b [mm]**	**Critical energy E_{cr}±s.d. [J]**	**Exponent exp for E_n**	**Normalised energy E_n±s.d [J/mm^{exp}]**
Outside	5.1	1.9±0.3	2.7	0.022±0.003
	7.7	5.8±0.8		0.022±0.003
Inside	5.3	1.8±0.2	2.3	0.041±0.006
	7.8	4.5±0.4		0.041±0.004

E_n is an estimate of the impact strength, which is dependent both on the impact side and on the thickness.

Notable differences were observed also between inside and outside impacts regarding the failure mechanisms. The critical energy produced on the specimens impacted on the outside a local indentation under the impactor, and a subsequent initiation and propagation of a crack in the longitudinal direction of the bamboo, which travelled across the whole thickness, causing the specimens to split into two halves. As a result, for specimens impacted on the outside, the critical energy E_{cr} corresponds to the energy required for complete failure of the structure.

Specimens impacted on the inside surface at the critical energy, experienced a wider local damage in the impact area, since the softer inside layers are able to partially crush under the impactor, and the propagation of a longitudinal crack, which crossed the specimen in the radial direction from the inside to the outside, was observed. However, critical impact energy on the inside did not produce a complete failure of the samples, instead crack propagated across the thickness but stopped before reaching the outer surface.

Further tests were performed in order to find the energy required to produce the complete failure of specimens impacted on the inside. The maximum feasible impact energy, equal to 9.4 J, was applied to three specimens with an average thickness of 9.5 mm. However, none of the tests produced the

complete failure of the samples, instead crack propagated up to about the 80% of the thickness. The different behaviour between outside and inside impacted specimens can be observed in Figure 4.4.

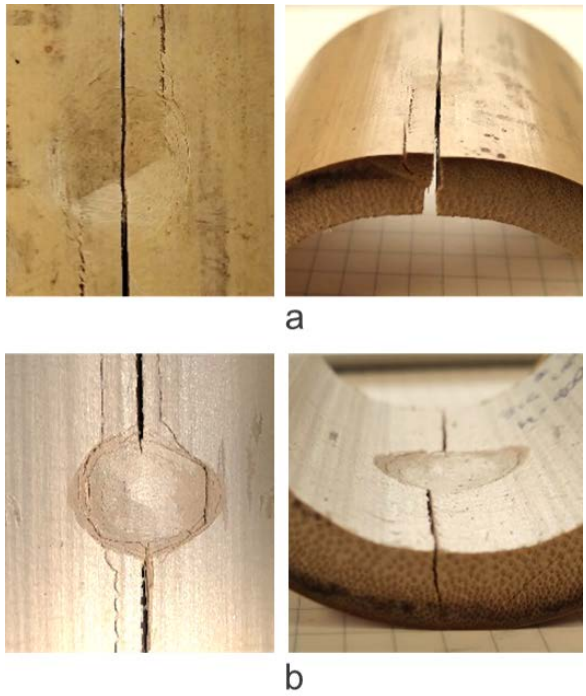

Figure 4.4. Impact area and propagated crack of specimens impacted a) on the outside at the critical energy level, and b) on the inside at 9.4 J.

The boundary conditions may affect the different response of the inside and outside impacted specimens, since it is not possible to guarantee the exact same testing conditions, as a result of the specimens shape. The above observations suggest that bamboo's graded structure may also have a significant role on the impact response. The softer inside layers, characterised by lower fibre density, may act as an energy absorbing structure, with a gradual crush of the cells. Such phenomena may enhance the impact resistance

of the structure when impacted from the inside. In addition, when a crack propagates from the inside to the outside, it meets outer layers richer in fibre content, which may be responsible for crack stopping
According to Low et al. [141], bamboo hardness decreased from the outside to the inside. Similar conclusions were reported also by Tan et al. [142], who performed nanoindentation tests across the radial direction of bamboo, finding that Young's modulus decreases from the outside to the inside, according to the fibre density distribution. In the same study, bending tests were performed on specimens with a notch on the inside or on the outside surface. Their results demonstrated that inside notched specimens had a higher resistance curve than the outside crack samples. Such difference was attributed to crack tip shielding through cellulose crack bridging, which was more evident in inside layers with lower fibre density.

4.1.2 Impact tests on bamboo abraded samples

Some bamboo samples were abraded on the outside surface, removing a layer of about 0.1 mm. Abraded samples were tested under impact both on the outside and on the inside. 15 tests were performed. Two thickness groups were considered for tests on the outside:

- $3 \text{ mm} \leq t_b \leq 6 \text{ mm}$;
- $6 \text{ mm} < t_b \leq 10 \text{ mm}$.

Tests on the inside were performed only on specimens with $3 \text{ mm} \leq t_b \leq 6 \text{ mm}$. The same procedure for the definition of the critical energy E_{cr} described in the previous section was applied. The normalised energy was evaluated using the exponents previously assessed for the not-abraded samples, since a lower number of tests were performed. Consequently, in this case the values of E_n were not intended to provide a normalisation within each thickness group, but were used for comparison purposes with the not-abraded samples.

The obtained results are reported in Table 4.2.

Table 4.2. Critical and normalised energy for abraded samples.

Impact side	**Average thickness t_b [mm]**	**Critical energy E_{cr}±s.d. [J]**	**Exponent exp for E_n**	**Normalised energy E_n±s.d [J/mm^{exp}]**
Outside	4.5 7.3	3.5±0.9 6.0±0.7	2.7	0.057±0.012 0.026±0.003
Inside	4.5	1.4±0.4	2.3	0.044±0.012

The comparison of the normalised energy En for not abraded and abraded specimens is shown in Figure 4.5, where error bars are also reported.

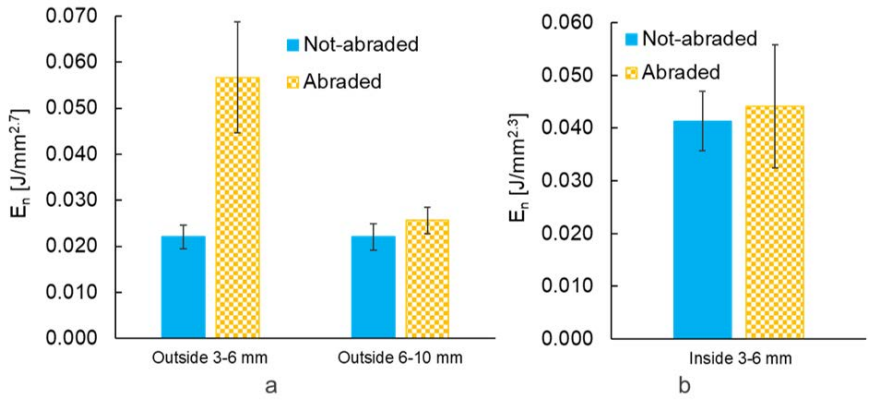

Figure 4.5. Comparison of E_n for not-abraded and abraded samples, for a) outside and b)inside impacted specimens.

For specimens impacted on the inside and on the outside with the biggest thickness, a slight increase in the average E_n was registered, but it was non-significant, as confirmed by the t test and the ANOVA ($p>0.05$). On the other hand, for samples with thickness between 3 and 6 mm impacted on

the outside, a significant increase in impact strength was observed. In this case, the abraded samples yielded an impact strength almost 2.6 times bigger than the non-abraded samples. Such statistically significant improvement in impact strength ($p<0.05$) may be explained considering the characteristics of bamboo structure. The harder outside layer probably behaves as a brittle structure, which is able to absorb a small amount of impact energy before cracking.

Focusing on specimens with thickness between 3 and 6 mm, the improvement obtained in normalised energy was significant for outside impacts ($p<0.05$) but not for inside impacts ($p>0.05$): this could be explained considering that bamboo has a graded structure which may enhance energy absorption properties when the outer hard layer is removed and the impact happens on the outside. Since this outer layer does not improve impact resistance (indeed it reduces it) one can assume that it has evolved for some other purpose, such as abrasion resistance or protection from pathogens.

The difference in critical and normalised energy between abraded and not-abraded specimens was mainly registered for thinner specimens, probably because in bigger specimens the hard outside layer is thicker and an abrasion 0.1 mm deep was not sufficient to affect the energy absorption properties. The different response between not-abraded and abraded samples impacted on the outside, is not limited to impact strength but it involves also the failure modes. Such dissimilarity is clear by comparing Figure 4.4a and Figure 4.6.

In abraded samples impacted on the outside, the damage in the impact area is less severe, as if the impact energy was distributed over a wider area after the local crushing of the structure. Longitudinal cracks were still produced by the impact, but they seemed to not cross the impact area. Instead cracks were produced near the edge of the impact region and they did not cause the separation of the specimens into two halves. As a consequence, abraded

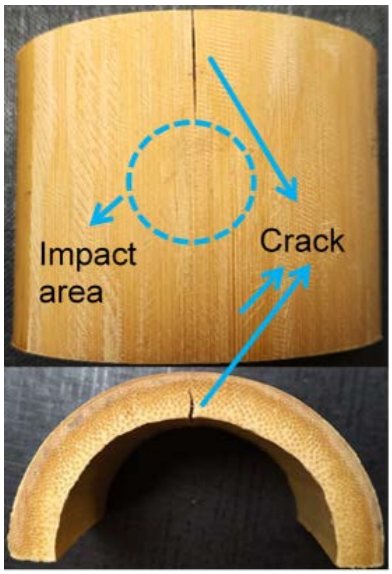

Figure 4.6. Abraded sample with t_b=7.1 mm impacted on the outside at 6.8 J.

samples impacted at E_{cr}, retained some residual strength.
Abraded specimens impacted on the inside did not exhibit any significant difference from the non-abraded samples.

4.1.3 Impact tests on whole cylindrical bamboo samples

Whole cylindrical sections of bamboo culms were subjected to low-velocity impact tests in the radial direction. 15 tests were performed and two thickness groups were considered for these tests:

- 3 mm $\leq t_b \leq$ 6 mm;
- 6 mm $< t_b \leq$ 10 mm.

The critical energy E_{cr} was evaluated as described in the previous sections. The normalised energy was evaluated using the exponents obtained for the

outside-impacted specimens. Applying the outside-tested specimens exponent was considered the most reasonable solution, since on the whole cylindrical specimens the impact happens on the outside. The values of E_n are not intended to provide a normalisation within each thickness group, but are used for comparison purposes with the not-abraded samples. The obtained results are reported in Table 4.3.

Table 4.3. Critical and normalised energy for whole cylindrical sections.

Average thickness t_b [mm]	**Critical energy E_{cr}±s.d. [J]**	**Exponent exp for E_n**	**Normalised energy E_n±s.d [J/mm^{exp}]**
4.0	0.9±0.2	2.7	0.021±0.003
6.3	2.0±0.3		0.012±0.003

Some tests were performed also on whole cylindrical sections abraded on the outside, but no significant difference was registered in impact properties. Whole cylindrical specimens, impacted at an energy equal to E_{cr}, experienced complete failure producing the fracture of the cylinder into two or more pieces, by cracks travelling in the longitudinal direction. The collapse behaviour was similar to that observed for non-abraded samples impacted on the outside.

The comparison, in terms of critical energy E_{cr}, among cylindrical samples, outside impacted samples and inside impacted samples is reported in Figure 4.7, along with error bars.

Testing the whole cylindrical samples affected the critical energy ($p<0.05$) for both thickness groups, in comparison with both outside and inside impacted samples. For both thickness classes, the whole cylindrical samples had a critical energy significantly lower than the samples of the corresponding class tested only on the inside or on the outside, and such reduction is more evident for the thicker samples. The low critical energy of whole cylindrical samples

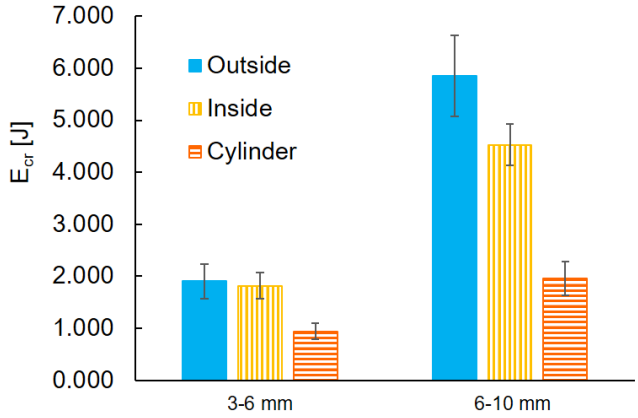

Figure 4.7. Comparison of E_{cr} among outside and inside impacted samples and whole cylindrical structures.

is probably the result of the completely different boundary conditions and shape of the specimens.

4.1.4 Optical microscopy and CT analysis

Optical microscopy and Computed tomography analysis were used to observe impact areas in order to acquire more information on collapse mechanisms. As observed in section 4.1.1, the impact area of samples tested on the inside, presented signs of a gradual local crush, which enabled a less severe damage than specimens impacted on the outside. Figure 4.8a shows a magnification of the impact area of a sample impacted on the inside at 9.4 J. It is possible to observe a gradual compression of the area subjected to impact and the presence of circular cracks which become deeper moving from the centre to the periphery of the impact area. Along the perimeter of one of the circular cracks, the starting point of the longitudinal crack is visible, probably triggered by the tensile stress produced in the circumferential direction during the impact. The impact area of a specimen tested on the outside at 6.8 J is

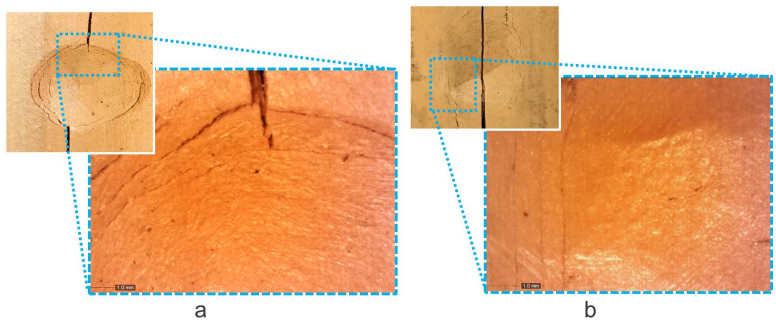

Figure 4.8. Impact region of specimens impacted a) on the inside and b) on the outside.

displayed in Figure 4.8b.

The graded structure of the bamboo had some influence also on crack path and propagation. Figure 4.9 shows crack path across the thickness in different samples.

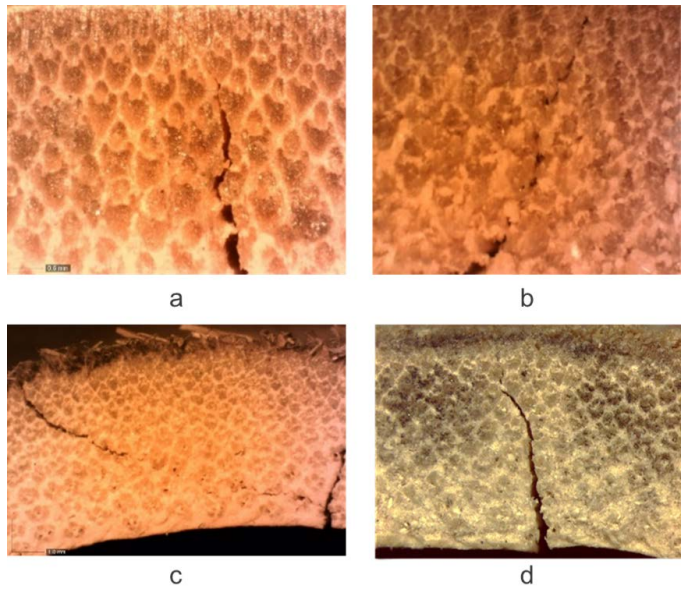

Figure 4.9. Crack path in samples impacted a) on the inside, b) on the outside, c) in an outside impacted abraded sample and d) in an inside impacted abraded specimen.

Regardless of the impact side, cracks seem to travel along cell boundaries, which probably represent low-energy interfaces. Cracks can travel across the thickness in an almost radial direction, as in Figure 4.9a, or they can follow a more complex path as visible in Figure 4.9c. In this case, the interfaces met by cracks during their propagation deflect them, providing a toughening mechanism which probably prevents total failure of the specimen.

The effect of impact side on collapse mechanisms was further investigated by means of µCT analysis. Figure 4.10 reports two tomographic images of samples impacted on the inside and on the outside.

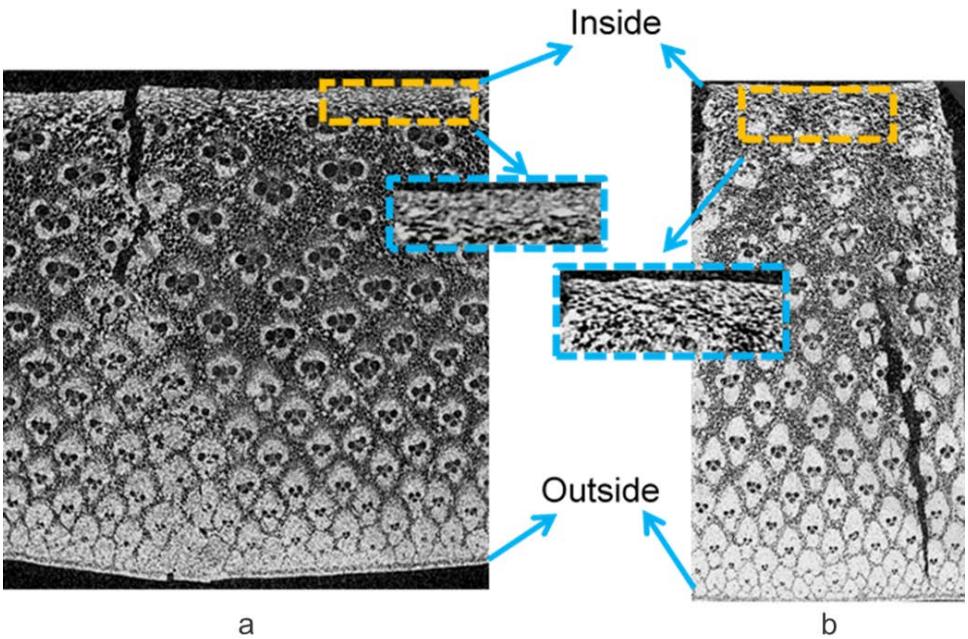

Figure 4.10. µCT images of bamboo samples impacted a) on the inside and b) on the outside.

In the sample impacted on the inside, a local crush of the cells below to the inside surface can be observed, in comparison to the outside impacted

specimen. Crack path is also visible in both cases, and seems to be partially driven by bundle interfaces.

4.2 Preliminary design of bamboo-inspired structures

The findings concerning the radial impact response of bamboo may prove to be useful in the design of bio-inspired impact-resistant structures. Indeed, transferring some of bamboo's key features to engineer structures it could be possible to obtain novel solutions for impact protection aims.

Despite the fact that countless ideas could be suggested by bamboo structure and its impact behaviour, some core concepts were considered in the design of some possible bamboo-inspired structures. Firstly, bamboo's graded structure, which seems to be strongly involved in energy absorption mechanisms, should be somehow resembled by the bio-inspired structures. Hierarchical assemblies may also be involved in impact response and could be introduced in the design of new structures. In addition, manufacturing feasibility should be considered, especially for marine applications, which may involve structures with large dimensions. For this reason, sandwich structures with corrugated cores were considered as a starting point for bio-inspired marine structures, taking into account also their well-proved crashworthy properties [143]. Some examples of corrugated structures for marine applications are showed in Figure 4.11.

According to these main principles, four bamboo-inspired structures were designed. The schematic of the bio-inspired design process is represented in Figure 4.12, where some possible applications in marine structures field are also presented.

The bamboo-inspired structures were designed considering the graded and hierarchical structure of bamboo. They were modelled as sandwich structures, in order to make them suitable for possible applications for impact

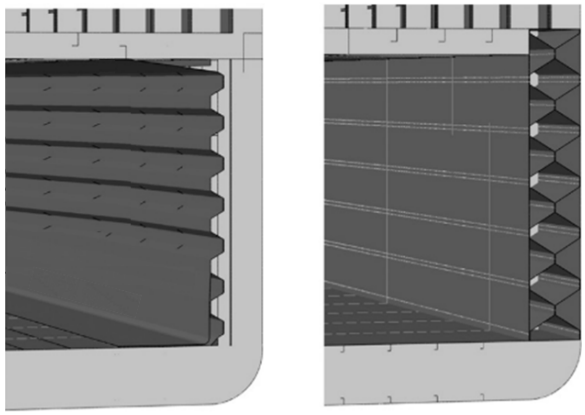

Figure 4.11. Examples of corrugated structures use in marine applications, reprinted from [143] with permission from Elsevier.

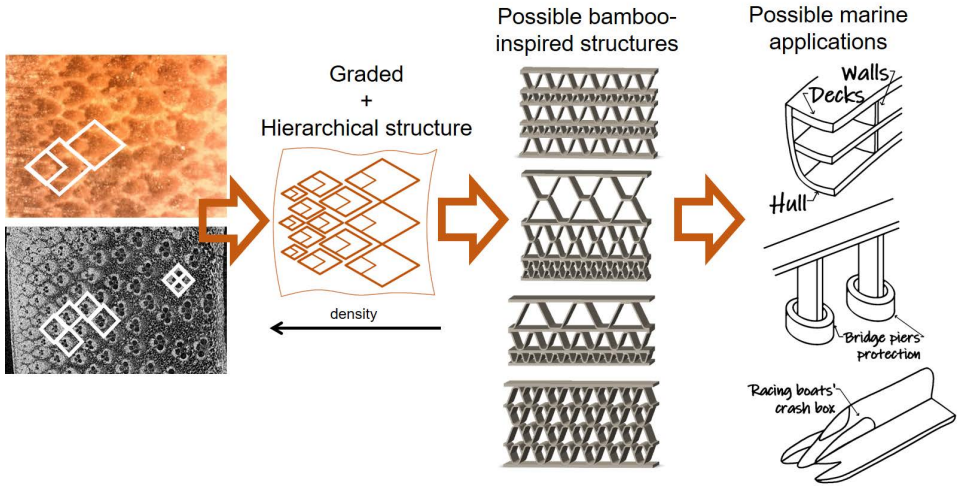

Figure 4.12. Schematic of bio-inspired design process.

protection in marine structures. They may be manufactured both with traditional industrial processes, but also with innovative additive manufacturing techniques. Differently from existing corrugated sandwich structures, which are usually made of a single layer or multi-layers with the same geometrical

characteristics [103, 107, 143], the sandwich structures here suggested include layers with different geometrical properties, arranged so as to resemble the graded and hierarchical structure of bamboo.

Multi-layer corrugated sandwich structures may be used in the marine applications as ship hulls - similarly to hulls with a Y-frame core [144] - as bulkheads, cabin decks or staircase landings [40].

In order to investigate the energy absorption properties of the modelled structures, some samples were manufactured in polylactic acid (PLA) with an Ultimaker2+ 3D printer based on fused deposition modelling technology. The nozzle had a 0.8 mm diameter, the printing speed was set at 50 mm/min and each layer thickness was equal to 0.2 mm.

The geometrical characteristics of the 3D printed samples are displayed in Figure 4.13. The width of all specimens was equal to 26 mm.

Geometrical dimensions were chosen so as to emulate the ratios of graded and hierarchical structure of bamboo measured with the aid of microscopic images.

Structure 1 was inspired by bamboo cellular structure, and consists of two layers with different geometrical characteristics, repeated along the specimen's height. Structure 2 and 3 consists of three layers, each with a double-corrugated core or a simple-corrugate core respectively, and with decreasing dimensions along the height, as to imitate bamboo graded structure. Structure 4 has 4 corrugated layers within which a smaller corrugation was included, with the aim of resembling the hierarchy observed in bamboo structure.

Bio-inspired samples were subjected to compression tests with a universal testing machine at a displacement rate of 10 mm/min. The compressed samples were fully supported on the bottom side and the compression loading was applied with a flat plate on the entire upper surface. The compression tests were recorded with a GOM Digital Image Correlation (DIC) system,

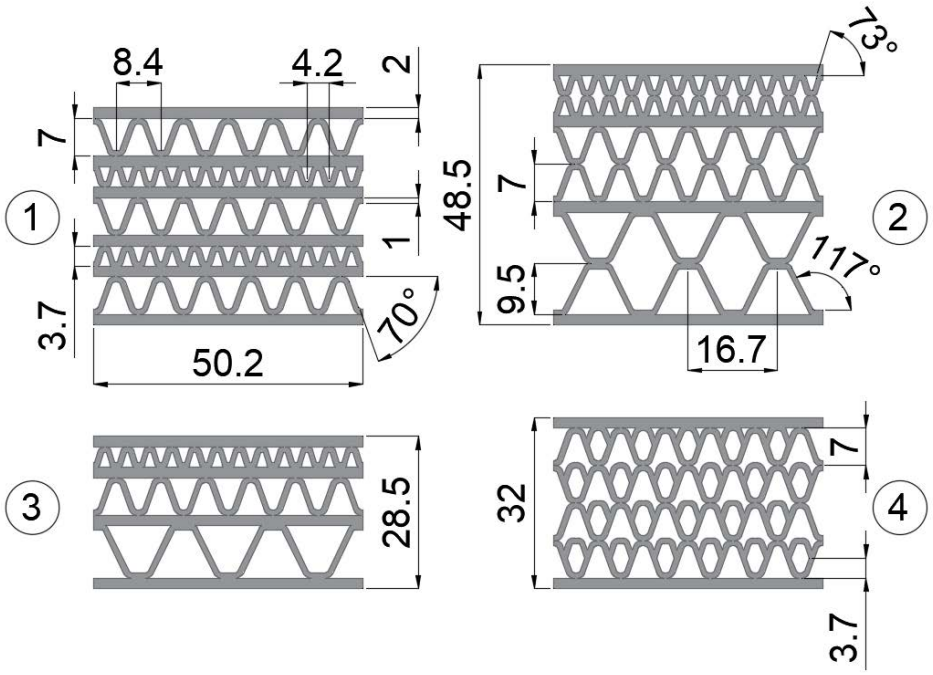

Figure 4.13. Geometrical characteristics of 3D printed samples.

to obtain images synchronised with the compression curves, in order to investigate the collapse mechanisms.

The results yielded by quasi-static compression tests, especially in terms of collapse mechanisms, give an acceptable estimate of low-velocity impact behaviour. The relationship between quasi-static compression and low-velocity impact is often reported in the literature [45, 145] and it is reasonable to consider that this applies also in the following analysis.

The stress-strain curves obtained with compression tests are reported in Figure 4.14. Stress was calculated as the ratio between the force values, measured by the load cell, and the overall area of the specimen's rectangular section.

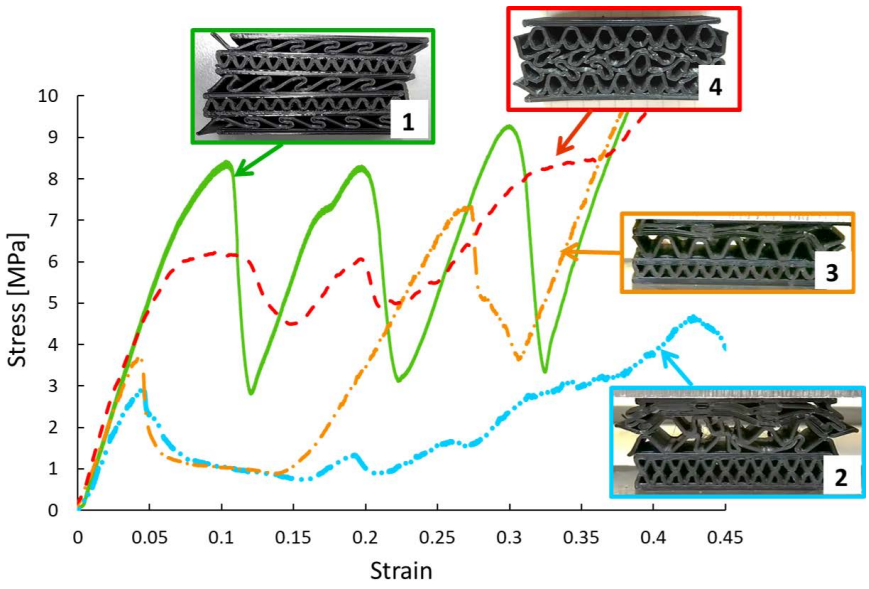

Figure 4.14. Stress-strain curves from compression tests.

In order to assess and compare the energy absorption capabilities of the considered structures, the total energy absorption was evaluated, as the area under the force-displacement curve obtained during a compression tests, according to equation 3.1. In order to provide a valid comparison among the results, the TEA was evaluated up to a displacement of 18 mm. The effect of different specimens' height was considered by evaluating the ratio between the TEA and the overall volume (V) of each specimen.
The compressive strength, the TEA and the ratio TEA/V evaluated for each structure are reported in Table 4.4. In addition, Table 4.4 reports a comparison with the aluminium honeycomb sandwich structure Type 1, analysed in chapter 3.

Table 4.4. Compressive properties of bio-inspired structures and Type 1 AHS.

Structure type	**Compressive strength σ_{cs} [MPa]**	**TEA [J]**	**TEA/V [J/mm^3]**
1	8.4	157.8	0.003
2	3	43.2	0.0007
3	3.7	114.8	0.0031
4	6.1	151.3	0.0036
AHS Type 1	11.8	86.8*	0.0023*

*calculated up to a displacement of 4.5 mm, due to the core thickness of the AHS equal to 9 mm.

The stress-strain curves of the aluminium honeycomb sandwich structure together with the bamboo-inspired structures are displayed in Figure 4.15. Since the AHS is significantly thinner than the bamboo-inspired structures, its TEA was calculated up to a displacement equal to 4.5 mm, which represents the 50% of the entire core thickness.

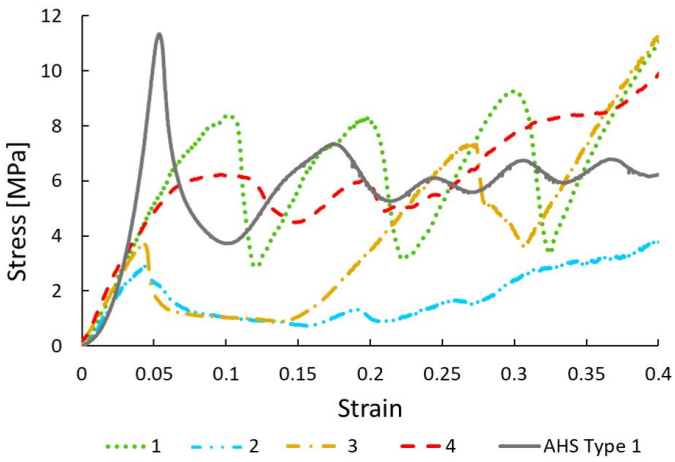

Figure 4.15. Comparison of compression stress-strain curves of bamboo-inspired structures and AHS Type 1.

The compressive response of the investigated structures can be compared to the well-known behaviour of cellular structures [55], as also visible from the comparison with the honeycomb sandwich panel:

- the stress (or load) has a linear trend up to a maximum value, which can be considered the compressive strength σ_{cs} of the structure; this first stage can be associated to the elastic response of the structure;
- then the stress falls as a consequence of the permanent failure in some point of the structure;
- the plateau phase, typical of cellular and foam structures, characterised by a constant stress value, is registered for structures 2 and 3, but it is almost absent for structures 1 and 4;
- other stress peaks follow the first one, as other layers fail after the first one;
- in the end, the load rises sharply as a result of the overall densification of the structure, which is not able to withstand further deformation.

Though the general trend during compression tests is similar for all structures, it is worth mentioning some peculiarities of bio-inspired structures 1 and 4 response.
In structure 1, differently from the others, the first stress peak is followed by two other peaks, almost identical to the first one. This is the result of the collapse mechanism, which produces the failure of the layers with the bigger corrugation, one at a time. Such collapse mode produces for the structure 1, the highest crush strength and TEA. The observed failure sequence for structure 1 could provide a protection mechanism for devices, cables and pipes [4] positioned between the collapsed layers and could delay the risk of complete failure of the structure. For bio-inspired structure 4, the load drop after the initial elastic region is less evident, providing the structure with a

more stable response. Interestingly, for structure 4, the crush phase starts from the central region, preserving the integrity of the outer layers. The TEA of structure 4 is considerably higher than structures 2 and 3 and the TEA per unit volume highlights that structure 4 has better energy absorption properties than structure 1. In addition, structure 4 has an initial peak load lower by about 3 kN than structure 1: this is an interesting property for crashworthy structures, where it is necessary to avoid the transmission of high load to other structures and passengers. The observed properties for structure 4 are the result of the hierarchical structure, which provides an efficient collapse mechanism at reduced volume expense.

The comparison with the honeycomb sandwich structure highlights the interesting compressive properties of the bamboo-inspired structures: even though the compressive strength of the AHS Type 1 is higher, it is necessary to consider that it is made of aluminium and it is a commercial sample with minimum manufacturing defects. In addition, even though the TEA was calculated for different displacement values, the ratio TEA/V for the honeycomb structure is lower than that obtained for the bio-inspired samples.

The obtained experimental results suggested that, among the tested specimens, the configuration of structure 1 and 4, which are inspired by bamboo cellular and hierarchical structure, are particularly suitable for energy absorption applications. Some initial considerations about manufacturing feasibility, indicated that structure 1 is more likely to be applied as an impact-resistant marine structure, thanks also to the collapse mechanisms which provides an effective solution to protect cables and pipes inserted between corrugated layers. Possible use of structure 1 in marine structures, could involve some revisions as the reduction of the number of layers, if needed, to make it cheaper to produce and easier to adapt to real components.

The collapse modes of the corrugated multi-layer sandwich structures were further investigated through the analysis of the frames recorded by a DIC system. By overlapping the acquired frames and the compression curves, the

load peaks were correlated with the collapse events responsible for their presence. The load-displacement curves with the frames recorded immediately after the load peaks, are reported in Figure 4.16.
As visible from the recorded frames, the load peaks are related to the collapse of the inclined walls under compression, which takes the form of buckling failure. The load increase between a peak and the following one is due to the densification of the layer which is failing, before another one starts to collapse.

4.2.1 Theoretical prediction of bio-inspired structures compressive performance

Since the considered bamboo-inspired structures have the shape of corrugated sandwich structures, the existing analytical models for such sandwich type can be applied to predict their compressive strength.
Compression loading in the out-of-plane direction, produces the failure of the core after buckling of the inclined cell walls. As a result, the buckling theory can be applied to the investigated configurations in order to estimate the failure load.
A corrugated core consists of a sequence of triangular or trapezoidal unit cells which extend along the width of the sandwich structure. When subjected to compression in the out-of-plane direction, each unit cell bears a load equal to the total load P divided for the number of cells n, which is further split between two consecutive cell walls. Considering the geometry of the cells, the load acting on each cell wall can be decomposed to a component N acting along the wall and another R acting perpendicularly to the wall. The loading conditions are schematised in Figure 4.17.
As suggested by Rejab and Cantwell [146], the application of the classical beam theory and the buckling theory, considering a perfect adhesion between

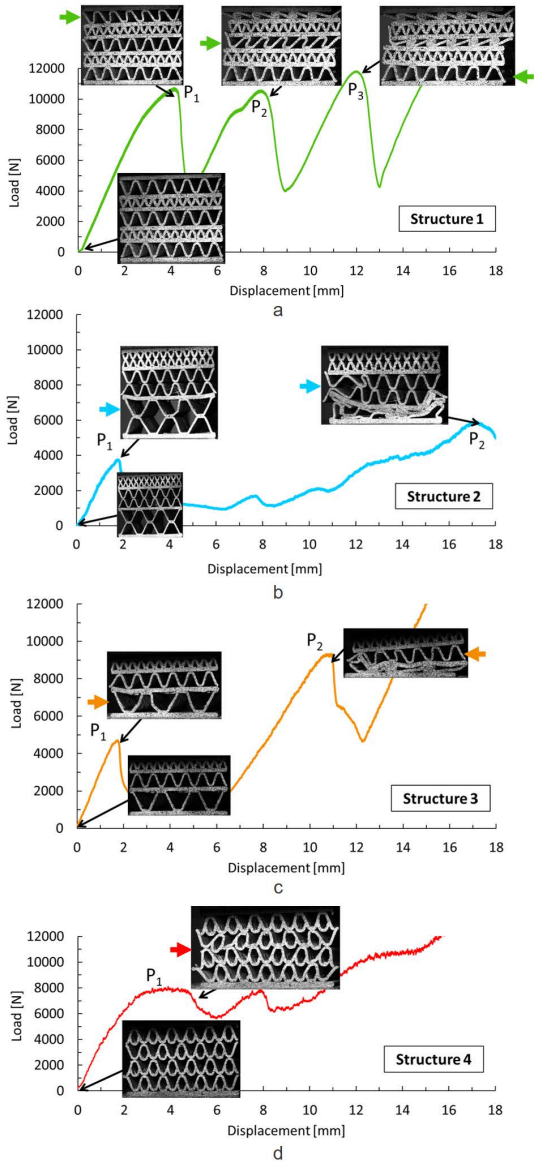

Figure 4.16. Load-displacement curves and images showing the collapse mode of bio-inspired structures a)1, b)2, c)3 and d)4.

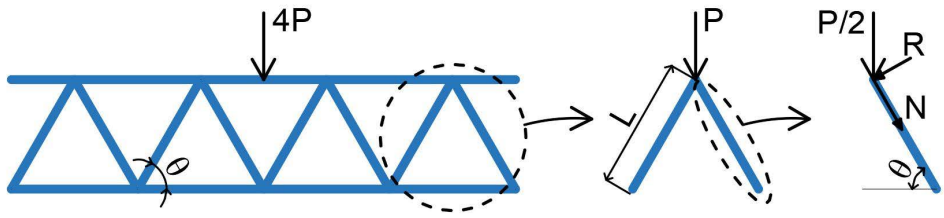

Figure 4.17. Schematisation of loading conditions for the corrugated core under compression.

core and skins, allow the identification of the critical buckling load P_{cr} for a corrugated structure:

$$P_{cr} = \frac{n\lambda^2\pi^2 E b f^3 (l^2 \sin^2\theta + f^2 \cos^2\theta)}{6l^2 \sin\theta} \tag{4.4}$$

In equation 4.4 n is the cell number, λ is a parameter dependent on the boundary conditions, E is the Young's modulus, b is the width of the structure, f is the thickness of the considered wall, l is the length of the wall.
Equation 4.4 was applied to the investigated structures, considering the presence of multiple layers with different geometrical characteristics. For each structure, the critical loads evaluated analytically for each layer, were compared to the load peaks registered during the compression tests. For all specimens b was equal to 26 mm and f to 1 mm; the Young's modulus of the PLA filament after 3D printing, is equal to 2346.5 MPa, according to the manufacturer data sheet. The results of the comparison are reported in Figure 4.18.
The boundary conditions considered in the analytical evaluation were selected on the basis of the collapse modes observed during experimental tests. The condition of both pinned ends suited best structure 1 and 3, where each corrugated layer is separated from the other layer by a solid skin; structures 2 and 4, where solid skins do not separate all the layers, were best modelled

Structure 1

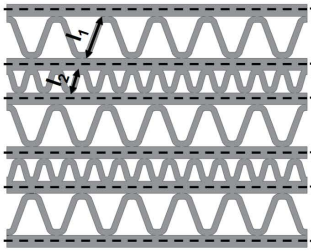

	n	L [mm]	θ [deg]	Boundary conditions	λ	P_{cr} analytical [kN]	P_{cr} experimental [kN]
Layer 1	6	7.9	70	both ends pinned	1	9.2	P_1=10.7
Layer 2	12	3.9	73	" "	1	76.9	N. A.
Layer 3	6	7.9	70	" "	1	9.2	P_2=10.3
Layer 4	12	3.9	73	" "	1	76.9	N. A.
Layer 4	6	7.9	70	" "	1	9.2	P_3=11.1

a

Structure 2

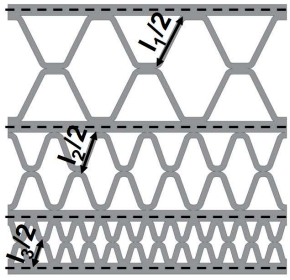

	n	L [mm]	θ [deg]	Boundary conditions	λ	P_{cr} analytical [kN]	P_{cr} experimental [kN]
Layer 1	3	17.5	63	both ends fixed	2	3.7	P_1=3.8
Layer 2	6	15.7	70	" "	2	9.2	P_2=5.9
Layer 3	12	3.9	73	" "	2	76.6	N. A.

b

Structure 3

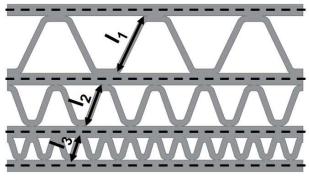

	n	L [mm]	θ [deg]	Boundary conditions	λ	P_{cr} analytical [kN]	P_{cr} experimental [kN]
Layer 1	3	8.5	63	both ends pinned	1	3.7	P_1=4.7
Layer 2	6	7.9	70	" "	1	9.2	P_2=9.3
Layer 3	12	3.9	73	" "	1	76.9	N. A.

c

Structure 4

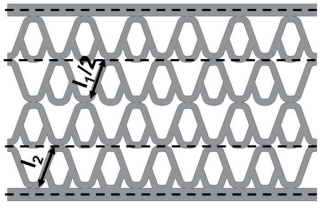

	n	L [mm]	θ [deg]	Boundary conditions	λ	P_{cr} analytical [kN]	P_{cr} experimental [kN]
Layer 1	6	7.9	70	both ends fixed	2	36.7	N. A.
Layer 2	6	15.7	70	" "	2	9.2	P_1=7.3
Layer 3	6	7.9	70	" "	2	36.7	N. A.

d

Figure 4.18. Analytical end experimental critical loads for corrugated layers of structures a)1, b)2, c)3 and d)4.

considering that both ends of one layer are fixed. In addition, for structures 1 and 3, the length l was considered equal to the length of the inclined wall between two consecutive skins; whereas for structures 2 and 4, l was considered equal to the length of two consecutive walls. Such considerations were derived from the observation of collapse mechanism during compression tests, which highlighted that the absence of skins between layers, makes two walls belonging to adjacent layers behaving as a single wall. Figure 4.18 shows the length l selected for each structure.

For structures 1, 2 and 3, the analytical prediction provides an excellent approximation of the experimental results for the first load peak.

For structure 4 the theoretical analysis yields a less accurate result, but within an acceptable range in comparison to the experimental value. The reasons of such difference between analytical and experimental results in structure 4, could lie in the geometrical complexity of the structure, which resemble the hierarchical system of bamboo structure. It is therefore difficult to match real and theoretical boundary conditions and to select the correct cell wall length.

In addition, for each structure several sources of deviation from the analytical model should be considered; for instance, the 3D printing process could be responsible for imperfect bonding between core and skins, geometrical inaccuracies, discrepancy between real and theoretical boundary conditions or material deterioration during 3D printing process.

Good matches were obtained also for the other load peaks for structure 1 and 3, whereas structure 2 registered a second load peak slightly lower than the predicted one. This is probably the result of bonding imperfections between two adjacent layers, which produces an asymmetric collapse of the intermediate layer, visible in Figure 4.16, not predictable with an analytical model.

However, the applied analytical model allow the identification of the collapse sequence of multi-layer corrugated structures, which starts from the

layer with the larger value of l, when other geometrical parameters are the same in the other layers.

In general, the buckling theory offers a simple and effective tool to predict the collapse load and the collapse sequence of multi-layer corrugated structures. Consequently, the design of lightweight sandwich structures based on a corrugated shape, could be supported by the application of buckling theory, when compression strength is required. Optimization processes, addressed to weight savings and compression resistance, could also be based on buckling consideration.
The performed analysis provided preliminary data for future development of bio-inspired impact-resistant marine structures. Further investigations, considering also metallic materials instead of polymeric ones, will be performed to provide guidelines for a more complex and optimised design.

4.3 Final remarks

The application of biomimetic approach could represent an innovative response for the design of lightweight marine structures. For this purpose, bamboo was examined under low-velocity impact conditions, evaluating the relationship between its structure and its mechanical response. The obtained responses were applied for the preliminary design of some bio-inspired lightweight impact-resistant structures. The detected impact response of bamboo can be related to a combination of mechanisms strongly dependent on its graded structure. The main conclusions deriving from experimental investigations on bamboo are the following:

- Critical impact energy depends on bamboo thickness; in addition, specimens impacted on the outside at E_{cr} failed completely, whereas specimens impacted on the inside at E_{cr} were still capable of absorbing a small amount of energy before splitting in two halves;

- A normalised energy E_n depending on thickness was defined for each impact condition and its value was found to be related to impact strength. In addition, this parameter is useful to provide energetic comparison among experimental data;
- Abraded specimens impacted on the outside had a higher normalised energy E_n than not-abraded specimens and show a less severe damage; this is the result of removing the harder outside layer which is probably a protection for the bamboo from other environmental factors, but it is not useful for impact resistance; in addition, abraded samples impacted on the outside experienced a higher improvement in energy absorption capabilities in comparison to abraded samples impacted on the inside and this could be the effect of the graded structures;
- Crack propagation may be influenced by bamboo's cellular graded structure, since cracks travel along fibre bundles interfaces.

Such observations suggested that graded cellular structures may be successfully applied to improve crashworthiness in several applications, including the marine industry. Taking inspiration from the phenomena involved in bamboo impact resistance, four multi-layer sandwich structures were designed in order to be applied, for instance, in marine applications, when low-velocity impact resistance combined with lightweight properties are required.

The bamboo-inspired structures where modelled as multi-layer corrugated sandwich structures, in order to take into account the manufacturing feasibility and the applicability in the marine field. A preliminary analysis of their energy-absorption properties was performed by testing under compression loading some samples manufactured in PLA with 3D printing technology.

The obtained results highlighted the predominance of cell walls buckling as the responsible mechanism in compression failure. This allowed the application of the buckling theory to analytically predict the failure load and

the collapse sequence in multi-layer corrugated sandwich panels subjected to compression. Good agreement between analytical and experimental results was observed. It is therefore reasonable to suggest that a proper application of such theoretical formulation, may support the design and optimisation of crashworthy and lightweight devices, based on bamboo structure.
The performed analysis could represent a preliminary step in the application of biomimetics principles to lightweight marine structure design. Future developments will consider the application of metallic materials, other loading conditions and manufacturing constraints, in order to obtain reliable data to support the design of complex lightweight marine structures.
The development of additive manufacturing techniques will probably enhance and encourage the design of innovative bio-inspired structures for marine industry. Nevertheless, at present, additive manufacturing techniques are not economically competitive for large structures production.
For such reason, the next chapter will deal with a comparison between a traditional GFRP structure and an AHS-based structure, rather than a bio-inspired solution.

5

Comparison of GFRP and aluminium honeycomb sandwich panels for marine structures

The benefits of lightweight philosophy applied to marine structures and the advantages offered by sandwich structures introduction were extensively discussed in Chapters 1, 2 and 3.

Almost exclusively, marine applications use fibre reinforced plastic (FRP) polymeric foam-cored sandwich structures, with some use of honeycomb cores in the very small high-performance/racing vessel sector of the industry. Further, a very high percentage of the FRP used in marine sandwich skins is glass reinforced polyester resin, commonly referred to as GFRP (glass fibre reinforced plastic). However, as observed in section 2.4.1.1, the major

drawback of composite sandwich panels is the difficulty of disposing of them - and of the waste disposable products of the production process - at end of life.

Indeed, concerns about the sustainability of the materials used are attracting the attention of customers and hence institutions and shipbuilders. Therefore, sustainability issues should be addressed right from the start of the design phase with an intelligent selection of materials, but which must also comply with the structural and weight constraints.

As pointed out in chapter 3, aluminium sandwich structures with cellular cores could represent a sustainable, lightweight and efficient solution for several marine applications. However, the success of aluminium sandwich components in marine applications depends on the knowledge of their performance, on their economical competitiveness but also on the availability of effective guidelines for their design and of methodologies for their selection and comparisons.

The organisation of scientific data and knowledge into practical tools and procedures, is a necessary step towards a wider use of aluminium sandwich components for structural applications in the marine industry and it is under the responsibility of researchers and experts of the field.

In light of the above considerations and of the investigations described in the previous chapters, a comparison of GFRP and aluminium honeycomb sandwich panels was outlined. The aim was to substantiating the advantages of the use of aluminium sandwich structures for marine applications by providing guidelines to their selection, based on comparisons with other materials and on analytical predictions of their mechanical properties.

The analysis was outlined in the following phases:

- A mechanical parameter was chosen to provide a valid equivalence with other material structural solutions already commonly used in the marine industry;

- Analytical formulations were used to evaluate this mechanical parameter for different sandwich structure options (core configurations, geometrical characteristics, core and skin materials, etc.);

- Material charts reporting the relationships between several mechanical and physical properties of these sandwich structures were provided, to assist in the optimal selection of the main sandwich structure design variables;

- An example case study regarding a specific marine structural design, based on the previous comparisons, was defined.

5.1 Mechanical properties equivalence and evaluation

In order to verify the effectiveness of aluminium and other metallic sandwich structures for marine applications, a preliminary equivalence with more common structural solutions - which are mainly represented by GFRP panels - is required. The substitution of an existing composites sandwich structure design approach with one using all-metal sandwich panels, needs to be carried out whilst ensuring that there is a common baseline criteria to which each approach conforms to – i.e. there must be some form of "equivalence" between the two designs. Only by providing a common baseline for the different structural design approaches may valid conclusions as to the advantages and disadvantages of each be drawn.
In addition, such an equivalence is useful to assess and decide upon the practical geometrical configuration of all-metal sandwich panels, which must also take into account which specific plate thicknesses, core configurations, alloys etc. are readily available in the commercial market.

The bending stiffness was selected as the parameter on which the equivalence of all-metal and composite sandwich structures was based. This was

because metallic sandwich panels in marine applications would be a candidate for replacement of GFRP sandwich structures, whose design is most often stiffness constrained. In addition, reliable analytical formulations for the bending stiffness of sandwich panels are well developed and accepted [43, 44] and their experimental evaluation is relatively straightforward.

In order to provide a realistic evaluation, the reference bending stiffness for the claimed purposes was established on data for marine structures reported in the literature. In particular, the study of Muscat-Fenech et al. [147] of impact damage testing on composite marine sandwich panels was identified as the reference work for the current bending stiffness benchmark. In their work the authors designed various candidate composite panels for a specific local boat builder according to the BS EN ISO 12215-5 standard for small craft. The selected materials were PVC foam for the core and glass-fibre reinforced plastics for the skins. They arrived at seven different candidate designs for the same small motor craft, with core thicknesses c varying from 10 to 30 mm and skin thicknesses t ranging from 0.81 to 1.76 mm. Panels were manufactured according to each design which were then tested to characterised their structural responses. ASTM D7250M-06 was used as the reference standard for flexural stiffness D evaluation with testing of 75 mm wide specimens. The stiffness values thus obtained by Muscat-Fenech et al., which are used as benchmark values "typical" of marine structure in the current study, are shown in Table 5.1.

From the values in Table 5.1 it is clear that relatively small variations in skin thickness and, most importantly, core thickness have a significant effect on bending stiffness. Therefore, these parameters need to be selected carefully in order to fulfil structural requirements, but also to satisfy other constraints such as weight or space requisites.

The bending stiffness of a sandwich panel under three-point bending was reported in equation 2.2, which was applied to assess the bending stiffness of

Table 5.1. Candidate marine composite sandwich geometrical parameters and flexural stiffness [147].

Panel	**Core thickness c [mm]**	**Skin thickness t [mm]**	**Bending stiffness D [N mm^2]**
A	10	0.81	$49.6{\cdot}10^6$
B	10	0.67	$45.3{\cdot}10^6$
C	15	1.35	$248{\cdot}10^6$
D	15	2.03	$374{\cdot}10^6$
E	20	1.22	$393{\cdot}10^6$
F	25	2.03	$945{\cdot}10^6$
G	30	1.76	$1160{\cdot}10^6$

several candidate commercially available all-metal sandwich panels in order to compare their bending stiffness with the target range (Table 5.1).
Some hybrid (metal-composite) sandwich structures were also included in the comparison in order to provide a more general overview on lightweight sandwich structures properties.
The sandwich structures included in the comparison and their properties are summarised in Table 5.2. Literature studies used to derive properties and information are also indicated.
The Young's modulus of the facings E_f for each sandwich structure was provided by the suppliers or taken from the literature; the Young's modulus of the cellular core E_c was evaluated from formulations established in the literature. In particular, for honeycomb core the Young's modulus E_c was evaluated according to the equation suggested by Gibson and Ashby [55]:

$$E_c = 2.3E_s \left(\frac{\sqrt{3}}{2}\right)^3 \left(\frac{\rho_c}{\rho_s}\right)^3 \tag{5.1}$$

where E_s is the Young's modulus of the solid material, ρ_c is the density of the core and ρ_s is the density of the solid material.

Table 5.2. Summary of the main properties for the sandwich structures included in the comparison.

Sandwich type	**Skin material**	**Core material**	**Considered core thickness c [mm]**	**Considered skin thickness t [mm]**	**Considered cell size s [mm]**	**Core density ρ_c [kg/m^3]**	**Ref.**
All-Aluminium honeycomb	Al series 3000	Al series 3000	3÷21	0.5 – 0.8 - 1	6	56	-
	Al series 1000	Al series 3000	3÷21	1	6	56	-
	AA 5754	AA 5052	9	1	3÷6	130- 80	Type 1 (3) [92, 93]
Aluminium-steel honeycomb	AISI 304	Al series 3000	5÷12	0.5 - 1	6	56	-
Aluminium foam	Al 3103	Al series 4000 (AlSi7)	3÷19	1	-	450	[148]: c=9 mm
	Al 99.5%	Al series 4000 (AlSi10)	3÷19	1	-	530	
GFRP-titanium lattice BCC	GFRP	Ti6Al4V8Si	7÷23	1	-	529	[109]: c=7.5 mm
Aluminium-aramid honeycomb	Al series 3000	HRH	3÷20	1	3.2	80	-
GFRP-PVC	GFRP	PVC foam	15÷30	15÷30	1.35÷1.76	100	[147]

For foam core, the following formulations by Gibson and Ashby [55] for the Young's modulus E_c was applied:

$$E_c = C_1 \left(\frac{\rho_c}{\rho_s}\right)^2 \tag{5.2}$$

where $C_1 \approx 1$ for open cell foams. For the GFRP titanium lattice with a body centred cubic (BCC) unit cell, the experimental results from Ref. [109] were adopted.

Flexural stiffness was calculated according to equation 2.2 for each sandwich structure and for each available combination of facing-core thickness. The panel width was set at 75 mm for all calculations to ensure equivalence with the values given in [147]. From the obtained results, the combinations which provided bending stiffness values similar to the range of those of Ref. [147] were selected as relevant. Panels A and B from [147] (see Table 5.1), which have the lowest values of D, were excluded from this comparison since very few of the all-metal and hybrid panels considered gave bending stiffness similar to those of panel A and B and these were the panels with very thin cores (3-4 mm), making them hardly dissimilar to a solid plate.

The all-metal and hybrid sandwich structures with a bending stiffness comparable to panels C-G from [147] were considered for further comparisons in order to evaluate the relationship of bending stiffness with other sandwich structures properties which can be crucial during the design process, such as the core thickness, overall panel density ρ_p and areal density ρ_A (the product of density and thickness). The bending stiffness was plotted against each of these parameters in Figures 5.1, 5.2 and 5.3, giving charts useful for sandwich selection in stiffness-constrained design. ρ_p and ρ_A of the panels from [147] were estimated analytically from the data reported in the reference.

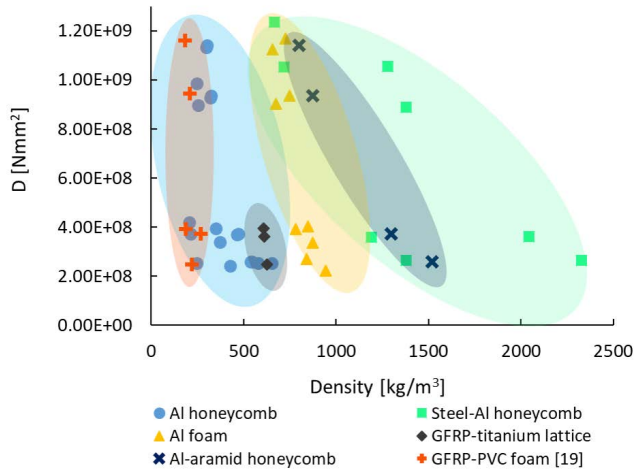

Figure 5.1. Bending stiffness vs sandwich panel density.

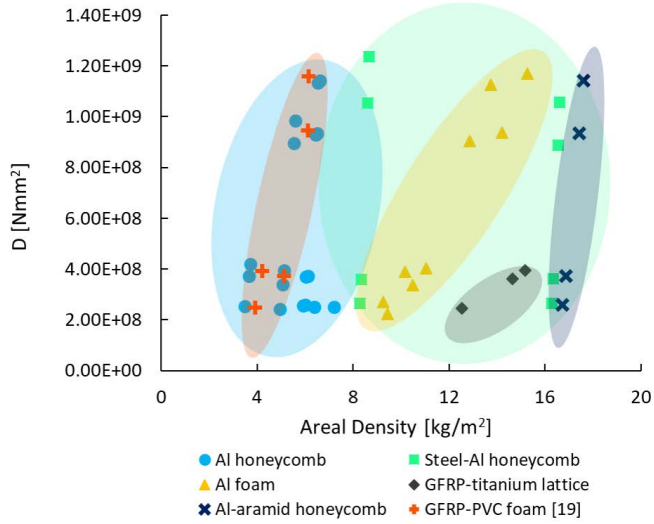

Figure 5.2. Bending stiffness vs sandwich panel areal density.

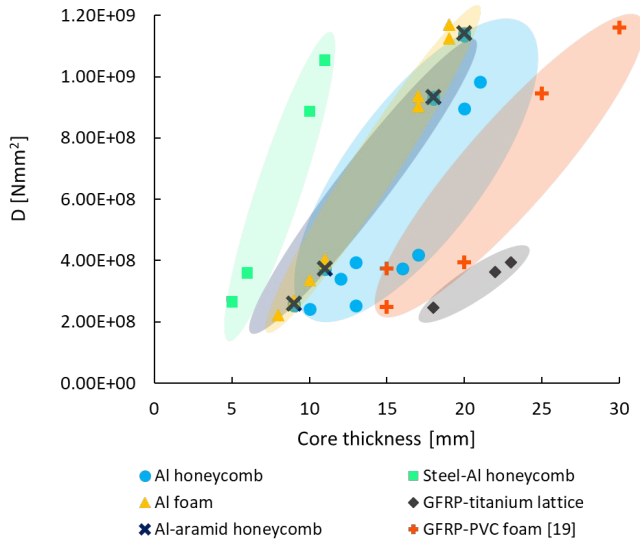

Figure 5.3. Bending stiffness vs core thickness.

Table 5.3 shows three examples of how a sandwich bending stiffness of approximately $2.5{\cdot}10^8$ Nmm^2 can be obtained using different combinations of core and skin thicknesses for an all-Al series 3000 aluminium honeycomb sandwich structure.

Table 5.3. Examples of AHS panels (Al series 3000 core and skin) with different core and skin thickness combinations giving approximately equal bending stiffness.

Core thickness c [mm]	**Skin thickness t [mm]**	**Resulting stiffness D [N mm^2]**	**Resulting density ρ_p [kg/m^3]**	**Resulting areal density ρ_A [kg/m^2]**
9	1	2.6 108	542.8	6
13	0.5	2.5 108	248.4	3.5
10	0.8	2.4 108	427.6	4.9

Figures 5.1 and 5.2 show that among all-metal or hybrid sandwich panels, all-

aluminium honeycomb sandwich structures provide the lowest density and areal density for a given bending stiffness. In addition, they have very similar properties to the sandwich panels from [147] and this suggest that they are attractive competitors for the GFRP sandwich structures, especially given their much improved recyclability. All-aluminium foam sandwich structures could also provide an alternative solution, whereas steel-aluminium honeycomb sandwich panels are not very particularly lightweight due to their heavy steel skins, especially with the thicker 1 mm skins. Although GFRP-titanium lattice sandwich panels provide intermediate properties, their elevated cost and their technological feasibility for large structures do not make them suitable for marine applications. Aluminium-aramid honeycomb sandwich panels do not offer any particular advantage in terms of a stiffness for density point of view, but their wide availability and the fact that they can be manufactured into complex shapes could be advantageous for some applications.

As shown in Figure 5.3, for a given flexural stiffness value, the composite sandwich panels - considered here as stiffness benchmarks - require the highest core thickness, whereas steel-aluminium honeycomb sandwich structures require the lowest core thickness, followed by aluminium foam and then aluminium honeycomb panels. In other words, for a given core thickness, GFRP-PVC foam panels produce a lower bending stiffness in comparison to the rigidity achievable with other sandwich panel solutions such as AHS or aluminium foam sandwich.

The advantages attainable by replacing polymer-based sandwich panels with all-metal ones, and in particular with aluminium honeycomb sandwich structures, are clearly deducible from the material charts presented in Figures 5.1-5.3. Consequently, wider applications of similar structures, supported by extensive experimental and analytical evidences, could lead to improvements in marine structures both from mechanical and environmental points of view. Plotting materials maps similar to those reported in Figures 5.1-

5.3 could support the preliminary selection of lightweight structures aimed at optimising some crucial aspect, such as weight, and at guaranteeing the structural equivalence with existent solutions.

5.2 Failure map-driven design for honeycomb sandwich structures

The materials charts developed in the previous section could aid in the selection of a convenient structure to improve the lightweight, environmental and volume properties of a marine structure, for instance when compared to common GFRP-based panel manufacture. Once an alternative structure is selected, the designer then needs to identify the main geometric variables to proceed with calculations and other analyses. Such a process might require the consideration of several aspects of the selected structures, such as mechanical or physical constraints.
Therefore, a procedure which takes into account the main issues encountered in the replacement of an existing polymer-based sandwich structure with an all-metal sandwich structure has been developed. The main steps of this method are summarised in Figure 5.4.

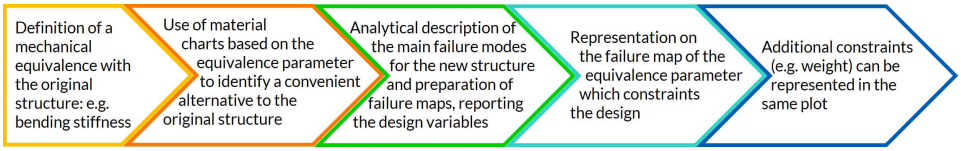

Figure 5.4. Sequence of the design procedure based on material comparisons and mechanical equivalence.

The preliminary comparison, performed in section 5.1, among different structural solutions in terms of panel density and volume criteria led to the selection of aluminium honeycomb sandwich structures as potential competitors for GFRP sandwich structures.

In order to perform further illustrative comparisons, a specific example of an aluminium honeycomb sandwich panel was selected. In particular, it was chosen the AHS Type 1 described in 3, whose main properties are given in Table 5.4.

Table 5.4. Properties of the selected aluminium honeycomb sandwich structure.

Skin material	AA 5754
Core material	AA 5052
Skin thickness [mm]	1
Cell diameter [mm]	3
Skin Young's modulus E_f [MPa]	67000
Core Young's modulus E_c [MPa]	11.8
Yield stress skin material σ_{fy} [MPa]	155
Compressive strength core material σ_{cc} [MPa]	3.3
Shear strength of the core τ_{cs} [MPa]	0.9

Since flexural stiffness was used as the equivalence parameter with traditional marine composite sandwich structural panels, the bending behaviour of the selected honeycomb sandwich structure was focused upon for further considerations.

As already observed in section 3.2.1.2, a previous experimental study performed on the selected aluminium sandwich structure [95], highlighted that under three-point bending conditions, two collapse modes occur:

- Mode I, which involves indentation under the load actuator, combined with the rotation of the two halves of the sample around the mid-plane and with the formation of 4 plastic hinges (see Figure 5.5a);
- Mode II, which is similar to core shear AB, reported by Kesler and Gibson for metallic foam core sandwich structures [122]. This mode consists of the formation of one plastic hinge in each skin at the load point, with one half of the beam entirely deforming in shear, but the other half deforming by shear only between the load application point

and the support, where two other plastic hinges form (see Figure 5.5b). Core compression is also seen in the load application area.

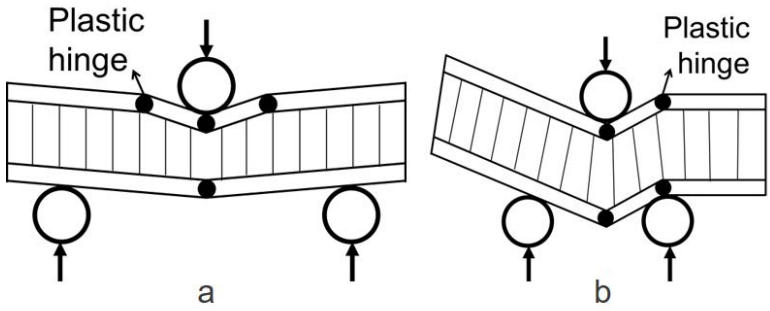

Figure 5.5. Scheme of collapse Mode a) I and b) II.

The manifestation of the two different collapse modes depends upon the boundary condition, and in particular on the support span: smaller support spans trigger the Mode II core shear failure, whilst for larger support spans Mode I indentation prevails. For a given sandwich design and loading conditions the dominant failure mechanism is that which produces the lowest failure load.

In Ref.[95] the analytical formulations to predict the failure load for both collapse modes were introduced and their reliability verified against experimental results. The expressions for the failure load of Mode I and Mode II are:

$$F_I = \left(bt\sqrt{3\sigma_{cc}\sigma_{fy}}\right) + \left[\sigma_{fy}\frac{bt^2}{L} + 2bc\tau_{cs}\left(1+\frac{2H}{L}\right)\right] \tag{5.3}$$

$$F_{II} = \sigma_{fy}\frac{bt^2}{L} + 2bc\tau_{cs}\left(1+\frac{2H}{L}\right) + \sigma_{cc}\frac{bL}{4}. \tag{5.4}$$

In equations 5.3 and 5.4, L is the support span and H is the overhang length on one side.

In order to evaluate the effect of various design parameters on the mechanical response of the sandwich structure, these same expressions were used to draw a failure map for the considered AHS structural panel.

A failure map displays the transition conditions between two different mechanisms, which occur when both mechanisms may produce the same failure load. For the aluminium honeycomb sandwich panels considered here, under three point bending only two failure mechanisms were observed. Hence the failure map will display only one transition line, which is obtained by equating the failure load for Mode I (equation 5.3) with that of Mode II (equation 5.4). In order to provide data in a convenient form for design purposes, the failure map is presented here in plots of core c against facing thickness t, both normalised with respect to the support span, L (i.e. plots of c/L against t/L). The equation of the transition line between Mode I and Mode II in terms of the parameters c/L and t/L is:

$$\frac{c}{L} = \frac{1}{-2b\tau_{cs}H}\left[-\sigma_{fy}bt\frac{t}{L} - \sigma_{cc}\frac{bL}{4} + bt\sqrt{3\sigma_{cc}\sigma_{fy}}\right]. \tag{5.5}$$

As observed above, the geometrical parameters such as c and t also affect flexural stiffness, and therefore reporting this information in the failure map should provide valuable data for selection of the sandwich panel structure during the design phase.

It is clear that some of the design variables need to be set in order to plot the failure map and the trend of bending stiffness in terms of c/L against t/L .In addition, in order to represent the bending stiffness in terms of a c/L against t/L plot it is necessary to introduce a simplification into its formulation.

As observed in section 2.3.1, the first and second term in the expression of bending stiffness 2.2 are negligible in common sandwich structures [43]. In

addition,if the facings are thin enough in comparison to the core then the distance d is approximately equal to that of c. Thus the flexural rigidity expression reduces to:

$$D \cong E_f \frac{btc^2}{2}. \tag{5.6}$$

Expressing D in terms of the variables c/L and t/L yields:

$$\frac{c}{L} = \sqrt{\frac{D}{L}\frac{2}{E_f b}\left(\frac{t}{L}\right)^{-1}} \tag{5.7}$$

Figure 5.6 presents a failure map for the currently considered aluminium honeycomb sandwich structural panel, for which facing thickness t and overall panel length, L_{tot} were set to 1 and 200 mm, respectively. Three different stiffness curves are plotted; one each for $D = 2.52 \cdot 10^8$, $3.93 \cdot 10^8$ and $9.45 \cdot 10^8$ Nmm^2.

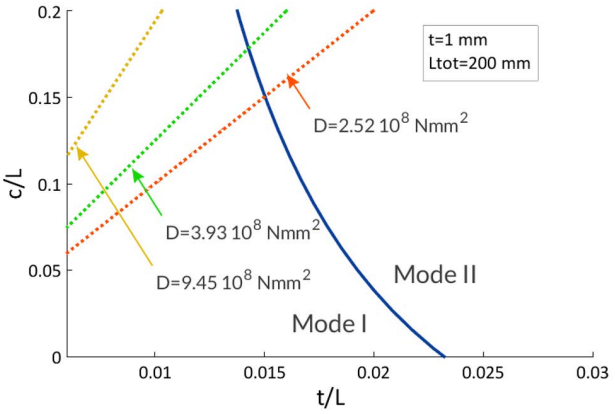

Figure 5.6. Failure map for the considered AHS, reporting three stiffness curves.

The values of $3.93 \cdot 10^8$ and $9.45 \cdot 10^8$ Nmm^2 for D correspond to those of panels E and F from Ref.[147] respectively, which are the target baselines for the current analysis. The value of $D = 2.52 \cdot 10^8$ Nmm^2 is obtained for the considered honeycomb sandwich panels with a core thickness equal to 9 mm, as used in Ref. [95] and in chapter 3.

As can be seen from Figure 5.6, after establishing certain parameters such as skin thickness (which for commercially available all-metal sandwich structures is usually limited to a few discrete options) and stiffness and beam overall length (which could be design constraints) it is possible to select a core thickness and support span to ensure the preferred failure mode for the final application case.

Further information to support preliminary design and selection of lightweight sandwich structures can be obtained by applying an optimisation procedure to one (or more) of the design variables. Since weight is a crucial issue for marine structures, an optimal selection of sandwich panels in terms of weight is desirable.

A single-objective optimisation procedure, similar to that described in Refs. [55, 149], can be applied to aid the selection of the main structural sandwich design variables with the aim of minimising weight.

The mass m of a sandwich panel, which is the objective function in the optimisation procedure, is equal to:

$$m = bL\left(2\rho_f t + \rho_c\right) \tag{5.8}$$

where ρ_f is the facing density.

This formulation of mass expressed in terms of c/L and t/L is:

$$\frac{c}{L} = \frac{m}{L^2 b \rho_c} - \frac{2\rho_f}{\rho_c}\frac{t}{L}. \tag{5.9}$$

Some of these variables need to be set in order to proceed with the design and its optimisation. By way of example, the variables selected to be fixed were ρ_f, ρ_c, b and L. To give a slightly different possible example to that shown in Figure 5.6, for the mass optimisation case it was decided to set the support span L as a design requirement whereas the skin and core thicknesses, t and c, were optimisation variables.

A graphical optimisation approach is useful to visualise the effects of different parameter variations, which are often constrained both by product commercial availability and technological limitations. An example is shown in Figure 5.7 where the following lines are plotted:

- the transition line between Mode I and Mode II, according to equation 5.5;
- a line representing the stiffness constraint of the design; a flexural rigidity of $2.52{\cdot}10^8$ Nmm^2, according to equation 5.7;
- the mass variation, according to equation 5.9: several of these parallel lines are shown, each for a different mass value.

The plot in Figure 5.7 presents the failure map, which allows the designer to distinguish between the zones of Mode I and Mode II failures, together with the stiffness constraint and also the panel weight, the latter of which is the optimisation parameter in the present example. The designer may then select the point on the stiffness constraint line which meets a minimum weight requisite, whilst ensuring that the corresponding core and skin thicknesses are both commercially readily available. Further, if one failure mode is desirable over the other then the closest $c/L - t/L$ combination both commercially available and falling within the relevant failure mode zone is readily identifiable from Figure 5.7.

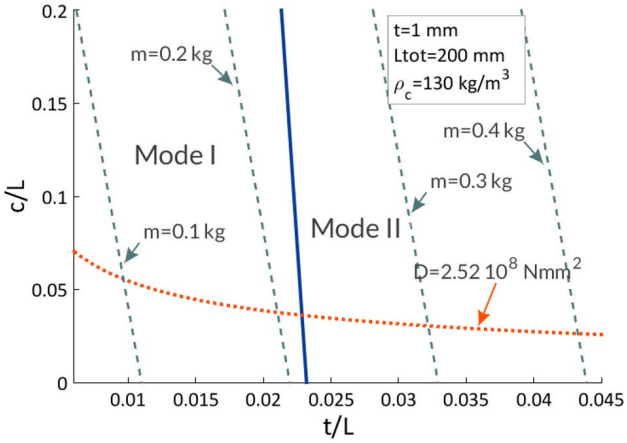

Figure 5.7. Graphical approach for design optimisation, considering stiffness, weight and failure modes, for the analysed AHS.

5.3 Replacement of GFRP sandwich with aluminium honeycomb sandwich: the case of a ship balcony overhang

In order to suggest a simple procedure to perform a preliminary selection of sandwich structure design variables, and to show the potential of metallic sandwich structures, an example of the application of materials charts and properties comparisons - discussed in sections 5.1 and 5.2 - in the design of a lightweight component for a real marine application was examined.

A ship balcony overhang was selected as the structure for the case study, since this is a plausible entry point where composites are very likely to enter into the structural design of cruise ships, ferries and other passengers ships [150]. The balcony structure used as a reference was deduced from the literature and, in particular, from the study by Kharghani and Guedes Guedes Soares [60] of a hybrid steel-GFRP balcony overhang.

This reference structure consists of a sandwich panel with balsa core and GFRP skins, integrated into a steel support which overlaps the sandwich

panel for part of its length. The balcony from Ref.[60] (which was already presented in chapter 2 in Figure 2.13) is displayed in Figure 5.8.

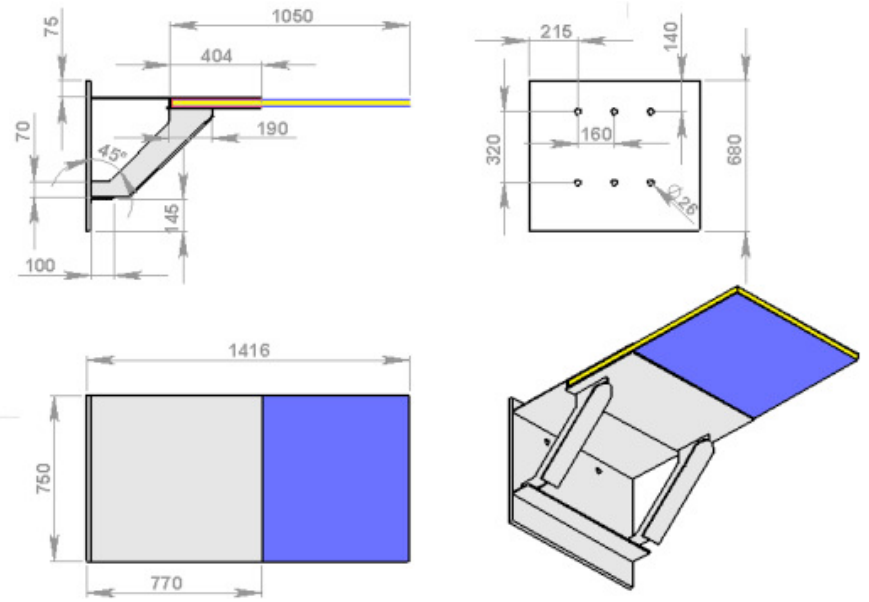

Figure 5.8. Balcony structure tested by Kharghani and Guedes Soares, reprinted from [60], with permission from Elsevier.

In the cited work the balcony structure was experimentally subjected to two types of loading condition: shear and bending controlled; the former obtained by applying the load in the proximity of the steel-sandwich overlap area, the latter by applying the load at the overhang extremity (as shown in Figure 2.13). Only the bending condition was used for comparison and design purposes in the current section. The main characteristic of this reference structure are summarised in Table 5.5.

The aim of the present section was to evaluate the potential advantages of the substitution of the composite panel used as the balcony overhang in Ref. [60] with an all-metal sandwich structure. The re-design process was focused

Table 5.5. Main properties of the reference structure [60].

Skins material	GFRP
Core material	Balsa wood
Skin thickness [mm]	2.5
Core thickness [mm]	30
Width [mm]	750
Overall length [mm]	1050
Length not overlapped by steel [mm]	646
Skin Young's modulus in the longitudinal direction [MPa]	26400
Weight of the entire structure (steel frame included) [kg]	150
Sandwich panel weight [kg]	15

solely on the sandwich panel, leaving the supporting steel frame, visible in Figures 2.13 and 5.8, unchanged. As proposed in section 5.1, the substitution was based on bending stiffness equivalence and aluminium honeycomb sandwich structures were selected to replace the composite sandwich panel.

The flexural rigidity D of the composite panel tested by Kharghani and Guedes Soares [60] was evaluated here according to equation 5.6 equal to $2.6{\cdot}10^{10}$ Nmm^2 and this was hence set as the target stiffness requirement for the replacement aluminium honeycomb sandwich panels. The width b and the length L of the balcony overhang were kept the same as in the original structure, i.e. 750 and 1050 mm, respectively. The selection of the design variables, namely the core and skin thicknesses and the core density, can be supported by plotting the rigidity boundary and the mass objective function on a c/L – t/L chart. In order to summarise all the information in a bi-dimensional plot, it is necessary to set some of the variables. In particular, in this case the desired mass for the replacement sandwich structure was set at 7 kg, in order to obtain a 50% reduction of the sandwich panel weight in comparison to the original structure. Once the mass is established, several lines representing the weight objective function, one for each core density, can be drawn according to equation 5.9. The obtained plot is shown in Figure 5.9.

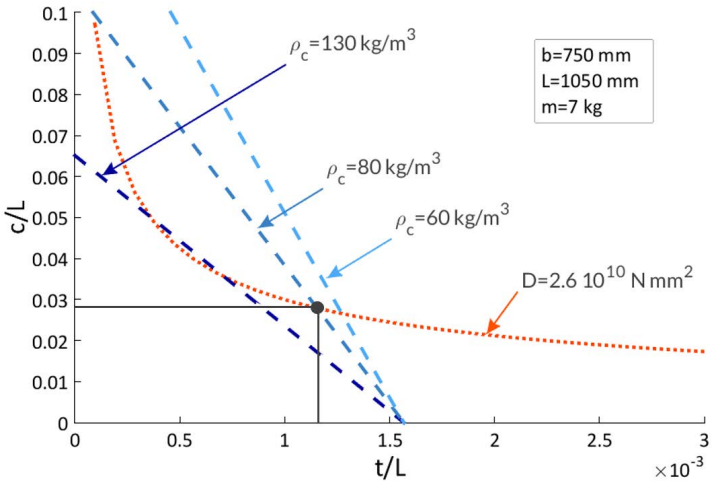

Figure 5.9. Graphical method for design variables definition, after establishing the flexural stiffness and the desired weight of the AHS panel.

The core density values (i.e. 130, 80 and 60 kg/m^3) displayed in Figure 5.9 were selected as examples of the commercially available solutions, but, in practice, this value could depend on several factors such as specific regulations or cost restrictions. Plotting different lines for different $_c$ is also useful to verify the effect of the variation of such a parameter on the other variables. Once the required core density is decided upon, the intersection between the stiffness constraint and the line representing the weight function allows the identification of the required core and skin thicknesses.

For instance, for a core density of 80 kg/m^3, as shown in Figure 5.9, the obtained design variables are summarised in Table 5.6 and compared with the original structure.

From Table 5.6 it is clear that, for the same bending stiffness, the aluminium honeycomb sandwich panel with $_c = 80$ kg/m^3 allows both a weight and skin thickness reduction of approximately 50%. An alternative approach could be to set the core density and then plot the objective function using the

Table 5.6. Design variables for the AHS panel with $D = 2.6 \cdot 10^{10}$ Nmm^2 and $m = 7$ kg compared with the original composite solution.

	Core density ρ_c [kg/m^2]	**Core thickness c [mm]**	**Skin thickness t [mm]**	**Panel weight m [kg]**
AHS panel	80	30	1.2	7
Original GFRP-balsa panel	155	30	2.5	15

weight as a parameter, as shown in Figure 5.7.

The overhang balcony could be required to fulfil other constraints, which could affect the selection of the design variables. For instance, the deflection δ of the overhang is a crucial aspect and it could be limited by specific comfort-related or other requirements.

The original composite structure tested by Kharghani and Guedes Soares [60] under bending conditions gave an initial linear response with a load-deflection stiffness ratio $P/$ equal to 230 N/mm.

Similarly to what was described in section 2.3.1 for three-point bending conditions, the deflection δ of a cantilever sandwich beam, subjected to a load P applied at its free extremity is the result of a bending (δ_b) and a shear (δ_s) contribution, according to equation 5.10 [43]:

$$\delta = \delta_b + \delta_s = \frac{PL^3}{3D} + \frac{PL}{AG_c}. \tag{5.10}$$

Focusing on the bending contribution, which is often predominant, and substituting the formulation of D from equation 5.6, it is possible to express the ratio P/δ in terms of c/L and t/L as:

$$\frac{c}{L} = \sqrt{\frac{P}{\delta}\frac{2}{3}\frac{1}{E_f b}\left(\frac{t}{L}\right)^{-1}}. \tag{5.11}$$

Hence, the overhang balcony design could be aimed not only at matching the flexural rigidity of the original composite sandwich panels whilst reducing the weight, but also at limiting the deflection of the balcony, i.e. ensuring high values of the ratio P/δ.

Since equation 5.10 is valid for cantilever beams, the following considerations will be made on a sandwich panel ideally clamped at one extremity and with a length L equal to the free length of the original composite panels (i.e. the length not overlapped by steel), which is equal to 646 mm. Obviously, the connection between the sandwich panels and the surrounding structure has a significant effect on the balcony functionality and on its mechanical response, but such considerations require a thorough and specific analysis, which is beyond the scope of the current section, and valid comparisons between sandwich structure solutions may be made using this simplification.

The constraint on the ratio P/δ can be plotted on a $c/L - t/L$ chart, together with the weight function, in order to identify the optimal design parameters. Since the considered length is reduced in comparison to the example reported in Figure 5.9, the target weight was set at 5 kg. The constraint on the ratio P/δ was represented for three different values: 230 N/mm, which is the value reported for the composite structure of [60], 400 N/mm and 800 N/mm. The plot for the present case study is displayed in Figure 5.10.

As previously discussed, the design variables are determined by the intersection between the weight function and P/δ constraint lines. For example, for a ratio P/δ=230 N/mm, which is the same of the original composite structure of [60], and for a density of aluminium honeycomb core of 80 kg/m^3 gives the resulting design variables indicated by the dark grey point and lines in Figure 5.10. The comparison of this solution with that of the original GFRP structure are reported in Table 5.7.

As shown in Table 5.7, the aluminium honeycomb sandwich structure with the same ratio P/δ of the original composite GFRP-balsa balcony, gives a

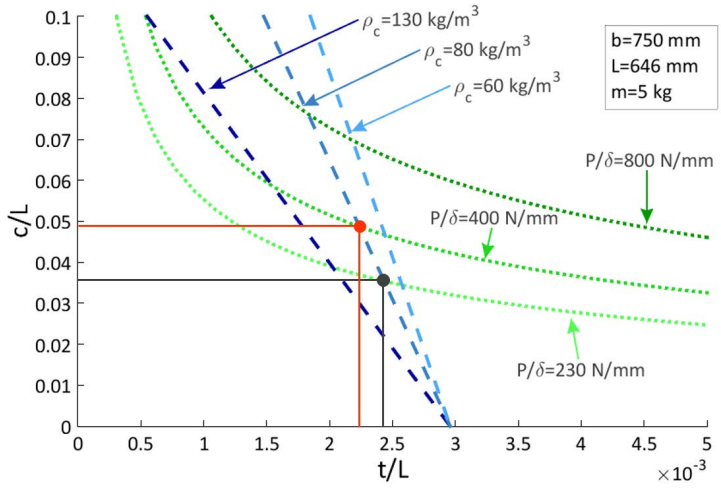

Figure 5.10. Graphical method for design variables definition, after establishing the P/δ ratio and the desired weight of the AHS panel.

Table 5.7. Design variables for the AHS, panel setting P/δ=230 N/mm and m=5 kg, and comparison with the original structure.

	Core density ρ_c [kg/m^2]	**Core thickness c [mm]**	**Skin thickness t [mm]**	**Panel weight m [kg]**
AHS panel	80	30	1.4	5
Original GFRP-balsa panel	155	30	2.5	9.2

weight and skin thickness reduction of approximately 50%. The potential advantages of AHS can be further demonstrated via a further example; for a ratio P/δ of 400 N/mm (almost double that of the original GFRP structure) and a core density of 80 kg/m^3 the resulting AHS properties summarised in Table 5.8 are obtained.

The values in Table 5.8 show the significant performance improvement attainable with an AHS structure; with a slight increase in the core thickness, but a reduction in skin thickness, it is possible to reduce the weight by a half

Table 5.8. Design variables for the AHS, panel with P/δ=400 N/mm and m=5 kg, and comparison with the original structure.

	P/δ [N/mm]	Core density ρ_c [kg/m^2]	Core thickness c [mm]	Skin thickness t [mm]	Panel weight m [kg]
AHS panel	230	80	32	1.4	5
Original GFRP-balsa panel	400	155	30	2.5	9.2

whilst doubling its stiffness, both of which are important parameters for a balcony overhang.

Another important design constraint could be the durability of the balcony overhang, which involves the investigation of impact, compression and contact events. Similar aspects represents future developments of the current section of the thesis.

The above-performed graphical procedure allows simple identification of the pertinent design variables to achieve different goals, such as a specific weight reductions and bending deflection limitations, whilst also enabling a clear understanding of the effects on the physical and mechanical properties of changes to the defining parameters.

Hence, the information obtained using the above described method can offer very useful support in the design phase. However, this approach would need to be integrated with specific further analyses where required. For instance, as previously stated, the connection between the sandwich panel and the main frame plays a crucial role in the mechanical response of the balcony and this aspect should be thoroughly investigated since the bonding methodology suitable for AHS may not be the same as that which should be used for the GFRP reference structure, although, the bonding of metal to metal structures may well be less problematic than that between composites and metal.

The failure modes of cantilever aluminium honeycomb sandwich panels would also need to be investigated in order to be considered during the design phase, as reported in section 5.2. However, although the methods described here obviously do not include all of the possible ensuing design issues, they do provide very useful and easy to use tools both to evaluate the potential advantages of AHS sandwich structures, and to guide the pertinent selection of their design parameters.

5.3.1 Preliminary numerical analysis

A complete and thorough analysis of the AHS-based balcony structure effectiveness should include a full-scale testing phase. Indeed, only evidences from experimental investigation are reliable sources to establish the AHS balcony response, its potentialities, its criticality and the possible improvements.

Nevertheless, a full-scale experimental analysis of a large structure requires a proper planning phase. Both the structure to analyse and the test setup have to be carefully designed and prepared in order to define the components assembly together with adequate testing configuration and procedure.

In view of the above considerations, a finite element model was developed with the aim of verifying the adequate selection of the AHS panel and of analysing the connection method between the panel and the supporting frame. The analysis was performed using Altair Hypermesh® for the preprocessing and Optistruct® as solver. The modelled structure is displayed in Figure 5.11 with the main characteristics.

The dimensions of the AHS panel were kept equal to those reported in Ref. [60] in order to provide a better comparison.

The characteristics of the honeycomb sandwich structures used in the model was selected taking into account the results obtained in section 5.3 and in particular in Tables 5.6, 5.7 and 5.6, on the basis of stiffness equivalence,

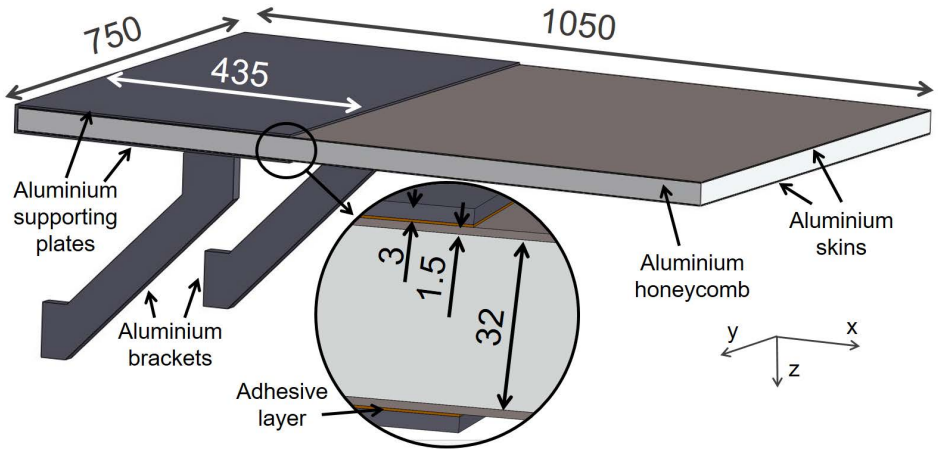

Figure 5.11. Characteristics of the AHS balcony structure.

mass and P/δ constraint and the commercial structures easily available from the main manufacturers.

Two aluminium plates, used to connect the balcony to the surrounding structures, were placed at the top and at the bottom of one side of the AHS panel, similarly to the reference structure by Khargani and Guedes Soares [60]. The bonding between the plates and the sandwich panel skins was provided with an adhesive layer. Two aluminium brackets were placed under the bottom plate in order to improve the structure stability and functionality, similary to the original structure [60].

In order to avoid time-consuming numerical analysis, the aluminium honeycomb panel can be modelled with an equivalent core sandwich panels [151, 152]. This consist of a sandwich structure where the honeycomb core is replaced with an orthotropic solid layer, whose properties are those of the equivalent honeycomb structure. For such purpose, some of the properties were provided by the honeycomb fabricator, with the others evaluated according to the analytical formulations reported by Gibson and Ashby [55]. The equivalent honeycomb core, the skins, the adhesive layer between the

skins and the brackets were modelled with first-order CHEXA solid elements, whereas the supporting plates were modelled with first-order CQUAD4 shell elements. All of the connections, were modelled, as a first approximation, by simply tying the nodes of the adjacent faces. The connections between the sandwich panels and external elements can be critical, although the joining of metallic components should be less challenging than that between composites and metal parts, where the large stiffness mismatch can initiate debonding and other problems. However, the stress in the adhesive layer needs to be evaluated in order to select an adequate structural adhesive and to guarantee the structure functionality. Since the main purpose of the model was to evaluate the adhesive performance and the general response of the assembly, rather than modelling the failure mechanisms, a linear elastic analysis was used.

The selected honeycomb has a cell size of 6 mm and a density equal to 83 kg/m3. The equivalent elastic parameters of the selected honeycomb core, used as input data for the numerical analysis, are summarised in Table 5.9.

Table 5.9. . Equivalent elastic parameters for the selected aluminium honeycomb core.

$\mathbf{E}_1$ [MPa]	$\mathbf{E}_2$ [MPa]	$\mathbf{E}_3$ [MPa]	$\mathbf{G}_{12}$ [MPa]	$\mathbf{G}_{23}$ [MPa]	$\mathbf{G}_{31}$ [MPa]	$\boldsymbol{\nu_{12}}$	$\boldsymbol{\nu_{23}}$	$\boldsymbol{\nu_{31}}$
2.7	2.7	1310	0.68	245	565	0.99	0.0001	0.3

The overall mass of the entire sandwich panel was estimated to be around 8.8 kg, i.e. almost 50% lighter than the original structure (15 kg) in Ref. [60].

The adhesive selected for the analysis was a two component, room temperature curing methacrylate adhesive system, with a tensile modulus of 1350 MPa and a tensile lap shear strength on aluminium of about 20 MPa.

On the free extremity of the balcony a load directed in the z direction equal to 6 kN was applied. This value was selected because it was the load level

at which initiation of non-linearity was recorded for the structure in Ref. [60]. Indeed, the numerical analysis was used to verify that the AHS-based balcony guarantees at least the same elastic range of the original structure. The opposite side of the sandwich panel and the supporting plates enclosing it were fully fixed in rotation and translation.

Figure 5.12 reports various stress contour plots obtained from the FEM model.

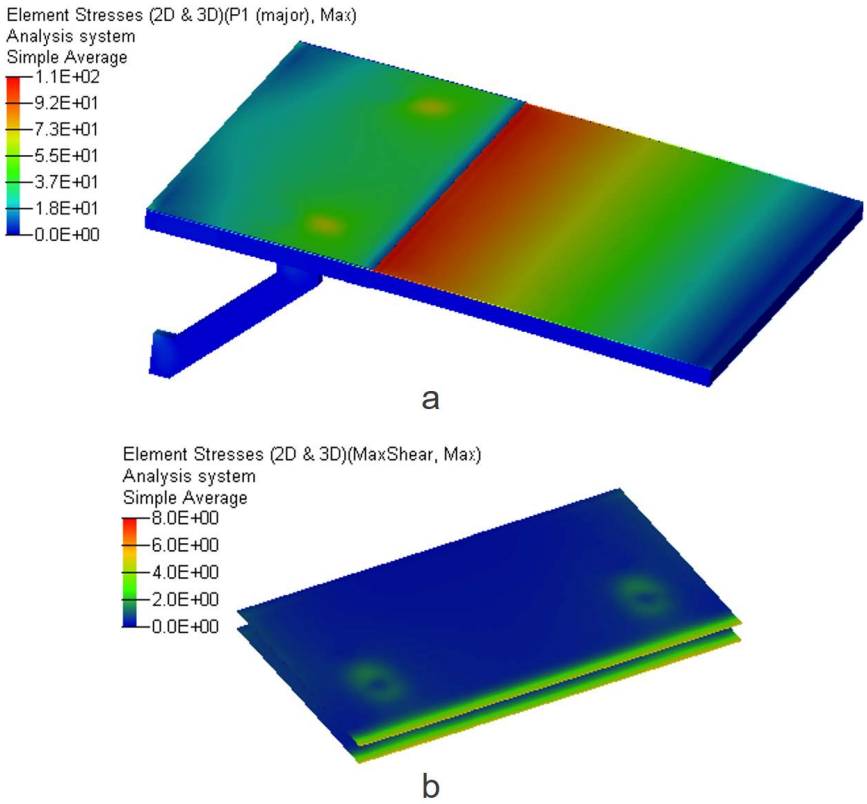

Figure 5.12. Contour plot of the analysed balcony for a) maximum principal stress and b)maximum shear stress in the adhesive layer.

As visible in Figure 5.12a, the maximum principal stress when a 6 kN downward load is applied at the free extremity of the balcony, does not reach the yield stress of the aluminium, and therefore it is reasonable to suppose that the structure is able to behave elastically for higher loads than does the original balcony design. In addition, the maximum shear stress in the adhesive layer, displayed in Figure 5.12b, is significantly lower than the tensile lap shear strength of the applied adhesive. This means that the integrity of the assembly and its elastic behaviour is at least comparable to those of the original structure.
The contour plot of the displacement in the z-direction obtained with the numerical model is displayed in Figure 5.13.

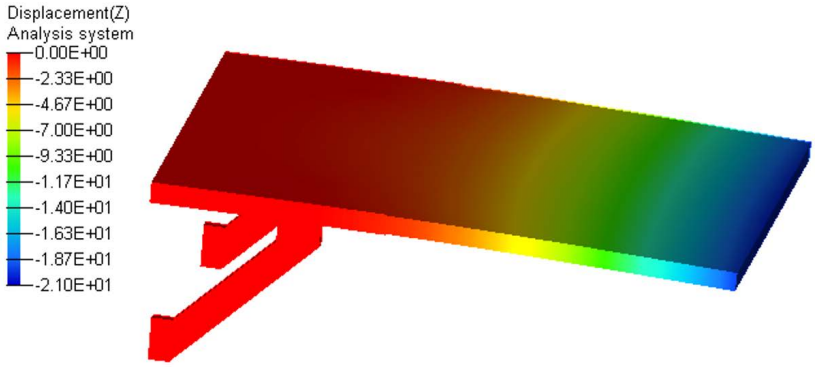

Figure 5.13. Contour plot of displacement in the z-direction

As visible in Figure 5.13, the maximum displacement is equal to 20 mm, which corresponds to the value reported at the same load level by Kharghani and Soares [60]. Indeed, as expected, since the AHS panel selection was based on a stiffness equivalence approach, the maximum displacement of both balconies is similar. This confirms the correct application of the bending stiffness equivalence approach.

Another advantage of the AHS-based design to consider is that its supporting plates of the AHS-based balcony are of aluminium and are only 3 mm thick, whereas the original structure had steel plates each 6 mm thick. As a result, the aluminium plates of the AHS balcony have a mass equal to 5.5 kg compared with the 42 kg of the steel plates of the original structure. From the numerical analysis it was observed that these plates are also subjected to a low stress level, and consequently their use, combined with that of the the AHS panel, would be beneficial to obtain a significant weight saving.
The numerical model was used also to perform a modal analysis on the balcony overhang structure. The first ten natural frequencies and mode shapes were evaluated. Table 5.10 reports the values of the natural frequencies.

Table 5.10. Results of the modal analysis performed with the numerical model.

Mode	**Frequency [Hz]**
1	70.2
2	164.7
3	324.2
4	473.5
5	484.0
6	501.5
7	505.2
8	512.8
9	651.1
10	768.4

Vibrations and resonance problems in a ship should be avoided by designing its structures in order to have natural frequencies far from the main exciting frequencies, such as those from the engine and propeller [153]. Therefore, knowing the natural frequencies of the balcony structure could be useful in view of its integration in a real marine vehicle. Figure 5.14 displays the mode shapes found with the numerical analysis, with the undeformed shape of the balcony shown for comparison.

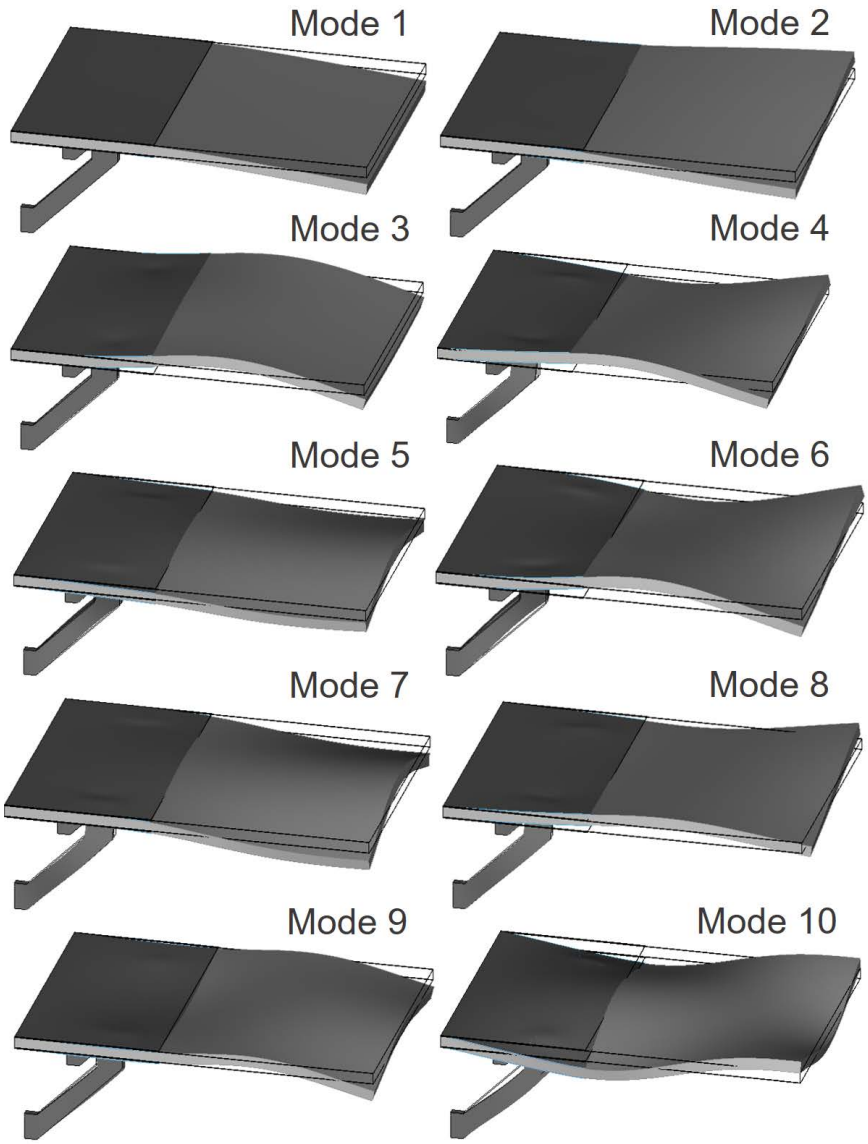

Figure 5.14. Mode shapes

In conclusion, the preliminary numerical model allowed the verification of the feasibility of the AHS-based balcony, with respect particularly to the response of the adhesive. Such information is very useful for the design of the experimental setup and procedure, which will be required to thoroughly and reliably investigate the mechanical performance of the AHS balcony. The modal analysis provided also useful information for future evaluations regarding the integration of the balcony in marine vehicle.
The full-scale tests will be performed at the CERISI Laboratories of the University of Messina. The designed setup for the full-scale test on the AHS balcony, along with the existing laboratory systems are showed in Figure 5.15.

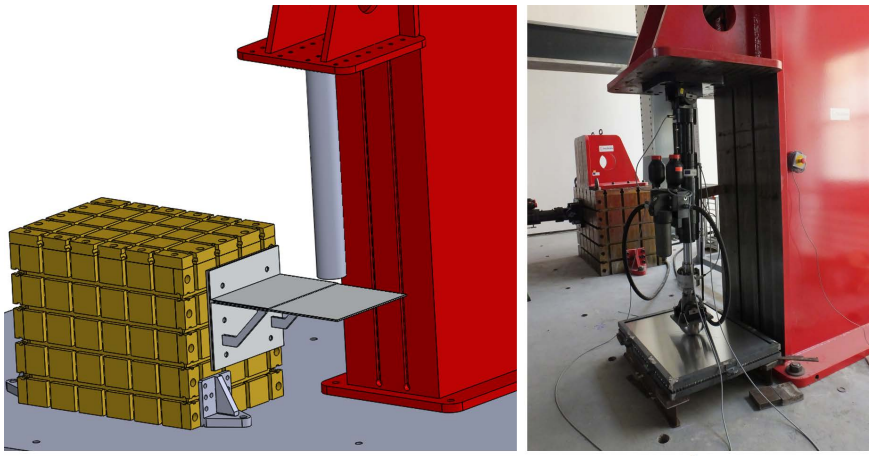

Figure 5.15. a)Designed setup for full-scale tests and b) part of the CERISI laboratories equipment.

Further developments will include the full-scale test of the AHS balcony and its integration with bi-metallic structures, which will be part of the supporting frame.

5.4 Final remarks

Aluminium honeycomb and GFRP-based sandwich structures were compared, with particular attention to possible marine applications, and a straightforward procedure to aid lightweight sandwich structure selection and design was proposed. In fact, all-metal sandwich structures, and in particular aluminium honeycomb sandwich structures, were seen to offer the possibility of combining lightweight properties with high environmental sustainability, which must be a crucial point to take into account in the design of future marine structures.

In order to guide the appropriate selection of all-metal sandwich structures for marine applications, an equivalence with more traditional structural solutions should be considered in order to give a suitable equivalent baseline from which valid and pertinent comparisons and design considerations can be drawn.

For this purpose, the bending stiffness was considered as the equivalence parameter on which the all-metal sandwich structure selection was based. In order to ensure realistic values of the bending stiffness for the preliminary phase of the analysis, these were based on data reported in the literature for GFRP panels commonly used in marine applications. The bending stiffnesses of several all-metal and hybrid lightweight sandwich candidate structures were then evaluated analytically, allowing the selection of candidate sandwich panels with bending stiffnesses within the range of those of the reference GFRP marine panels.

Subsequently, further design criteria were compared in order to evaluate various aspects of sandwich panel selection and design. In particular, for each sandwich structure solution the bending stiffness was plotted against the core thickness, the overall panel density and the areal density, to give materials charts which proved very useful for selection of the specific parameters of the sandwich structures. These charts identified that aluminium honey-

comb sandwich structures offer the potential to provide significant savings in weight (density) and volume (core thickness) in comparison to traditional composite sandwich panels.

Further aspects of aluminium honeycomb sandwich panels design were considered via failure maps combined with stiffness and weight constraints, and the plots produced were seen to support the selection of design variables such as core and skin thickness, whilst also giving clear insights into the effect of each of these variables on the resulting mechanical and physical properties.

Finally, a case study example regarding a ship balcony overhang was outlined. A structure reported in the literature incorporating sandwich panels with composite GFRP skins and balsa core was used as a baseline. The bending stiffness and the load/deflection ratio of this baseline structure were used as the constraints for an alternative aluminium honeycomb sandwich structure. The resulting AHS design, as compared to the baseline GFRP structure, demonstrated the potential of aluminium honeycomb sandwich structures in terms of both weight reduction and mechanical performance improvement. In addition, the outlined procedure facilitates the identification of the pertinent optimised main design variables.

The new AHS balcony was analysed with a simplified numerical model, where the honeycomb structure was modelled with an equivalent core sandwich panel. The aim of the FEM analysis was to perform a preliminary investigation of the feasibility of the AHS-based balcony, with particular attention to the adhesive response. Such information is useful for the design of the experimental setup and procedure, which is required to thoroughly evaluate the mechanical performance of the AHS balcony. It was verified the capability of the selected adhesive to bear the same load that in the original structure caused the initial non-linear response. In addition, at the same load level, the stress in the skins, in the plates and brackets were far from the aluminium yield stress and the maximum displacement corresponded to

that of the original structure, according to the stiffness equivalence design approach.

6
Conclusions

The aim of the present thesis was to investigate the potentialities of lightweight structures in the marine industry, focusing on experimental activities to acquire useful data and information for the design phase.

Particular attention was reserved to all-aluminium sandwich structures, in view of the recognised sustainability and recyclability of aluminium. In fact, aluminium sandwich structures, combine lightweight properties with high environmental sustainability, which should be carefully considered in the design of future marine structures.

The theme of biomimetic design was also presented as an innovative solution to common engineering problems.

In chapter 2 the state-of-art of sandwich structures mechanics and applica-

tions was proposed. The main formulations and theories regarding sandwich structures basic mechanics were reviewed. Bending, impact and fatigue behaviour were particularly addressed, since they are common conditions for sandwich marine structures and they were at the basis of the activities developed in the following chapters.
A literature survey of marine sandwich structures applications was also presented. Applications were distinguished according to the sandwich structure category (composite, hybrid or metal) and both scientific and technical references were provided.

Chapter 3 was focused on aluminium honeycomb sandwich structures (AHS), which were selected, among other lightweight solutions, because they combine sustainability, low density, excellent their energy absorption capabilities and high stiffness to weight and strength to weight ratios, which make them suitable for structural applications where weight reduction is a primary concern.
The importance of AHS response to dynamic events - which are less investigated in literature and more difficult to describe analytically - was highlighted and therefore two different types of dynamic conditions were investigated: low-velocity impact loading and fatigue loading.

In the first part of the chapter, an extensive experimental investigation on single and double-layer honeycomb sandwich structures was described. Six types of structures were tested under low-velocity impact conditions.
Their energy absorption capabilities were confirmed by a comparison with other lightweight structures from literature. It was observed that the good crashworthiness of honeycomb structure can be further improved by combining different honeycomb layers. For this purpose the arrangement and the honeycomb characteristics are crucial. As a consequence, the application of multi-layer honeycomb structures for energy absorption purposes should

consider thoroughly the exact aim (such as the protection of people or devices) and the more likely impact scenarios in order to provide an adequate selection and arrangement of honeycomb sandwich structures.

3D Computed Tomography technique was applied to observe, in a non-destructive way, the impacted areas. Cell walls buckling was recognised as the mechanism responsible for the exceptional energy absorption properties of honeycomb structures. In addition, accurate measurements of the impacted regions were taken.

The application of a theoretical approach to the mono-layer structures allowed the deduction of the parameters for the analytical description of the low-velocity impact phenomena, which could be applied to support the design of impact-resistant components. In addition, the comparison of the contact parameters obtained for the small-scale panels with those resulting from tests on a large honeycomb sandwich, allowed the identification of a size effect. Such findings may give useful information in the design phase of large structures, which is often the case for marine applications.

The second part of the chapter was focused on fatigue bending response of aluminium honeycomb sandwich structures, which is seldom studied in literature.

Differences and analogies between static and fatigue behaviour of aluminium honeycomb sandwich structures were observed.

The mechanisms involved in the bending response were identified, in a non-destructive way, by combining mechanical quasi-static tests with computed tomography technique. The performed analysis pointed out the significant effect of wall buckling on honeycomb sandwich structures load carrying capabilities.

Three-point bending fatigue tests were performed with different supports spans and it was found that they affect the collapse mechanisms. Two failure modes were identified: core shear mixed mode AB for small supports spans

and skin failure for large supports spans.
For one of the boundary condition the S-N curve was obtained. In addition, it was observed that supports span reduction, for a given stress range, produces a a decrease in fatigue life.
An analytical model was developed and applied to predict the collapse mechanisms and the fatigue limit loads. The good accordance between experimental and analytical results confirms the effectiveness of the considered model, which may represents an useful tool for sandwich structures design in several applications, including the marine ones.

Chapter 4 introduced the topic of biomimetic approach to respond to engineering and technological challenges, such as providing marine structures with both lightweight and impact-absorption capabilities.
In collaboration with Trinity College of Dublin, the biomimetic principles were applied to develop some bio-inspired lightweight crashworthy structures, with possible applications in the marine industry.
The applied method started from the selection of a natural structure to analyse and use as inspiration for novel engineering structures. In particular, bamboo was examined under low-velocity impact conditions, evaluating the relationship between its structure and its mechanical response.The detected impact response of bamboo can be related to a combination of mechanisms strongly dependent on its graded and hierarchical structure. Therefore, it was concluded that such characteristics, if properly mimicked, could improve the crashworthiness of engineering structures.
Inspired by the phenomena involved in bamboo impact response, four lightweight impact-resistant structures were designed.
The bamboo-inspired structures where modelled as multi-layer corrugated sandwich structures, in order to take into account the manufacturing feasibility and the applicability in the marine field. A preliminary analysis of their energy-absorption properties was performed by testing under compression

loading some samples manufactured in PLA with 3D printing technology. Cell walls buckling was found to be the predominant mechanism responsible for samples compression failure. This suggested that the the buckling theory could be applied to analytically predict the failure load and the collapse sequence in multi-layer corrugated sandwich panels subjected to compression. Good agreement between analytical and experimental results was obtained. Consequently, a proper application of buckling formulations, may support the design and optimisation of crashworthy and lightweight devices, based on bamboo structure.

Finally, chapter 5 describes a design methodology - partly based on the knowledge acquired from the investigations reported in the other chapters - and a case study for a realistic aluminium honeycomb sandwich structure application in the marine industry.
In particular, aluminium honeycomb structures were compared to their main competitors in the marine field, which are GFRP-based sandwich structures. An mechanical equivalence between existing and novel structures was considered crucial to guide an appropriate and rational selection of all-metal sandwich structures. Therefore, the bending stiffness was selected as a representative and easily-determinable equivalence parameter. The bending stiffnesses of several all-metal and hybrid lightweight sandwich candidate structures were evaluated analytically and they were combined with other design criteria. In particular, the bending stiffness was plotted against the core thickness, the overall panel density and the areal density. Material charts were obtained and their analysis highlighted the potentialities of aluminium honeycomb sandwich structures in offering significant savings in weight and volume in comparison to composite sandwich panels of the same stiffness.
Subsequently, a design methodology based on the combination of stiffness equivalence, failure maps and weight constraints was developed. The out-

puts of the procedure were plots which proved to be useful in the selection of design variables such as core and skin thickness.

In conclusion, a case study regarding a ship balcony overhang was outlined. A reference structure from literature, based on GFRP skins and balsa core, was identified. The developed design procedure was applied and the baseline bending stiffness and load/deflection ratio were used as the constraints for an alternative balcony, where composite panel is replaced with an aluminium honeycomb sandwich structure. The AHS panel, used as the balcony floor, was estimate to provide a weight and skin thickness reduction of approximately 50%. In addition, only with a small increase in core and skin thickness, a reduction in the expected balcony deflection was considered attainable. If the overall balcony design is considered, additional advantages are viable. Focusing on the supporting steel plates of the original design, their substitution with aluminium panels could provide a considerable weight reduction.

A simplified numerical model, which included an equivalent core sandwich panel, was developed to preliminary evaluate the feasibility of the AHS-based balcony, with particular attention to the adhesive response. Such information is functional to a correct design of a future full-scale investigation. According to the FEM results, when the AHS balcony is subjected to the load that in the original structure caused the initial non-linear response, the shear stress in the adhesive layer are significantly lower than its tensile lap shear strength. Under the same loading, the stress in all the other components, including the aluminium supporting plates, are barely half of the the aluminium yield stress. In addition, the maximum displacement matched that of the reference structure, confirming the correct application of the bending stiffness equivalence approach.

The main novelties presented in the thesis can be summarised as follows:

- The crashworthiness of aluminium honeycomb sandwich structures can be improved by assembling double-layer structures, where core arrangements and characteristics play a crucial role. Future developments of controlled energy absorbers could be based on these findings.

- A size effect regarding the contact parameters of AHS subjected to low-velocity impact and indentation was identified and it may be useful in the design phase of large marine structures.

- The response of aluminium honeycomb sandwich structures under three-point fatigue bending conditions was investigated. Two main failure modes were identified and an analytical model, which was in good agreement with experimental results, was developed for collapse mechanisms and the fatigue limit loads prediction.

- The biomimetic approach was applied to the development of possible lightweight impact-resistant structures for marine applications. Taking inspiration from bamboo structures and its influence on impact properties, four bio-inspired structures were designed and tested. They were modelled as multi-layer corrugated sandwich panels to account for manufacturing feasibility and the applicability in the marine field. In addition, this confirmed the effectiveness of the multi-layer design, already observed with aluminium honeycomb sandwich structures.

- The aluminium honeycomb sandwich structures represent a valid and sustainable alternative to common composite sandwich panels in the marine industry, both for their lightweight properties and their mechanical performance. This was demonstrated by suggesting and evaluating, with the aid of a numerical model, the replacement of a ship balcony based on a GFRP-balsa sandwich panel with an AHS panel. For this purpose a straightforward and accessible design methodology was also developed, starting from bending stiffness equivalence and

including other design constraints.

The conclusions of the thesis indicate that a broader application of aluminium honeycomb sandwich structure - and in general of all-metal sandwich structures - in marine applications is possible and it could provide several benefits, from sustainability to weight savings. Experimental, analytical and numerical analysis combination is required to guide a reliable and effective design of lightweight structures.

Nomenclature

Symbols		Unit of measurement
Latin symbols		
a	Sandwich plate length	mm
AG_c	Sandwich beam shear stiffness	mm
b	Sandwich beam width	mm
c	Sandwich core thickness	mm
C	Empirical constant for S-N curve definition	
d	Distance between the centroid axis of the sandwich skins	mm
D	Sandwich beam bending stiffness	Nmm^2
D_p	Sandwich plate bending stiffness	Nmm
E_b	Energy spent for bending deformation during impact	J
E_{bs}	Energy spent for bending and shear deformation during impact	J
E_c	Core Young's Modulus	GPa
E_{cn}	Energy spent in contact effect	J
E_{cr}	Critical energy required to produce a visible crack in a bamboo sample subjected to impact	J
E_f	Skin Young's Modulus	GPa
e_i	Error for the definition of a fitting function for bamboo impact tests	J
E_i	Impact energy of the i-th test on bamboo	J
E_m	Energy spent for membrane deformation during impact	J
E_n	Normalised energy	$\mathrm{J/mm}^{exp}$
E_s	Young's Modulus of the solid material	GPa
E_{sh}	Energy spent for shear deformation during impact	J
E_3	Out-of plane Young's modulus of the core	GPa
f	Cell foil thickness	mm
G_c	Core shear modulus	GPa
h	Sandwich overall thickness	mm
H	Overhang length on one side of the specimen in a bending test configuration	mm
I	Area moment of inertia	mm^4
k_b	Bending deflection coefficient	
K_b	Stiffness in the spring-mass model correlated to bending deformation effect	N/m
K_{bs}	Stiffness in the spring-mass model combining K_b and K_s	N/m
K_c	Stiffness in the spring-mass model correlated to non-linear contact effect	$\mathrm{N/m}^n$

K_m	Stiffness in the spring-mass model correlated to non-linear membrane effect	N/m^3
k_s	Shear deflection coefficient	
K_s	Stiffness in the spring-mass model correlated to shear deformation effect	N/m
l	Wall length in the corrugated core	mm
L	Sandwich beam length or supports span	mm
m	Empirical constant for S-N curve definition	
m_1	Projectile mass	kg
m_2	Sandwich structure mass	kg
M	Bending moment	Nmm
n	non-dimensional contact parameter	
P	Load	N
$P_{AB,f\ max}$	Fatigue limit load for core shear mode AB	N
P_{cr}	Critical buckling load	N
$P_{i,f\ max}$	Fatigue limit load for indentation	N
$P_{s,f\ max}$	Fatigue limit load for skin failure	N
q	Load per unit area	N/mm^2
R	Load ratio	
R_c	Radius of curvature	mm
s	Core cell size	mm
S	First moment of area	mm^3
t	Sandwich skin thickness	mm
T	Shear force	N
t_b	Bamboo sample thickness	mm
v	Impact velocity	m/s
W	Section modulus	mm^3
w_b	Deflection at impact point	mm
w_i	Impactor displacement	mm
Greek symbols		
α	Indentation depth	mm
β_1, β_2	Coefficients for plate deflection evaluation	
β_3-β_7	Coefficients for plate stresses evaluation	
γ	Shear strain	
δ	Sandwich beam or plate deflection	mm
δ_b	Bending contribute to sandwich beam deflection	mm
δ_p	Sandwich plate deflection	mm
δ_s	Shear contribute to sandwich beam deflection	mm
$\Delta\sigma$	Stress range	MPa
ε_c	Core strain	
ε_f	Skin strain	
θ	Specimen rotation during bending test	deg
λ	Parameter for critical buckling load evaluation	
ν_f	Skin Poisson's ratio	
ρ	Parameter for plate deflection evaluation	
ρ_c	Core density	
ρ_p	Sandwich panel density	kg/m^3
ρ_s	Skin density	kg/m^3
σ_c	Core stress	MPa
σ_{cc}	Core out-of-plane compressive strength	MPa
$\sigma_{c,f}$	Fatigue compressive strength of the core	MPa
σ_{cs}	Sandwich compressive strength	MPa

σ_f	Skin stress	MPa
σ_{fi}	Critical in-plane stress in the skin for intra-cell dimpling	
σ_{fy}	Yield stress of the sandwich skin	MPa
σ_{fw}	Critical compressive stress for wrinkling	MPa
σ_{max}	Maximum stress in a fatigue test	MPa
$\sigma_{s,f}$	Fatigue tensile strength of the skin	MPa
τ_c	Core shear stress	MPa
$\tau_{c,f}$	Fatigue hear strength of the core	MPa
τ_{cs}	Core shear strength	MPa

Abbreviations

AHS	Aluminium honeycomb sandwich structure
AM	Additive manufacturing
ANOVA	Analysis of Variance
BCC	Body centred cubic
CT	Computed Tomography
DIC	Digital Image Correlation
exp	Exponent for normalised energy definition
EMSA	European Maritime Safety Agency
EU	European Union
FRP	Fibre reinforced plastic
GFRP	Glass-fibre reinforced plastics
IEA	International Energy Agency
IMO	International Maritime Organization
s.d.	Standard deviation
SEA	Specific energy absorption
TEA	Total energy absorption

Bibliography

[1] IEA, "Tracking transport 2020," 2020.

[2] H. Helms and U. Lambrecht, "The potential contribution of lightweighting to reduce transport energy consumption," *The International Journal of Life Cycle Assessment*, vol. 12, pp. 58–64, 2007.

[3] A. Johnson and G. Sims, "Mechanical properties and design of sandwich materials," *Composites*, vol. 17, pp. 321–328, oct 1986.

[4] SANDCORe Co-ordination Action, "Best Practice Guide for Sandwich Structures in Marine Applications," tech. rep., NewRail, University of Newcastle upon Tyne, 2013.

[5] J. Nunes and J. Silva, "Sandwiched composites in aerospace engineering," in *Advanced Composite Materials for Aerospace Engineering*, pp. 129–174, Elsevier, 2016.

[6] D. Herzog, V. Seyda, E. Wycisk, and C. Emmelmann, "Additive manufacturing of metals," *Acta Materialia*, vol. 117, pp. 371–392, sep 2016.

[7] Directorate General Maritime Affairs and Fisheries, "The EU Blue Economy Report. 2019," tech. rep., 2019.

[8] Directorate General Maritime Affairs and Fisheries, "The EU Blue Economy Report. 2020," tech. rep., 2020.

[9] H. He-ping, "The Development Trend of Green Ship Building Technology," 2008.

[10] A. Rahman and M. M. Karim, "Green Shipbuilding and Recycling: Issues and Challenges," *International Journal of Environmental Science and Development*, vol. 6, no. 11, pp. 838–842, 2015.

[11] "The Hong Kong International Convention for the Safe and Environmentally Sound Recycling of Ships."

[12] I. Stenius, A. Rosén, and J. Kuttenkeuler, "On structural design of energy efficient small high-speed craft," *Marine Structures*, vol. 24, pp. 43–59, jan 2011.

[13] D. Mead, "The Damping Properties of Elastically Plates Supported," *Journal of Sound and Vibration*, vol. 24, no. 3, pp. 275–295, 1972.

[14] M. R. Maheri, R. D. Adams, and J. Hugon, "Vibration damping in sandwich panels," *Journal of Materials Science*, vol. 43, no. 20, pp. 6604–6618, 2008.

[15] Plascore, "Lightweight Panel Solutions for Marine Vessel Interiors."

[16] Hexcel, "Composite Materials for High Performance Yachts and Racing Boats."

[17] L. Sutherland, "A review of impact testing on marine composite materials: Part I – Marine impacts on marine composites," *Composite Structures*, vol. 188, pp. 197–208, mar 2018.

[18] Z. Wang, Z. Lu, H. Tian, S. Yao, and W. Zhou, "Theoretical assessment methodology on axial compressed hexagonal honeycomb' s energy absorption capability," *Mechanics of Advanced Materials and Structures*, vol. 23, no. 5, pp. 503–512, 2016.

[19] J. W. Ringsberg, "Characteristics of material, ship side structure response and ship survivability in ship collisions," *Ships and Offshore Structures*, vol. 5, pp. 51–66, mar 2010.

[20] B. Liu, Y. Garbatov, L. Zhu, and C. Guedes Soares, "Numerical assessment of the structural crashworthiness of corroded ship hulls in stranding," *Ocean Engineering*, vol. 170, no. November, pp. 276–285, 2018.

[21] European Maritime Safety Agency, "Annual Overview of Marine Casualties and Incidents 2019," tech. rep., 2019.

[22] European Maritime Safety Agency, "Marine Casualties and Incidents - Preliminary annual overview of marine casualties and incidents 2014-2019," *Marine Casualties and Incidents*, no. March, 2020.

[23] P. Noury, B. Hayman, D. McGeorge, and J. Weitzenböck, "Lightweight construction for advanced shipbuilding-recent development," in *Proceedings of the 37th WEGEMT Summer School*, DET NORSKE VERITAS, 2002.

[24] C. Nasso, U. La Monaca, A. Marinò, S. Bertagna, and V. Bucci, "The Strip Planking: an Eco-Friendly Solution for the End-of-Life of Ships," in *Technology and Science for the Ships of the Future. Proceedings of NAV 2018: 19th International Conference on Ships and Maritime Research*, pp. 444–451, 2018.

[25] M. Mahfoud and D. Emadi, "Aluminum recycling - Challenges and opportunities," in *Advanced Materials Research*, vol. 83-86, pp. 571–578, 2010.

[26] M. E. Schlesinger, *Aluminum Recycling*. CRC Press Taylor & Francis Group, second ed., 2014.

[27] V. K. Soo, J. R. Peeters, P. Compston, M. Doolan, and J. R. Duflou, "Economic and environmental evaluation of aluminium recycling based on a belgian case study," *Procedia Manufacturing*, vol. 33, pp. 639–646, 2019.

[28] J. B. Fogagnolo, E. M. Ruiz-Navas, M. A. Simón, and M. A. Martinez, "Recycling of aluminium alloy and aluminium matrix composite chips by pressing and hot extrusion," *Journal of Materials Processing Technology*, vol. 143-144, no. 1, pp. 792–795, 2003.

[29] G. Ingarao, D. Baffari, E. Bracquene, L. Fratini, and J. Duflou, "Energy demand reduction of aluminum alloys recycling through friction stir extrusion processes implementation," *Procedia Manufacturing*, vol. 33, pp. 632–638, 2019.

[30] B. A. Behrens, A. Bouguecha, K. Brunotte, M. Dannenberg, A. Huskic, and M. Bonhage, "Reprocessing of aluminum chips by hot backward extrusion," *Production Engineering*, vol. 10, pp. 375–382, 2016.

[31] O. Schmitt, "Some interesting and useful biomimetic transforms," in *Proceeding Third International Biophysics Congress*, p. 297, 1969.

[32] D. Taylor, "Fatigue-resistant components: What can we learn from nature?," *Proceedings of the Institution of Mechanical Engineers, Part C: Journal of Mechanical Engineering Science*, vol. 229, no. 7, pp. 1186–1193, 2015.

[33] G. A. Pauli, *The blue economy: 10 years, 100 innovations, 100 million jobs*. Paradigm publications, 2010.

[34] R. Kaminski, T. Speck, and O. Speck, "Biomimetic 3D printed lightweight constructions: a comparison of profiles with various geometries for efficient material usage inspired by square-shaped plant stems," *Bioinspiration & Biomimetics*, vol. 14, p. 046007, jun 2019.

[35] X. Zhenhai, *Biomimetic Principles and Design of Advanced Engineering Materials*. John Wiley & Sons, 2016.

[36] L. Zhao, J. Ma, T. Wang, and D. Xing, "Lightweight Design of Mechanical Structures based on Structural Bionic Methodology," *Journal of Bionic Engineering*, vol. 7, pp. S224–S231, dec 2010.

[37] L. Li, C. Guo, Y. Chen, and Y. Chen, "Optimization design of lightweight structure inspired by glass sponges (Porifera, Hexacinellida) and its mechanical properties," *Bioinspiration & Biomimetics*, vol. 15, p. 036006, mar 2020.

[38] D. Leidenfrost, "the 46M Sailing Yacht Exo : Structural Design Inspired By Nature," in *24th International HISWA Symposium on Yacht Design and Yacht Construction*, no. November, 2016.

[39] HexCel, "HexWeb Honeycomb sandwich design technology," 2000.

[40] P. Kujala and A. Klanac, "Steel sandwich panels in marine applications," *Brodogradnja*, vol. 56, no. 4, pp. 305–314, 2005.

[41] G. Epasto, G. Palomba, D. D'Andrea, E. Guglielmino, S. Di Bella, and F. Traina, "Ti-6Al-4V ELI microlattice structures manufactured

by electron beam melting: Effect of unit cell dimensions and morphology on mechanical behaviour," *Materials Science and Engineering: A*, vol. 753, pp. 31–41, apr 2019.

[42] F. J. Plantema, *Sandwich construction*, vol. 966. Wiley New York, 1966.

[43] H. G. Allen, *Analysis and Design of Structural Sandwich Panels*. Franklin Book Co, 1969.

[44] D. Zenkert, *The Handbook of Sandwich Construction*. 1997.

[45] S. Abrate, *Impact on Composite Structures*. Cambridge University Press, 1998.

[46] K. N. Shivakumar, W. Elber, and W. Illg, "Prediction of Impact Force and Duration Due to Low-Velocity Impact on Circular Composite Laminates," *Journal of Applied Mechanics*, vol. 52, no. September 1985, 1985.

[47] N. Apetre, B. Sankar, and D. Ambur, "Low-velocity impact response of sandwich beams with functionally graded core," *International Journal of Solids and Structures*, vol. 43, pp. 2479–2496, may 2006.

[48] B. V. Sankar, "Scaling of Low-Velocity Impact for Symmetric Composite Laminates," *Journal of reinforced plastics and composites*, vol. 2, pp. 296–309, 1992.

[49] N. Sharma, R. F. Gibson, and E. O. Ayorinde, "Fatigue of Foam and Honeycomb Core Composite Sandwich Structures: A Tutorial," *Journal of Sandwich Structures & Materials*, vol. 8, pp. 263–319, jul 2006.

[50] K. Kanny and H. Mahfuz, "Flexural fatigue characteristics of sandwich structures at different loading frequencies," *Composite Structures*, vol. 67, pp. 403–410, mar 2005.

[51] M. Burman and D. Zenkert, "Fatigue of foam core sandwich beams—1: undamaged specimens," *International Journal of Fatigue*, vol. 19, pp. 551–561, oct 1997.

[52] M. Burman and D. Zenkert, "Fatigue of Undamaged and Damaged Honeycomb Sandwich Beams," *Journal of Sandwich Structures & Materials*, vol. 2, pp. 50–74, jan 2000.

[53] G. Belingardi, P. Martella, and L. Peroni, "Fatigue analysis of honeycomb-composite sandwich beams," *Composites Part A: Applied Science and Manufacturing*, vol. 38, pp. 1183–1191, apr 2007.

[54] A.-M. Harte, N. Fleck, and M. Ashby, "The fatigue strength of sandwich beams with an aluminium alloy foam core," *International Journal of Fatigue*, vol. 23, pp. 499–507, jul 2001.

[55] L. J. Gibson and M. F. Ashby, *Cellular Solids-Structure and Properties*. Cambridge University Press, 1999.

[56] A. Petras and M. Sutcliffe, "Failure mode maps for honeycomb sandwich panels," *Composite Structures*, vol. 44, pp. 237–252, apr 1999.

[57] J. R. Vinson, "Sandwich Structures: Past, Present, and Future," in *Sandwich Structures 7: Advancing with Sandwich Structures and Materials*, pp. 3–12, Berlin/Heidelberg: Springer-Verlag, 2005.

[58] D. Zenkert, A. Shipsha, P. Bull, and B. Hayman, "Damage tolerance assessment of composite sandwich panels with localised damage," *Composites Science and Technology*, vol. 65, pp. 2597–2611, dec 2005.

[59] G. Di Bella, G. Galtieri, and C. Borsellino, "Three-Point Flexural Properties of Bonded Reinforcement Elements for Pleasure Craft Decks," *Applied Composite Materials*, vol. 25, pp. 21–34, feb 2018.

[60] N. Kharghani and C. Guedes Soares, "Experimental and numerical study of hybrid steel-FRP balcony overhang of ships under shear and bending," *Marine Structures*, vol. 60, pp. 15–33, jul 2018.

[61] J. Cao, J. L. Grenestedt, and W. J. Maroun, "Testing and analysis of a 6-m steel truss/composite skin hybrid ship hull model," *Marine Structures*, vol. 19, pp. 23–32, jan 2006.

[62] W. J. Maroun, J. Cao, and J. L. Grenestedt, "Steel truss/composite skin hybrid ship hull, Part II: Manufacturing and sagging testing,"

Composites Part A: Applied Science and Manufacturing, vol. 38, pp. 1763–1772, jul 2007.

[63] J. Cao, J. L. Grenestedt, and W. J. Maroun, "Steel truss/composite skin hybrid ship hull. Part I: Design and analysis," *Composites Part A: Applied Science and Manufacturing*, vol. 38, pp. 1755–1762, jul 2007.

[64] A. Mouritz, E. Gellert, P. Burchill, and K. Challis, "Review of advanced composite structures for naval ships and submarines," *Composite Structures*, vol. 53, pp. 21–42, jul 2001.

[65] I. Grabovac and D. Turley, "Present and future of composite materials for marine applications," *ICCM/9. Metal Matrix Composites.*, vol. 1, pp. 89–96, 1993.

[66] M. Gaiotti, E. Ravina, C. M. Rizzo, and A. Ungaro, "Testing and simulation of a bolted and bonded joint between steel deck and composite side shell plating of a naval vessel," *Engineering Structures*, vol. 172, pp. 228–238, oct 2018.

[67] J. Summerscales, M. Singh, and K. Wittamore, "Disposal of composite boats and other marine composites," in *Marine Applications of Advanced Fibre-Reinforced Composites* (J. Graham-Jones and J. Summerscales, eds.), Woodhead Publishing Series in Composites Science and Engineering, pp. 185 – 213, Woodhead Publishing, 2016.

[68] J. Romanoff, A. Laakso, and P. Varsta, "Improving the shear properties of web-core sandwich structures using filling material," in *Proc. of 2nd Intl. Conference on Analysis and Design of Marine Structures, Editors Guedes Soares and Das, Taylor & Francis Group*, pp. 133–138, 2009.

[69] T. Grafton and J. Weitzenböck, "Steel-concrete-steel sandwich structures in ship and offshore engineering," in *Adv. Mar. Struct.-Proc. 3rd Int. Conf. Mar. Struct. MARSTRUCT*, pp. 549–558, 2011.

[70] K. Sohel, J. Richard Liew, J. Yan, M. Zhang, and K. Chia, "Behavior of Steel–Concrete–Steel sandwich structures with lightweight cement composite and novel shear connectors," *Composite Structures*, vol. 94, pp. 3500–3509, dec 2012.

[71] S. Sujiatanti, A. Zubaydi, and A. Budipriyanto, "Finite Element Analysis of Ship Deck Sandwich Panel," *Applied Mechanics and Materials*, vol. 874, pp. 134–139, 2018.

[72] K. Niklas and J. Kozak, "Experimental investigation of Steel–Concrete–Polymer composite barrier for the ship internal tank construction," *Ocean Engineering*, vol. 111, pp. 449–460, jan 2016.

[73] J. J. Kortenoeven, B. B. Boon, and A. A. D. Bruijn, "Application of Sandwich Panels in Design and Building of Dredging Ships," *Journal of ship production*, vol. 3, no. 24, pp. 125–134, 2008.

[74] S. Mueller and L. M. Volpone, "Friction stir welding of steel/aluminium sandwich panels," *Welding International*, vol. 23, no. 9, pp. 699–705, 2009.

[75] T. Bitzer, "Honeycomb Marine Applications," *Journal of Reinforced Plastics and Composites*, vol. 13, pp. 355–360, apr 1994.

[76] T. Bitzer, *Honeycomb Technology: materials, design, manufacturing, applications and testing*. Springer, Dordrecht, 1st ed., 1997.

[77] A. Hazizan and W. J. Cantwell, "The low velocity impact response of an aluminium honeycomb sandwich structure," *Composites: Part B*, vol. 34, pp. 679–687, 2003.

[78] J. Kee Paik, A. K. Thayamballi, and G. Sung Kim, "The strength characteristics of aluminum honeycomb sandwich panels," *Thin-Walled Structures*, vol. 35, pp. 205–231, nov 1999.

[79] L. Aktay, A. F. Johnson, and B.-H. Kröplin, "Numerical modelling of honeycomb core crush behaviour," *Engineering Fracture Mechanics*, vol. 75, pp. 2616–2630, jun 2008.

[80] M. K. Khan, T. Baig, and S. Mirza, "Experimental investigation of in-plane and out-of-plane crushing of aluminum honeycomb," *Materials Science & Engineering A*, vol. 539, pp. 135–142, 2012.

[81] G. Sun, X. Huo, D. Chen, and Q. Li, "Experimental and numerical study on honeycomb sandwich panels under bending and in-panel compression," *Materials & Design*, vol. 133, pp. 154–168, nov 2017.

[82] G. Cricrì, M. Perrella, and C. Calì, "Honeycomb failure processes under in-plane loading," *Composites Part B: Engineering*, vol. 45, no. 1, pp. 1079–1090, 2013.

[83] Z. Li, T. Wang, Y. Jiang, L. Wang, and D. Liu, "Design-oriented crushing analysis of hexagonal honeycomb core under in-plane compression," *Composite Structures*, vol. 187, no. December 2017, pp. 429–438, 2018.

[84] Z. Wang, "Recent advances in novel metallic honeycomb structure," *Composites Part B: Engineering*, vol. 166, no. August 2018, pp. 731–741, 2019.

[85] B. P. Russell, T. Liu, N. A. Fleck, and V. S. Deshpande, "Quasi-static three-point bending of carbon fiber sandwich beams with square honeycomb cores," *Journal of Applied Mechanics, Transactions ASME*, vol. 78, pp. 031008–1, may 2011.

[86] G. Zhou, M. Hill, J. Loughlan, and N. Hookham, "Damage Characteristics of Composite Honeycomb Sandwich Panels in Bending under Quasi-static Loading," *Journal of Sandwich Structures & Materials*, vol. 8, pp. 55–90, jan 2006.

[87] Y. Xiao, Y. Hu, J. Zhang, C. Song, and X. Huang, "The bending responses of sandwich panels with aluminium honeycomb core and CFRP skins used in electric vehicle body," *Advances in Materials Science and Engineering*, 2018.

[88] S. D. Pan, L. Z. Wu, Y. G. Sun, Z. G. Zhou, and J. L. Qu, "Longitudinal shear strength and failure process of honeycomb cores," *Composite Structures*, vol. 72, no. 1, pp. 42–46, 2006.

[89] J. d. D. Rodriguez-Ramirez, B. Castanie, and C. Bouvet, "Experimental and numerical analysis of the shear nonlinear behaviour of Nomex honeycomb core: Application to insert sizing," *Composite Structures*, vol. 193, no. February, pp. 121–139, 2018.

[90] M. N. Wang, B. Wang, C. Liu, G. Zhang, Y. Wan, and F. Zhang, "Mechanical respond and failure mode of large size honeycomb sandwiched composites under in-plane shear load," *Molecules*, vol. 24, no. 23, 2019.

[91] U. B. Shah and R. K. Kapania, "Crush dynamics and shear failure of alternate sandwich panel honeycomb core for space structures," *AIAA Scitech 2019 Forum*, no. January, 2019.

[92] G. Palomba, G. Epasto, V. Crupi, and E. Guglielmino, "Single and double-layer honeycomb sandwich panels under impact loading," *International Journal of Impact Engineering*, vol. 121, pp. 77–90, nov 2018.

[93] G. Palomba, V. Crupi, and G. Epasto, "Collapse modes of aluminium honeycomb sandwich structures under fatigue bending loading," *Thin-Walled Structures*, vol. 145, p. 106363, dec 2019.

[94] B. G. Vijayasimha Reddy, K. V. Sharma, and T. Yella Reddy, "Deformation and impact energy absorption of cellular sandwich panels," *Materials and Design*, vol. 61, pp. 217–227, sep 2014.

[95] V. Crupi, G. Epasto, and E. Guglielmino, "Collapse modes in aluminium honeycomb sandwich panels under bending and impact loading," *International Journal of Impact Engineering*, vol. 43, pp. 6–15, 2012.

[96] V. Crupi, G. Epasto, and E. Guglielmino, "Comparison of aluminium sandwiches for lightweight ship structures: Honeycomb vs. foam," *Marine Structures*, vol. 30, pp. 74–96, 2013.

[97] V. Crupi, E. Kara, E. Guglielmino, and A. Aykul, "Prediction model for the impact response of glass fibre reinforced aluminium foam sandwiches," *International Journal of Impact Engineering*, vol. 77, no. May, pp. 97–107, 2015.

[98] V. Crupi, E. Kara, G. Epasto, E. Guglielmino, and H. Aykul, "Theoretical and experimental analysis for the impact response of glass fibre reinforced aluminium honeycomb sandwiches," *Journal of Sandwich Structures & Materials*, vol. 20, pp. 42–69, feb 2018.

[99] A. Hazizan and W. J. Cantwell, "The low velocity impact response of foam-based sandwich structures," *Composites: Part B*, vol. 33, 2002.

[100] Y. Yasui, "Dynamic axial crushing of multi-layer honeycomb panels and impact tensile behavior of the component members," *International Journal of Impact Engineering*, vol. 24, 2000.

[101] J. Fazilati and M. Alisadeghi, "Multiobjective crashworthiness optimization of multi-layer honeycomb energy absorber panels under axial impact," *Thin-Walled Structures*, vol. 107, pp. 197–206, oct 2016.

[102] Z. Wang, J. Liu, Z. Lu, and D. Hui, "Mechanical behavior of composited structure filled with tandem honeycombs," *Composites Part B: Engineering*, vol. 114, pp. 128–138, apr 2017.

[103] B. T. Cao, B. Hou, Y. L. Li, and H. Zhao, "An experimental study on the impact behavior of multilayer sandwich with corrugated cores," *International Journal of Solids and Structures*, vol. 109, pp. 33–45, 2017.

[104] L. Shiqiang, L. Xin, W. Zhihua, W. Guiying, G. Lu, and L. Zhao, "Sandwich panels with layered graded aluminum honeycomb cores under blast loading," *Composite Structures*, 2017.

[105] C. Kılıçaslan, . K. Odacı, and M. Güden, "Single- and double-layer aluminum corrugated core sandwiches under quasi-static and dynamic loadings," *Journal of Sandwich Structures & Materials*, vol. 18, pp. 667–692, nov 2016.

[106] A. Bonanno, V. Crupi, G. Epasto, E. Guglielmino, and G. Palomba, "Aluminum honeycomb sandwich for protective structures of earth moving machines," *Procedia Structural Integrity*, vol. 8, pp. 332–344, 2018.

[107] C. Kiliçaslan, M. Güden, I. K. Odaci, and A. Taşdemirci, "The impact responses and the finite element modeling of layered trapezoidal corrugated aluminum core and aluminum sheet interlayer sandwich structures," *Materials and Design*, vol. 46, pp. 121–133, 2013.

[108] Y. Wu, J. Fu, and Q. Li, "Dynamic crash responses of bio-inspired aluminum honeycomb sandwich structures with CFRP panels," *Composites Part B: Engineering*, vol. 121, pp. 122–133, jul 2017.

[109] S. Abrate, G. Epasto, E. Kara, V. Crupi, E. Guglielmino, and H. Aykul, "Computed tomography analysis of impact response of lightweight sandwich panels with micro lattice core," *Proceedings of the Institution of Mechanical Engineers, Part C: Journal of Mechanical Engineering Science*, no. Special Issue "Lightweight Design in Transportation Engineering", 2018.

[110] S. Abrate, "Localized impact on sandwich structures with laminated facings," *Applied Mechanics Reviews*, vol. 50, no. 2, 1997.

[111] G. Minak and D. Ghelli, "Influence of diameter and boundary conditions on low velocity impact response of CFRP circular laminated plates," *Composites: Part B*, vol. 39, pp. 962–972, 2008.

[112] Y. Bay, *Marine Structural Design*. Elsevier, 2003.

[113] E. Knox, M. Cowling, and I. Winkle, "Adhesively bonded steel corrugated core sandwich construction for marine applications," *Marine Structures*, vol. 11, pp. 185–204, may 1998.

[114] Y.-M. Jen and L.-Y. Chang, "Evaluating bending fatigue strength of aluminum honeycomb sandwich beams using local parameters," *International Journal of Fatigue*, vol. 30, pp. 1103–1114, jun 2008.

[115] S. Belouettar, A. Abbadi, Z. Azari, R. Belouettar, and P. Freres, "Experimental investigation of static and fatigue behaviour of composites honeycomb materials using four point bending tests," *Composite Structures*, vol. 87, pp. 265–273, feb 2009.

[116] Y.-M. Jen, F.-L. Teng, and T.-C. Teng, "Two-stage cumulative bending fatigue behavior for the adhesively bonded aluminum honeycomb sandwich panels," *Materials & Design (1980-2015)*, vol. 54, pp. 805–813, feb 2014.

[117] G. Demelio, K. Genovese, and C. Pappalettere, "An experimental investigation of static and fatigue behaviour of sandwich composite panels joined by fasteners," *Composites Part B:Engineering*, vol. 32, no. 4, pp. 299–308, 2001.

[118] A. Partovi Meran, T. Toprak, and A. Muğan, "Numerical and experimental study of crashworthiness parameters of honeycomb structures," *Thin-Walled Structures*, vol. 78, pp. 87–94, may 2014.

[119] J. Zhang and M. Ashby, "The out-of-plane properties of honeycombs," *International Journal of Mechanical Sciences*, vol. 34, pp. 475–489, jun 1992.

[120] C. Kılıçaslan, M. Güden, . K. Odacı, and A. Taşdemirci, "Experimental and numerical studies on the quasi-static and dynamic crushing responses of multi-layer trapezoidal aluminum corrugated sandwiches," *Thin-Walled Structures*, vol. 78, pp. 70–78, may 2014.

[121] J. Lukács, Á. Meilinger, and D. Pósalaky, "High cycle fatigue and fatigue crack propagation design curves for 5754-H22 and 6082-T6 aluminium alloys and their friction stir welded joints," *Welding in the World*, vol. 62, no. 4, pp. 737–749, 2018.

[122] O. Kesler and L. Gibson, "Size effects in metallic foam core sandwich beams," *Materials Science and Engineering: A*, vol. 326, pp. 228–234, mar 2002.

[123] M. Ashby, A. Evans, N. Fleck, L. Gibson, and J. Hutchinson, *Metal Foams: a Design Guide*. 2000.

[124] Y.-M. Jen and H.-B. Lin, "Temperature-dependent monotonic and fatigue bending strengths of adhesively bonded aluminum honeycomb sandwich beams," *Materials & Design*, vol. 45, pp. 393–406, mar 2013.

[125] G. X. Gu, M. Takaffoli, and M. J. Buehler, "Hierarchically Enhanced Impact Resistance of Bioinspired Composites," *Advanced Materials*, vol. 29, p. 1700060, jul 2017.

[126] R. Ballarini and A. H. Heuer, "Secrets in the Shell: The Body Armor of the Queen Conch Is Much Tougher than Comparable Synthetic Materials. What Secrets Does It Hold?," *American Scientist*, vol. 95, no. 5, pp. 422–429, 2007.

[127] P. Tran, T. D. Ngo, A. Ghazlan, and D. Hui, "Bimaterial 3D printing and numerical analysis of bio-inspired composite structures under

in-plane and transverse loadings," *Composites Part B: Engineering*, vol. 108, pp. 210–223, jan 2017.

[128] N. Zhao, Z. Wang, C. Cai, H. Shen, F. Liang, D. Wang, C. Wang, T. Zhu, J. Guo, Y. Wang, X. Liu, C. Duan, H. Wang, Y. Mao, X. Jia, H. Dong, X. Zhang, and J. Xu, "Bioinspired Materials: from Low to High Dimensional Structure," *Advanced Materials*, vol. 26, pp. 6994–7017, nov 2014.

[129] Y. Zhang, M. Lu, C. H. Wang, G. Sun, and G. Li, "Out-of-plane crashworthiness of bio-inspired self-similar regular hierarchical honeycombs," *Composite Structures*, vol. 144, pp. 1–13, jun 2016.

[130] P. Tran, T. D. Ngo, and P. Mendis, "Bio-inspired composite structures subjected to underwater impulsive loading," *Computational Materials Science*, vol. 82, pp. 134–139, 2014.

[131] U. G. K. Wegst, H. Bai, E. Saiz, A. P. Tomsia, and R. O. Ritchie, "Bioinspired structural materials," *Nature Materials*, vol. 14, pp. 23–36, jan 2015.

[132] L. Keogh, P. O'Hanlon, P. O'Reilly, and D. Taylor, "Fatigue in bamboo," *International Journal of Fatigue*, vol. 75, pp. 51–56, jun 2015.

[133] J. Fu, Q. Liu, K. Liufu, Y. Deng, J. Fang, and Q. Li, "Design of bionic-bamboo thin-walled structures for energy absorption," *Thin-Walled Structures*, vol. 135, pp. 400–413, feb 2019.

[134] M. Ansell, "Natural fibre composites in a marine environment," *Natural Fibre Composites*, pp. 365–374, jan 2014.

[135] S. Corradi, T. Isidori, M. Corradi, F. Soleri, and L. Olivari, "Composite boat hulls with bamboo natural fibres," *International Journal of Materials and Product Technology*, vol. 36, no. 1/2/3/4, p. 73, 2009.

[136] S. S. Suhaily, A. H. Khalil, W. W. Nadirah, and M. Jawaid, "Bamboo Based Biocomposites Material, Design and Applications," in *Materials Science - Advanced Topics* (H. P. S. A. Khalil, ed.), p. Ch. 19, Rijeka: IntechOpen, 2013.

[137] G. Palomba, T. Hone, D. Taylor, and V. Crupi, "Bio-inspired protective structures for marine applications," *Bioinspiration & Biomimetics*, jul 2020.

[138] M. Zou, S. Xu, C. Wei, H. Wang, and Z. Liu, "A bionic method for the crashworthiness design of thin-walled structures inspired by bamboo," *Thin-Walled Structures*, vol. 101, pp. 222–230, apr 2016.

[139] Z. Meng, W. Can-gang, L. Jian-qiao, X. Shu-cai, and Z. Xiong, "The energy absorption of bamboo under dynamic axial loading," *Thin-Walled Structures*, vol. 95, pp. 255–261, oct 2015.

[140] D. Taylor, "Impact damage and repair in shells of the limpet Patella vulgata.," *The Journal of experimental biology*, vol. 219, pp. 3927–3935, jan 2016.

[141] I. M. Low, Z. Che, B. A. Latella, and K. Sim, "Mechanical and Fracture Properties of Bamboo," *Key Engineering Materials*, vol. 312, pp. 15–20, jun 2006.

[142] T. Tan, N. Rahbar, S. Allameh, S. Kwofie, D. Dissmore, K. Ghavami, and W. Soboyejo, "Mechanical properties of functionally graded hierarchical bamboo structures," *Acta Biomaterialia*, vol. 7, pp. 3796–3803, oct 2011.

[143] P. Hogström and J. W. Ringsberg, "Assessment of the crashworthiness of a selection of innovative ship structures," *Ocean Engineering*, vol. 59, pp. 58–72, feb 2013.

[144] V. Rubino, V. Deshpande, and N. Fleck, "The dynamic response of clamped rectangular Y-frame and corrugated core sandwich plates," *European Journal of Mechanics - A/Solids*, vol. 28, pp. 14–24, jan 2009.

[145] L. Sutherland and C. Guedes Soares, "The use of quasi-static testing to obtain the low-velocity impact damage resistance of marine GRP laminates," *Composites Part B: Engineering*, vol. 43, pp. 1459–1467, apr 2012.

[146] M. Rejab and W. Cantwell, "The mechanical behaviour of corrugated-core sandwich panels," *Composites Part B: Engineering*, vol. 47, pp. 267–277, apr 2013.

[147] C. De Marco Muscat-Fenech, J. Cortis, and C. Cassar, "Impact damage testing on composite marine sandwich panels, part 1: Quasi-static indentation," *Journal of Sandwich Structures & Materials*, vol. 16, pp. 341–376, jul 2014.

[148] V. Crupi, G. Epasto, and E. Guglielmino, "Comparison of aluminium sandwiches for lightweight ship structures: Honeycomb vs. foam," *Marine Structures*, vol. 30, pp. 74–96, 2013.

[149] M. F. Ashby, "Multi-objective optimization in material design and selection," *Acta Materialia*, vol. 48, pp. 359–369, 2000.

[150] "MOSAIC project final publishable report," tech. rep., 2015.

[151] I. Aydincak and A. Kayran, "An approach for the evaluation of effective elastic properties of honeycomb cores by finite element analysis of sandwich panels," *Journal of Sandwich Structures and Materials*, vol. 11, no. 5, pp. 385–408, 2009.

[152] J. Yuan, L. Zhang, and Z. Huo, "An Equivalent Modeling Method for Honeycomb Sandwich Structure Based on Orthogonal Anisotropic Solid Element," *International Journal of Aeronautical and Space Sciences*, 2020.

[153] V. Bertram, *Practical Ship Hydrodynamics*. Elsevier, second edi ed., 2012.